QUANTUM MECHANICAL AND OPTICAL PROPERTIES OF ASYMMETRIC DOUBLE WELLS AND TWO ELECTRON QUANTUM DOTS

Menberu Mengesha Woldemariam

A Thesis Submitted to

The Department of Physics

PRESENTED IN FULFILMENT OF THE
REQUIREMENTS FOR THE DEGREE OF DOCTOR OF PHILOSOPHY (CONDENSED MATTER PHYSICS)

ADDIS ABABA UNIVERSITY
ADDIS ABABA, ETHIOPIA
JUNE 2012

ADDIS ABABA UNIVERSITY
DEPARTMENT OF
PHYSICS

This is to certify that the thesis prepared by **Menberu Mengesha Woldemariam** Graduate Studies entitled "**Quantum mechanical and optical properties of asymmetric double wells and two electron quantum dots**" in fulfillment of the requirements for the degree of **Doctor of Philosophy (Condensed Matter Physics)** complies with the regulations of the University and meets the accepted standards with respect to originality and quality. .

Dated: June 2012

Examiner: _____
Dr. Nandakumar Kalarikkal

Examiner: _____
Dr. Mulgeta Bekele

Research Supervisor: _____
Prof. Malnev.V

_____

ADDIS ABABA UNIVERSITY

Date: **June 2012**

Author: **Menberu Mengesha Woldemariam**

Title: **Quantum mechanical and optical properties of asymmetric double wells and two electron quantum dots**

Department: **Physics**

Degree: **Ph.D.** Convocation: **July** Year: **2012**

Permission is herewith granted to Addis Ababa University to circulate and to have copied for non-commercial purposes, at its discretion, the above title upon the request of individuals or institutions.

Signature of Author

To my family.

Table of Contents

Abstract

In this dissertation the energy of the ground and excited state of symmetric and asymmetric parabolic double quantum wells (DQWs) are investigated by using our formulated trial wave functions and the Hamiltonian. For symmetric DQWs, calculation of the frequency corresponding to the ground state energy splitting describes that tunneling takes place in the duration of short time when the frequency of the photon is in tera hertz (THz) region. However the tunneling time for excited state energy splitting is shorter than that of the ground state energy splitting due to the decrement of barrier width for parabolic DQWs.

The asymmetric DQWs with resonant levels (the ground state energy level in one well coincides with the first excited state energy in another well) is analyzed. The splitting of these levels and the tunneling times are calculated. If the typical life time of the excited state is much smaller than the tunneling time between wells, the charged particle can radiate as the result of quantum transition from the excited state to the ground state. In the opposite case, the asymmetric DQWs can be treated as a metastable excited nano-system regardless of that the dipole transition from the excited state to the ground state is permitted. The life time of this metastable state can be considerably reduced by putting it in the resonant cavity. The possibility of coherent radiation of an ensemble of asymmetric DQWs is discussed.

Moreover the analytical expressions of absorption coefficients and refractive index changes for parabolic asymmetric DQWs have been determined using the compact density matrix approach. The calculation shows that at some frequency range the asymmetric DQWs become left handed media with negative values of total refractive

index. This behavior of the asymmetric DQWs at some frequency range is of great importance for metamaterial science.

The low lying energy levels of 3D two electron QDs with parabolic confinement and rigid confinement (the wave functions vanish at the surface of the QD) are obtained by the variational method and perturbation techniques. The quantum states of the QD are divided in to the para- and ortho- states like in the theory of helium atom. Our numerical calculations show that the energy differences between the ground and first excited states of the para- dots are practically linear function of the coupling constant λ. This allows one to propose the phenomenological formulas for the energy levels as a function of a typical size of QD. The spin function of the para-dot is singlet with total spin zero. One of the spin function of the ortho-dot is not factorizable symmetric combination. The two functions relate to the entanglement states, which are important for quantum information processing.

The lowest transition energy of one and two electron GaAs QDs are calculated by solving the corresponding Schrödinger equation. For the two electron GaAs QD we calculated the real and imaginary parts of the dielectric constant, the refractive index, and the absorption coefficients as functions of the incident photon energy. The maxima of these quantities show a blue shift comparing with those of the one electron QD due to the Coulomb and exchange interaction between electrons.

Reducing the size of quantum dots results in blue shift of the maxima of the above mentioned quantities for both one and two electron QDs. But the blue shift in the case of two electron QD is larger than that one electron QD due to the energies of Coulomb and exchange.

Acknowledgements

First of all I would like to thank the almighty of God.

I am thankful to graduate office of Addis Ababa University for financial support in my all research activities.

I am deeply indebted to my advisor, Prof. Vadim Mal'nev, not only academically but also in every aspect of my life after I met him. I am thankful to him for giving me opportunities to indulge myself in this wonderfully intriguing research field, guiding me to the right research direction, and sharing his deep insights in to physics.

I would like to thank the Department of Physics for facilitating all the necessary materials while I am doing my research work. I am thankful to Dr. Lemi Demeyu (head Department of Physics) Prof. P. Singh, Dr. Mulgeta Bekele, Dr. Fisseha Kassahun, and Dr. Gizaw Mengiste for their valuable suggestion.

I would also like to acknowledge my sponsor, Bonga College of Teacher education, for a material support. Last but not the least I would like to express my thanks to my brothers Mesfin Mengesha, Dinkayehu Mengesha, Abraham Mengesha, Sebsibe Mengesha and to my sisters Workayehu Mengesha, Zelalem Mengesha, Maedot Mengesha, and Bezawork Mengesha and all my family members for their endless support and love.

List of Figures

List of Tables

Introduction

The study of confined quantum systems has been an interesting subject of investigation since the beginning of quantum theory. It is about fifty years since Richard Feyman famously declared that there is plenty of room at the bottom [1]. In his paper, in 1960 he predicted that the miniaturization of physical systems towards nanometer length scales would result in the discovery of fundamentally new physics. The field of semiconductor nanotechnology began in the late 1960's and early 1970's. It received a sudden impulse in the mid seventies due to the advent of new crystal growth technique known as MBE (molecular beam epitaxy) [2] that enabled the growth of mixed semiconductor crystals with atomic layer precision. For the first time, this development enabled the growth of high quality quantum well structures in which electrons and holes show quantization of their energy spectrum predicted by simple quantum mechanics for particles localized with in rectangular potential. These effects were first exactly observed in 1975 by R. Dingle using optical absorption measurements [3]. Since then the technology for the growth of semiconductor crystals and nanostructure fabrication has improved dramatically resulting in a gradual shift of interest from quantum wells to "lower dimensional" systems in which carrier motion is restricted in two (quantum wires) or all three spatial dimensions (quantum dots). Some of the most milestones in low dimensional systems in III/V, II-VI and

IV/IV hetrostructures are:ultra high vacuum (UHV) techniques in the growth of single crystals of GaAs with Ga and As_4 and As_2 respectively was introduced in 1968 [4]; first attempts to fabricate quantum well structures and superlattices using III-V materials was demonstrated in 1970 [5]; a double barrier resonant tunneling structure was demonstrated in 1972 [6]; first attempts to perform strained layer epitaxy SiGe hetrostructures in 1975 [7]; experimental discovery of the fractional Hall effect in 1982 [8]; first demonstration of epitaxial growth of self-assembled quantum dots in 1985 [9]; realization of the first single electron transistor (SET) in the semiconductor in 1987 [10]; first observation of single electron transport through quantum dots in 1991 [11]; DNA analysis nanodevice developed in 1992; first attempt to propose nano-imprinting in 1994; nano-pore DNA sequencing was realized in 1996; nano-alloy polymer technology invented in 2001; graphene successfully isolated in 2004; iron-based layered superconductor discovered in 2008; and nowadays it is difficult to find optical semiconductor component whose operation is not based on quantum structure.

The interest in the study of physical properties of confined systems such as quantum wells, wires and dots has increased with the recent progress in semiconductor technology [12-14]. In these structures precise engineering enables us to confine the charge carrier motion in one two or three dimensions, which allows us to control the physical properties of structures. The controlling of physical properties of these structures is attractive not only from fundamental scientific point of view but also for their potential applications in the development of semiconductor optoelectronic devices. The increasing interest in low-dimensional semiconductor nanostructures is mainly motivated by the search of materials with tunable optical properties of evident technological relevance. It is important to emphasize at the outset that quantum

confinement and layered structures produce not only quantitative but also qualitative differences in physics from that in bulk structures, which is of course another major motivation for the interest in them. There are many examples of these differences. Excitonic effects become much stronger because of the quantum confinement giving clear absorption resonances even at room temperature. The optical absorption spectrum breaks up in to a series of steps associated with a quantum confined electron and hole levels. The relative importance of direct Coulomb screening and exchange effects is quite different in quantum dots, wires and wells (the Coulomb screening is relatively much weaker), giving very different optical saturation behavior. Modulation doping, which is only possible with layered structures, allows high concentration of electrons with out any impurity scattering leading to the observation of Fermi level correlation singularities, a phenomenon never clearly observed in bulk semiconductors. Electro absorption is totally different from that in bulk semiconductors because of the confinement of the electrons, resulting in very large shifts of optical absorption peaks (the quantum confinement Stark effect). Potential semiconductor nanostructures, in general, porous silicon [15] nano-crystalline silicon [16] GaAs, [17] and nano-crystalline materials have been the subject of intense studies over the last decade primarily due to their interesting size dependent electronic and optical properties. Blue-shift of the optical absorption spectrum, size dependent luminescence, enhanced oscillator strength; non-linear optical effects are some examples of the interesting properties exhibited by these nano-structures. Nonlinear optical properties are of major interest for photonic device application such as all optical switching. Intensity dependent changes in the optical properties are prominent at high intensities of pump laser particularly third order nonlinear effects.

Semiconductor nano-crystals having analogous interior bonding geometries compared to their bulk counter parts exhibit variation in their optical properties with size variation [18, 19]. Nanostructure semiconductors have large nonlinear response as compared to bulk semiconductors. In bulk semiconductors the physical origin of nonlinear absorption and refraction is associated with the optically created high density many particle system causing screening, band gap re-normalization and band filling. The mechanism of nonlinearity in low dimensional systems such as quantum wells, quantum wires and quantum dots is of a basically different kind [20]. With decreasing size the optical nonlinearity is strongly influenced by quantum confinement. The interband absorption spectrum should change from continuous band to a set of discrete lines as the size of crystallite is decreased. The quantum confinement of electronic envelope wave functions over dimensions of the order of the carrier de-Broglie wavelengths provides a novel means to engineer optical nonlinearities. The optical properties of nanostructures are strongly affected because of the quantum confinement of electrical carriers, the huge local electric field enhancement, and the significantly enhanced surface and interface effects [21].

Quantum wells (QWs) have promised a lot of device applications such as modulation doped field effect transistors and quantum well lasers [22, 23]. In addition to this QWs have been found to play a key role in optoelectronics applications such as infrared detectors, wave guides, fast switching and others. The main difference between the QW and the bulk semiconductor is that the electrons are confined in a two dimensional space in the QW and along the growth direction several discrete energy levels are formed. Theoretical studies show that the optical properties of the quantum wells mainly depend on the asymmetry of the confining potential. Such an

asymmetry in the potential profile can be obtained either by applying an electric field to a symmetric QW or by compositionally grading the QW [24]. In asymmetric QW structures the changes in the absorption coefficients were predicted theoretically and confirmed experimentally to be larger than the changes that occur in conventional surface QWs.

Double quantum wells (DQWs) have attracted a great deal of interest recently because of their potential application as optoelectronic devices such as photo detectors, electro optical switches, tera hertz oscillators and for the study of exciton condensation [25-28]. High mobility double quantum well hetrostructures have been important for the study of correlated electron states in two dimensional electron systems, and are potentially important for novel field effect transistors that add functionality by controlling electron transfer between the quantum wells [29]. DQW structures are very interesting as far as the device industry is concerned, since by the inter layer distance between wells and the barrier varies, an improvement in the transport properties is achieved [30]. Asymmetric double quantum well (ADQW) structures, which consist of two different size wells coupled by a thin barrier have been commonly used to investigate electron and hole tunneling [31].

The tera hertz portion of the electromagnetic spectrum spans the frequency range between microwave and mid infrared (100 GHz -30 THz). In spite of many potential applications, this frequency range still represents the least exploited region of the spectrum owing to the very limited availability of suitable sources and detectors [32-35]. In present times there is an impression for such devices as a relatively long list of applications has been envisioned for the THz range: wireless communication, atmospheric sensing, chemical detection, astronomy, biological, and medical imaging

are among the possible applications for this region. Inter well transfer can also be promoted by tera hertz photon assisted tunneling, opening the possibility of fast, voltage tunable tera hertz detectors, inversion doubling of ammonia in the ammonia maser (molecular physics) and electron tunneling through hetrostuctures (condensed matter physics) [36, 37].

In symmetric double well the potential of the two wells are separated by the central barrier. If the barrier were impenetrable, the energy levels would correspond to the motion of a particle in one of the two wells. But since for a finite barrier, tunneling is possible, each energy level split in to two and these two levels correspond to the motion of the particle in one of the two wells at the same time.

When the confining potential $V(\xi)$ tends to infinity on both sides of the central maximum, that is $V(\xi) \to \infty$ as $\xi \to \pm\infty$, the motion of the particle will be restricted to a part of the ξ-axis. Depending on the number of maxima of $V(\xi)$, we can have the eigenvalue problem for a double or multiple well potential. The energy eigenvalues are almost even in each parity sector, for solution of double well oscillator with the potential $\frac{\hbar\omega}{2}(|\xi| - \xi_0)^2$. As the parameter ξ_0 is varied from 0 to ∞, the potential changes from the limit of single harmonic oscillator well to the other limit of two separate oscillator wells divided by an infinitely high and broad potential well. In the first case we have non degenerate energy eigenvalues however; in the second case the energy levels are doubly degenerate, since the system may occupy an eigenstate of either the harmonic oscillator well on the left or on the right.

For finite barrier the energy levels form doublets $(E_1, E_2), (E_3, E_4)$ which are well separated from each other. Since each doublet is composed of the states of opposite

parity, electromagnetic dipole radiation causes transition between them and this allows for accurate measurement of the splitting of the energy levels. The originally degenerate energy levels in each well mix into symmetric and anti-symmetric combinations due to quantum tunneling [38-40].

Among semiconductor nanostructures, quantum dots (QDs) have gained considerable attention due to their unusual electronic and optical properties. Quantum size effect in these structures lead to the formation of atomic-like discrete energy levels, and discrete charges of physical properties of these quasi-zero dimensional structures [41-43]. Essentially QDs (artificial atoms) are boxes about 100 nm on a side, contained in a semiconductor, and holding a number of electrons that may be varied at will. As in real atoms, the electrons are attracted to a positively charged nucleus. In artificial atoms, electrons are typically trapped in a bowl-like parabolic potential well in which electrons tend to fall in towards the bottom of the bowl. One can consider the QD as tiny laboratory in which quantum mechanics and the effect of electron-electron interaction can be studied. The typical characteristics of a QD differ considerably from that of natural atom for one important reason: artificial atoms are typically much larger than real atoms. The electron orbits do not simply scale with size. A real atom containing many electrons whose size is continuously variable. As it is made larger, the Coulomb energy arising from the repulsion, between electrons orbiting around, the nucleus decreases because the average spacing between electrons increases. However, there is another energy scale in the problem: the separation in energy of the different orbits of electrons in the QD. As a QD size increases, the differences in the orbital energies decrease faster than the coulomb energy. It follows that in a large QD, the effect of electron-electron interactions are relatively more important than in

a small QD.

In particular, QDs in which only few electrons are bound at semiconductor interface have been the subject of intense research studies over the last few years. The electron motion in QDs are confined to a region with dimensions comparable to the de Broglie wave length of the particle. In two electron QDs the Hamiltonian operator $\hat{H}$ is symmetrical with respect to the two electrons because of their identity. The wave function Ψ must be antisymmetric with respect to interchange of electrons as they obey the Pauli principle. As a result there are two possibilities. The first possibility signifies that the coordinate wavefunction is symmetric and the spin function is antisymmetric, while the second possibility represents the opposite situation. We have therefore two classes of wave functions for the possible states of QD namely the para- and ortho- states. That is the level of the QD with antiparallel spins (singlet levels) is the para- QD and the QD with parallel spins (triplet levels) is called the ortho- QD.

For theoretical studies, one of the most important problems is the two electron QD problem. Although there are only two electrons in the system with a confining potential, it is not yet possible to find an exact analytical solution due to the presence of Coulomb interaction. Even though accurate results could easily be obtained by numerical approaches like exact diagonalization [44, 45], the series expansion method [46, 47] and the quantum Monte Carlo technique [48, 49], many researchers are interested in finding a simple but accurate analytical method to gain insight into the competition between the confinement potential and the Coulomb interaction.

This dissertation focuses on theoretical analysis of: (I) the energy doublets and tunneling properties in symmetric parabolic DQWs with zero electric field; (II) The

energy doublets and THz radiation under tunneling in parabolic DQWs with applied electric field; (III) Optical absorption coefficients and refractive index changes in parabolic DQWs in the presence of electric field ; (IV) Two electron QDs with parabolic confinement (Low lying para- and ortho- states); and (V) Optical properties of two-electron quantum dots in low lying para- and ortho- states.

Chapter 1

The energy doublets in parabolic double quantum wells with zero electric field

The energy splitting of the ground and excited state energy levels of symmetric parabolic DQWs is investigated employing our formulated trial wave functions and Hamiltonian. Calculation of the frequency corresponding to the ground state energy splitting reveals that tunneling takes place in the duration of short time when the frequency is in tera hertz (THz) region. Moreover the tunneling time for excited state energy splitting is too short to that of ground state energy splitting.

1.1 Introduction

The quantum mechanical tunneling in symmetric DQWs was studied intensively for last few decades. The originally degenerate energy levels in each well mix into symmetric and antisymmetric combinations due to quantum tunneling. Different methods have been proposed to calculate the energy splitting: the WKB approximation [50], the numerical methods [51], the instanton method [52], analytical transfer matrix

method [53], and highly accurate refined spectral method [54]. The WKB approximation is commonly used for its ease mathematical form. However taking the quadratic connection formula instead of those related to the Airy functions to modify the WKB result for the ground state diminishes the accuracy. Instanton method is useful for understanding the quantum tunneling, which has no classical counterpart. However the quantitative calculation of the energy splitting in the double well potential by this method is less accurate because of the Euclidean propagator can be obtained only in the limit of infinite separation between the potential minima which corresponds to zero tunneling probability. The refined spectral method or numerical method is relatively accurate as compared to the other methods. However its accuracy depends on the number of basis elements (usually infinite number of basis functions) and controlling the round of errors is difficult. Moreover, the scarcity of sophisticated softwares to manipulate this matrix limits its application. In this part of thesis the energy splitting of the ground state as well as excited state is found by simple approach employing our model Hamiltonian and wave functions.

1.2 Statement of the problem

In this chapter we recall some known results concerning the splitting of the ground state energy of the symmetrical double well with the Hamiltonian

$$\hat{H} = -\frac{\hbar^2}{2m^*}\frac{d^2}{dx^2} + \frac{m^*\omega^2}{2}(|x| - a)^2. \tag{1.2.1}$$

Here a is a distance between the minima of the two parabolic wells, m^* is the effective mass of the particle, ω is the frequency, and x is a coordinate of the particle. It would

be more convinent to introduce a dimensionless variable $\xi = \sqrt{\frac{m^*\omega}{\hbar}}x$ and rewrite (1.2.1) in a more simple form

$$\frac{\hat{H}}{\hbar\omega} = -\frac{1}{2}\frac{d^2}{d\xi^2} + \frac{1}{2}\Big(|\xi| - \xi_0\Big)^2, \quad \xi_0 = \sqrt{\frac{m^*\omega}{\hbar}}a. \tag{1.2.2}$$

Further, for the sake of simplicity, we consider the case of "far separated wells" when the height of the barrier between wells $V(0) = \frac{1}{2}m^*\omega^2a^2$ is much larger than the level spacing $\hbar\omega$. In the dimensionless variables, we obtain the following inequality

$$\frac{2V(0)}{\hbar\omega} = \xi_0^2 >> 1. \tag{1.2.3}$$

The solution of the Schrödinger equation corresponding to Hamiltonian (1.2.2), we seek in the form

$$\psi_0 = c_1\psi_{0L}(\xi) + c_2\psi_{0R}(\xi), \tag{1.2.4}$$

where

$$\begin{cases} \psi_{0L} = (\frac{1}{\pi})^{\frac{1}{4}} exp\{-\frac{1}{2}(\xi + \xi_0)^2\}, \\ \psi_{0R} = (\frac{1}{\pi})^{\frac{1}{4}} exp\{-\frac{1}{2}(\xi - \xi_0)^2\} \end{cases} \tag{1.2.5}$$

are the ground state wave functions of the left (L) and right (R) wells with equilibrium positions at $\xi = \pm\xi_0$.

1.3 The ground state energy doublet in parabolic DQWs

For "far" separated wells $\xi_0^2 >> 1$, the functions 1.2.5 are practically localized in their wells and correspond to the ground state energy $\frac{E_0}{\hbar\omega} = \frac{1}{2}$. The coefficients c_1 and c_2

of the linear combination (1.2.4) satisfy the system of algebraic equations

$$\begin{cases} c_1(H_{11} - E) + c_2(H_{12} - sE) = 0, \\ c_1(H_{21} - sE) + c_2(H_{22} - E) = 0, \end{cases} \tag{1.3.1}$$

where,

$$\begin{cases} H_{11} = \int \psi_{0L} H \psi_{0L} d\xi \\ H_{12} = \int \psi_{0L} H \psi_{0R} d\xi \\ H_{21} = \int \psi_{0R} H \psi_{0L} d\xi \\ H_{22} = \int \psi_{0R} H \psi_{0R} d\xi \end{cases} \tag{1.3.2}$$

$$\begin{aligned} H_{11} = \Big(\frac{1}{\pi}\Big)^{\frac{1}{2}} & \\ & \int_{-\infty}^{0} e^{-\frac{1}{2}(\xi+\xi_0)^2} \Big(-\frac{1}{2}\frac{d^2}{d\xi^2} + \frac{1}{2}(\xi+\xi_0)^2 \Big) e^{-\frac{1}{2}(\xi+\xi_0)^2} d\xi \\ & + \Big(\frac{1}{\pi}\Big)^{\frac{1}{2}} \int_{0}^{\infty} e^{-\frac{1}{2}(\xi+\xi_0)^2} \Big(-\frac{1}{2}\frac{d^2}{d\xi^2} + \frac{1}{2}(\xi-\xi_0)^2 \Big) e^{-\frac{1}{2}(\xi+\xi_0)^2} d\xi \end{aligned} \tag{1.3.3}$$

The Hamiltonian H_{11} can be separated in to kinetic K_{11} and potential V_{11} terms as follows.

$$K_{11} = -\frac{1}{2}\Big(\frac{1}{\pi}\Big)^{\frac{1}{2}} \int_{-\infty}^{\infty} e^{-\frac{1}{2}(\xi+\xi_0)^2} \frac{d^2}{d\xi^2} (e^{-\frac{1}{2}(\xi+\xi_0)^2}) d\xi \tag{1.3.4}$$

The solution of this integral gives, $K_{11} = \frac{1}{4}$

$$\begin{aligned} V_{11} = \frac{1}{2}\Big(\frac{1}{\pi}\Big)^{\frac{1}{2}} & \\ & \int_{-\infty}^{0} e^{-\frac{1}{2}(\xi+\xi_0)^2} (\xi+\xi_0)^2 e^{-\frac{1}{2}(\xi+\xi_0)^2} d\xi \\ & + \frac{1}{2}\Big(\frac{1}{\pi}\Big)^{\frac{1}{2}} \int_{0}^{\infty} e^{-\frac{1}{2}(\xi+\xi_0)^2} (\xi-\xi_0)^2 e^{-\frac{1}{2}(\xi+\xi_0)^2} d\xi \end{aligned} \tag{1.3.5}$$

The solution of this integral is, $V_{11} = \frac{1}{4}$. Combining the solutions of the integral of kinetic and potential energy terms,

$$H_{11} = H_{22} = \frac{1}{2} \tag{1.3.6}$$

The matrix element H_{12} of the Hamiltonian is,

$$H_{12} = \Big(\frac{1}{\pi}\Big)^{\frac{1}{2}} \int_{-\infty}^{0} e^{-\frac{1}{2}(\xi+\xi_0)^2}\Big(-\frac{1}{2}\frac{d^2}{d\xi^2} + \frac{1}{2}(\xi+\xi_0)^2\Big)e^{-\frac{1}{2}(\xi-\xi_0)^2}d\xi + \Big(\frac{1}{\pi}\Big)^{\frac{1}{2}} \int_{0}^{\infty} e^{-\frac{1}{2}(\xi+\xi_0)^2}\Big(-\frac{1}{2}\frac{d^2}{d\xi^2} + \frac{1}{2}(\xi-\xi_0)^2\Big)e^{-\frac{1}{2}(\xi-\xi_0)^2}d\xi \quad (1.3.7)$$

The kinetic and potential part of this matrix element are,

$$K_{12} = -\frac{1}{2}\Big(\frac{1}{\pi}\Big)^{\frac{1}{2}} \int_{-\infty}^{\infty} e^{-\frac{1}{2}(\xi+\xi_0)^2}\frac{d^2}{d\xi^2}(e^{-\frac{1}{2}(\xi-\xi_0)^2})d\xi \quad (1.3.8)$$

$$V_{12} = \frac{1}{2}\Big(\frac{1}{\pi}\Big)^{\frac{1}{2}} \int_{-\infty}^{0} e^{-\frac{1}{2}(\xi+\xi_0)^2}(\xi+\xi_0)^2 e^{-\frac{1}{2}(\xi-\xi_0)^2}d\xi + \frac{1}{2}\Big(\frac{1}{\pi}\Big)^{\frac{1}{2}} \int_{0}^{\infty} e^{-\frac{1}{2}(\xi+\xi_0)^2}(\xi-\xi_0)^2 e^{-\frac{1}{2}(\xi-\xi_0)^2}d\xi \quad (1.3.9)$$

After some manipulation of the integral we obtain,

$$K_{12} = (\frac{1}{4} - \frac{\xi_0^2}{2})e^{-\xi_0^2} \quad (1.3.10)$$

$$V_{12} = \Big(\frac{1}{4} - \frac{\xi_0}{\sqrt{\pi}} + \frac{\xi_0^2}{2}\Big)e^{-\xi_0^2} \quad (1.3.11)$$

Combining equation (1.3.10) and (1.3.11) the matrix element H_{12} or H_{21} is

$$H_{12} = H_{21} = \Big(\frac{1}{2} - \frac{\xi_0}{\sqrt{\pi}}\Big)e^{-\xi_0^2} \quad (1.3.12)$$

The matrix elements of the Hamiltonian (1.2.2) on the wave functions (1.2.5) and the overlapping integral s with account of $\xi_0^2 >> 1$ are as follows

$$\begin{cases} H_{11} = H_{22} = \frac{1}{2}, \\ H_{12} = H_{21} = -\frac{\xi_0}{\sqrt{\pi}} exp\{-\xi_0^2\} \\ s = \int \psi_{0L}\psi_{0R}d\xi = exp\{-\xi_0^2\}. \end{cases} \quad (1.3.13)$$

The nontrivial solution of (1.3.1) is obtained from the condition of vanishing the determinant of the system (1.3.1)

$$\begin{vmatrix} H_{11} - E & H_{12} - sE \\ H_{21} - sE & H_{22} - E \end{vmatrix} = 0. \tag{1.3.14}$$

The solution (1.3.14) gives two energy levels of the ground state energy doublet appearing as a result of removing the double fold degeneracy of the ground state

$$E_0^{s,a} = \hbar\omega\Big[\frac{1}{2} \pm \frac{\xi_0}{\sqrt{\pi}} exp\{-\xi_0^2\}\Big]. \tag{1.3.15}$$

Here the lower index of energy E stands for the ground state $n = 0$, the upper indexes s and a relate to the following symmetrical and antisymmetrical functions

$$\psi_{s,a} = \frac{1}{\sqrt{2}}\Big[\psi_{0L}(\xi) \pm \psi_{0R}(\xi)\Big], \tag{1.3.16}$$

where $\psi_{0L}(\xi)$ and $\psi_{0R}(\xi)$ are given by (1.2.5). The ground state energy doublet is given by

$$\Delta E_0 = E_0^a - E_0^s = 2\hbar\omega\sqrt{\frac{2V_0}{\hbar\omega\pi}} exp\Big\{-\frac{2V_0}{\hbar\omega}\Big\}. \tag{1.3.17}$$

It coincides with limiting case $\xi_0^2 >> 1$ of the known exact solution of the parabolic double well [55]. Now we obtain the splitting of the ground state level with the help of the method proposed by Landau [56]. According to this method the splitting ΔE_0 is given by the formula

$$\Delta E_0 = \frac{2\hbar^2}{m^*}\psi_s(0)\frac{d\psi_a(x)}{dx}\Big|_{x=0}. \tag{1.3.18}$$

The usage of (1.3.18) with account of (1.3.16), (1.2.5) and $x = \sqrt{\frac{\hbar}{m^*\omega}}\xi$ gives exactly the same result as (1.3.17). The expression (1.3.17) is the first doublet of energy of the far separated parabolic double wells $\frac{V(0)}{\hbar\omega} >> 1$.

1.4 Tunneling property due to the splitting of ground state energy level of parabolic DQWs

The frequency corresponding to the ground state energy splitting is, $\frac{\Delta E_0}{\hbar} = \omega' = 2\omega\sqrt{\frac{2V_0}{\hbar\omega\pi}}e^{-\frac{2V_0}{\hbar\omega}}$. The time taken for the system to change from its initial state to a final state is given by, $T = \frac{\pi}{2\omega}\sqrt{\frac{\hbar\omega\pi}{2V_0}}e^{\frac{2V_0}{\hbar\omega}}$ and this clearly reveals that the particles have exchanged in an entirely quantum mechanical fashion. The ratio of the time T during which the exchange takes place to the period of harmonic oscillator is given approximately by $T\frac{\omega}{2\pi} = \frac{1}{4}\sqrt{\frac{\hbar\omega\pi}{2V_0}}e^{\frac{2V_0}{\hbar\omega}}$. If the barrier V_0 is high compared to $\hbar\omega$, the tunneling is strongly inhibited by the presence of exponential factor.

The wave functions corresponding to energy E_1 and E_2 has a symmetric and antisymmetric combinations of, ψ_{0L} and ψ_{0R}

$$\psi_0(E_1) = \frac{1}{\sqrt{2}}(\psi_{0L} + \psi_{0R}) \tag{1.4.1}$$

$$\psi_0(E_2) = \frac{1}{\sqrt{2}}(\psi_{0L} - \psi_{0R}). \tag{1.4.2}$$

Let us assume that the system is represented by $\psi_0(E_1)$ at $t = 0$. At latter time,the system has,

$$\psi_0(E_1, t_0 = 0; t) = \frac{1}{\sqrt{2}}(e^{-\frac{iE_1t}{\hbar}}\psi_{0L} + e^{-\frac{iE_2t}{\hbar}}\psi_{0R}) \tag{1.4.3}$$

Solving the above equation gives,

$$\psi_0(E_1, t_0 = 0; t) = \frac{1}{2\sqrt{2}}e^{-\frac{iE_1t}{\hbar}}\left[\psi_{0L} + e^{-\frac{i(E_2-E_1)t}{\hbar}}\psi_{0R} + \psi_{0L} + e^{-\frac{i(E_2-E_1)t}{\hbar}}\psi_{0R}\right] \tag{1.4.4}$$

$$\psi_0(E_1, t_0 = 0; t) = \frac{1}{2\sqrt{2}} e^{-\frac{iE_1 t}{\hbar}} \Big[\psi_{0L} + \psi_{0R} + e^{-i\omega' t}\psi_{0L} + e^{-i\omega' t}\psi_{0R} + \psi_{0L} - \psi_{0R} + e^{-i\omega' t}\psi_{0R} - e^{-i\omega' t}\psi_{0L}\Big] \tag{1.4.5}$$

$$\psi_0(E_1, t_0 = 0; t) = \frac{1}{2\sqrt{2}} e^{-i\frac{E_1 t}{\hbar}} e^{-i\frac{\omega' t}{2}} \Big[(\psi_{0L} + \psi_{0R})(e^{i\frac{\omega' t}{2}} + e^{-i\frac{\omega' t}{2}}) + (\psi_{0L} - \psi_{0R})(e^{i\frac{\omega' t}{2}} - e^{-i\frac{\omega' t}{2}})\Big] \tag{1.4.6}$$

$$\psi_0(E_1, t_0 = 0; t) = e^{-\frac{i(E_1+E_2)t}{2\hbar}} \Big[(\psi_{0L} + \psi_{0R})cos\frac{\omega' t}{2} + i(\psi_{0L} - \psi_{0R})sin\frac{\omega' t}{2}\Big] \tag{1.4.7}$$

This clearly shows that the particle oscillates back and forth between states $\psi_{0L}+\psi_{0R}$ and $\psi_{0L}-\psi_{0R}$. This oscillatory behavior can also be considered from the view point of tunneling in quantum mechanics. A particle initially confined to the right hand side can tunnel through the classically forbidden region to the left hand side, then back to the right hand side and so on. At time $t = \frac{\pi\hbar}{E_1-E_2}$ the system is found in pure $\psi_0(E_2)$. At $t = \frac{2\pi\hbar}{E_1-E_2}$ the system come back to pure $\psi_0(E_1)$ and so forth. Thus in general the system has an oscillation between $\psi_0(E_1)$ and $\psi_0(E_2)$ with angular frequency $\omega' = \frac{(E_1-E_2)}{\hbar}$. For infinitely high barrier; the states ψ_{0L} and ψ_{0R} are degenerate, so $\psi_0(E_1)$ and $\psi_0(E_2)$ are also energy eigenkets even though they are not parity eigenkets. Once the system is found in $\psi_0(E_1)$ it remains so forever (oscillation time between ψ_{0L} and ψ_{0R} is now ∞). Here calculation for tunneling time is carried out on typical AlGaAs/GaAs parabolic DQWs for ground state energy splitting. The material parameters adopted are $m^* = 0.082m_0$ (m_0 is the free electron mass), $\omega = 10^{12}s^{-1}$, and $a = 100$ nm. Fig. 1.1 describes the time taken for a particle to

change a state from its initial state to a final state and the ratio of the time T during which the exchange takes place to the period of harmonic oscillator for ground state energy doublet. The tunneling time and the ratio of tunneling time to the period of harmonic oscillator for the above parameters are ($T = 1.333 \times 10^{-9}s$) and $T\frac{\omega}{2\pi} = 209$ respectively. The time taken for a particle to change a state depends on the height or width of the barrier. A slight increase of the barrier height or width elongates the time taken for a particle to oscillate between the two wells. This reveals that the time taken to change a state is too large to the period of harmonic oscillator even in THz regime. At visible frequency regime ($10^{14} - 10^{15}$)Hz the time taken to change a state is the super astronomical.

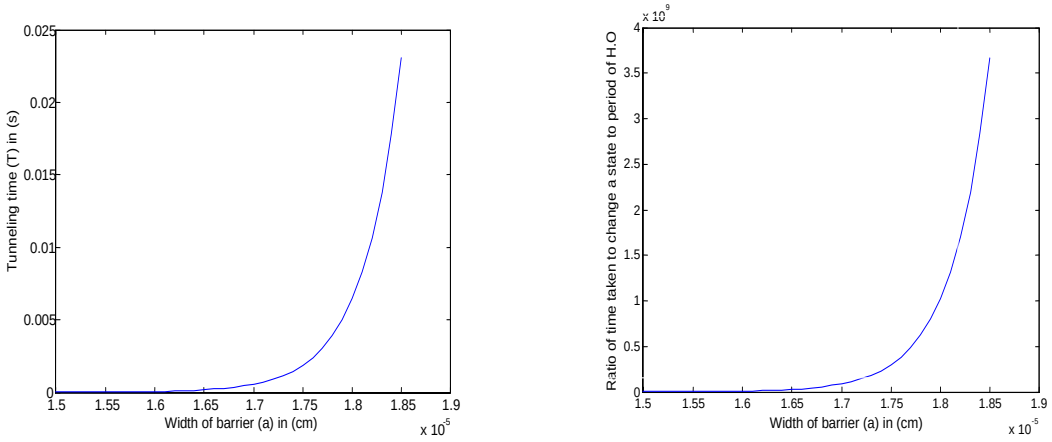

Figure 1.1: *The time taken for the system to change from its initial state to a final state and the ratio of the time during which the exchange takes place to the period of harmonic oscillator.*

1.5 The first excited state energy doublet in parabolic DQWs

Now we consider the splitting of the first excited state energy level. The wave functions related to the left and right wells have the form

$$\begin{cases} \psi_{11} = N_1(x+a)exp\{-\frac{m^*\omega}{2\hbar}(x+a)^2\}, \\ \psi_{12} = N_1(x-a)exp\{-\frac{m^*\omega}{2\hbar}(x-a)^2\}. \end{cases} \tag{1.5.1}$$

with the normalization constant $N_1 = \left(\frac{2}{\sqrt{\pi}}\right)^{\frac{1}{2}}\left(\frac{m\omega}{\hbar}\right)^{\frac{3}{4}}$. Using dimensionless variable, equation (1.5.1) can be rewritten as

$$\begin{cases} \psi_{1L} = \left(\frac{2}{\sqrt{\pi}}\right)^{\frac{1}{2}}(\xi+\xi_0)exp\{-(\xi+\xi_0)^2\}, \\ \psi_{1R} = \left(\frac{2}{\sqrt{\pi}}\right)^{\frac{1}{2}}(\xi-\xi_0)exp\{-(\xi-\xi_0)^2\}. \end{cases} \tag{1.5.2}$$

The matrix elements of the Hamiltonian for the first excited state are determined in the same way as we did for the ground state. The matrix elements are,

$$\begin{aligned} H_{11} = 2\Big(\frac{1}{\pi}\Big)^{\frac{1}{2}} & \\ & \int_{-\infty}^{0}(\xi+\xi_0)e^{-\frac{1}{2}(\xi+\xi_0)^2}\Big(-\frac{1}{2}\frac{d^2}{d\xi^2}+\frac{1}{2}(\xi+\xi_0)^2\Big)(\xi+\xi_0)e^{-\frac{1}{2}(\xi+\xi_0)^2}d\xi \\ & + 2\Big(\frac{1}{\pi}\Big)^{\frac{1}{2}}\int_{0}^{\infty}(\xi+\xi_0)e^{-\frac{1}{2}(\xi+\xi_0)^2}\Big(-\frac{1}{2}\frac{d^2}{d\xi^2}+\frac{1}{2}(\xi-\xi_0)^2\Big)(\xi+\xi_0)e^{-\frac{1}{2}(\xi+\xi_0)^2}d\xi \end{aligned} \tag{1.5.3}$$

This matrix element of the Hamiltonian can be separated in to kinetic and potential terms for simplification. The kinetic part of this Hamiltonian matrix element is,

$$K_{11} = -\Big(\frac{1}{\pi}\Big)^{\frac{1}{2}}\int_{-\infty}^{\infty}(\xi+\xi_0)e^{-\frac{1}{2}(\xi+\xi_0)^2}\frac{d^2}{d\xi^2}(\xi+\xi_0)(e^{-\frac{1}{2}(\xi+\xi_0)^2})d\xi \tag{1.5.4}$$

After integration for we obtain, $K_{11} = \frac{3}{4}$

The potential term in H_{11} is,

$$V_{11} = \Big(\frac{1}{\pi}\Big)^{\frac{1}{2}} \int_{-\infty}^{0} (\xi+\xi_0)e^{-\frac{1}{2}(\xi+\xi_0)^2}(\xi+\xi_0)^2(\xi+\xi_0)e^{-\frac{1}{2}(\xi+\xi_0)^2}d\xi + \Big(\frac{1}{\pi}\Big)^{\frac{1}{2}} \int_{0}^{\infty} (\xi+\xi_0)e^{-\frac{1}{2}(\xi+\xi_0)^2}(\xi-\xi_0)^2(\xi+\xi_0)e^{-\frac{1}{2}(\xi+\xi_0)^2}d\xi \quad (1.5.5)$$

The solution of this integral is, $V_{11} = \frac{3}{4}$

The Hamiltonian matrix H_{11} is the sum of K_{11} and V_{11} and is given by,

$$H_{11} = K_{11} + V_{11} = \frac{3}{2} \quad (1.5.6)$$

Similarly, the Hamiltonian matrix element H_{12} for the first excited state is,

$$H_{12} = 2\Big(\frac{1}{\pi}\Big)^{\frac{1}{2}} \int_{-\infty}^{0} (\xi+\xi_0)e^{-\frac{1}{2}(\xi+\xi_0)^2}\Big(-\frac{1}{2}\frac{d^2}{d\xi^2} + \frac{1}{2}(\xi+\xi_0)^2\Big)(\xi-\xi_0)e^{-\frac{1}{2}(\xi-\xi_0)^2}d\xi + 2\Big(\frac{1}{\pi}\Big)^{\frac{1}{2}} \int_{0}^{\infty} (\xi+\xi_0)e^{-\frac{1}{2}(\xi+\xi_0)^2}\Big(-\frac{1}{2}\frac{d^2}{d\xi^2} + \frac{1}{2}(\xi-\xi_0)^2\Big)(\xi-\xi_0)e^{-\frac{1}{2}(\xi-\xi_0)^2}d\xi \quad (1.5.7)$$

$$K_{12} = -\Big(\frac{1}{\pi}\Big)^{\frac{1}{2}} \int_{-\infty}^{\infty} (\xi+\xi_0)e^{-\frac{1}{2}(\xi+\xi_0)^2}\frac{d^2}{d\xi^2}(\xi-\xi_0)(e^{-\frac{1}{2}(\xi-\xi_0)^2})d\xi \quad (1.5.8)$$

After integration in (1.5.8) we get further

$$K_{12} = \Big(\frac{3}{4} - 3\xi_0^2 + \xi_0^4\Big)e^{-\xi_0^2}. \quad (1.5.9)$$

$$V_{12} = \Big(\frac{1}{\pi}\Big)^{\frac{1}{2}} \int_{-\infty}^{0} (\xi+\xi_0)e^{-\frac{1}{2}(\xi+\xi_0)^2}(\xi+\xi_0)^2)(\xi-\xi_0)e^{-\frac{1}{2}(\xi-\xi_0)^2}d\xi + \Big(\frac{1}{\pi}\Big)^{\frac{1}{2}} \int_{0}^{\infty} (\xi+\xi_0)e^{-\frac{1}{2}(\xi+\xi_0)^2}(\xi-\xi_0)^2)(\xi-\xi_0)e^{-\frac{1}{2}(\xi-\xi_0)^2}d\xi \quad (1.5.10)$$

The solution of this integral for this potential term is,

$$V_{12} = \Big(\frac{3}{4} - \frac{2\xi_0}{\sqrt{\pi}} + \frac{2\xi_0^3}{\sqrt{\pi}} - \xi_0^4\Big)e^{-\xi_0^2} \quad (1.5.11)$$

The matrix elements of the Hamiltonian H_{12} or H_{21} are,

$$\Big(\frac{3}{2} - 3\xi_0^2 - \frac{2\xi_0}{\sqrt{\pi}} + \frac{2\xi_0^3}{\sqrt{\pi}}\Big)e^{-\xi_0^2} \tag{1.5.12}$$

The matrix elements of the Hamiltonian (1.2.2) on the wave functions (1.5.2) and the overlapping integral s with account of $\xi_0^2 >> 1$

$$\begin{cases} H_{11} = H_{22} = \frac{3}{2}, \\ H_{12} = H_{21} = (\frac{3}{2} - 2\frac{\xi_0}{\sqrt{\pi}} - 3\xi_0^2 + \frac{2\xi_0^3}{\sqrt{\pi}})exp\{-\xi_0^2\} \\ s = \int \psi_{1L}\psi_{1R}d\xi = [1 - 2\xi_0^2]exp\{-\xi_0^2\}. \end{cases} \tag{1.5.13}$$

The nontrivial solution of this system is obtained from the condition of vanishing the determinant

$$\begin{vmatrix} H_{11} - E & H_{12} - sE \\ H_{21} - sE & H_{22} - E \end{vmatrix} = 0. \tag{1.5.14}$$

The solution (1.5.14) gives two energy levels of the excited state energy doublet appearing as a result of removing the double fold degeneracy of the excited state

$$E_1^{s,a} = \hbar\omega\Big(\frac{3}{2} \mp \Big(\frac{3}{2} - \frac{2\xi_0}{\sqrt{\pi}} - 3\xi_0^2 + \frac{2\xi_0^3}{\sqrt{\pi}}\Big)exp\{-\xi_0^2\}\Big), \tag{1.5.15}$$

with the above accepted approximation of the "far" separated wells, the energy splitting of the first excited energy level is

$$\Delta E_1 = E_1^s - E_1^a = 8V_0\sqrt{\frac{2V_0}{\hbar\omega\pi}}exp\Big\{-\frac{2V_0}{\hbar\omega}\Big\}. \tag{1.5.16}$$

The symmetric and antisymmetric wave functions describing energy levels of the first excited state doublet (1.5.16) with account of (1.5.15) are given by

$$\psi_{1s,1a} = \frac{1}{\sqrt{2}}\Big[\psi_{1L}(x) \pm \psi_{1R}(x)\Big]. \tag{1.5.17}$$

It is interesting to compare this result with the splitting of the first excited state obtained by the Landau method with the help of

$$\Delta E_1 = \frac{2\hbar^2}{m^*}\psi_{1s}(0)\frac{d\psi_{1a}(x)}{dx}\Big|_{x=0}. \tag{1.5.18}$$

The calculations according to (1.5.18) gives the same splitting as (1.5.16).

Now we compare splitting of the first excited level and ground state level

$$\frac{\Delta E_1}{\Delta E_0} = \frac{4V_0}{\hbar\omega} >> 1.$$

In the accepted approximation $\hbar\omega << V_0$, the splitting of the first excited level is much larger then the splitting of the ground state level being exponentially small. This is understandable because in the case of parabolic oscillator the width of the barrier decreases with the number of level. In the case of arbitrary symmetric well, we can see this from the known formula [56]

$$\Delta E_n = \frac{\hbar\omega_n}{\pi}exp\Big(-\frac{1}{\hbar}\int_{-a}^{a}|p(x)|dx\Big), \tag{1.5.19}$$

where $|p(x)| = \sqrt{2m^*[V(x)-E_n]}$, ω_n is a frequency of the classical periodic motion in the potential well $V(x)$ for the energy E_n, $\pm a/2$ is a turning points corresponding to energy E_n (See Fig 1.2). It is clear that $|p|$ decreases with the number of the level and provides increasing in ΔE_n. Application of (1.5.19) to calculation of the splitting ΔE_0 of the parabolic potential double well gives

$$\Delta E_0 = \frac{2\hbar\omega}{\sqrt{\pi}}\sqrt{\frac{2V_0}{\hbar\omega\pi}}exp\Big\{-\frac{2V_0}{\hbar\omega}\Big\}.$$

This result differs from (1.3.17) by a factor $\frac{1}{\sqrt{\pi}} \sim 1$. For the excited levels the splitting obtained with the help of (1.5.19) is $\Delta E_1 = \frac{2}{3\sqrt{3\pi}}8V_0\sqrt{\frac{2V_0}{\hbar\omega\pi}}exp(-\frac{2V_0}{\hbar\omega})$ and differs from (1.5.16) by a factor $\frac{2}{3\sqrt{3\pi}}$. The ratio of the excited state energy splitting to the ground state energy splitting is $\simeq 1.5396(\frac{V_0}{\hbar\omega})$ and greater than unity. So this result is also approximately true.

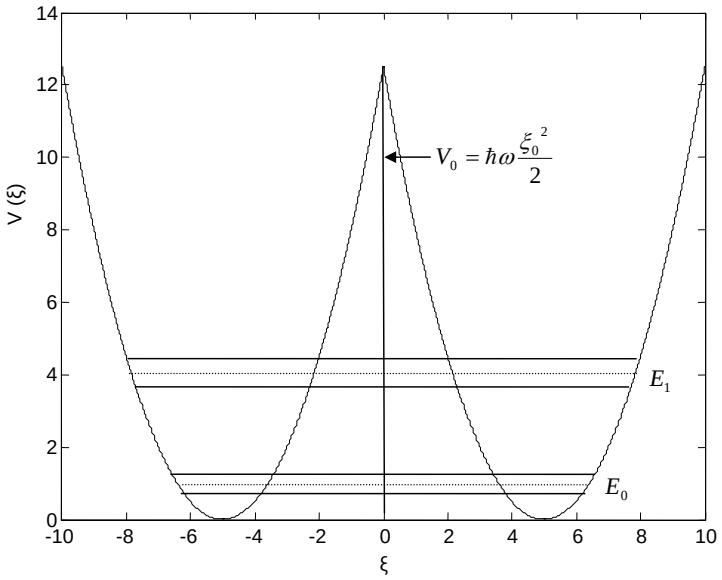

Figure 1.2: *Potential of symmetric DQWs.*

1.6 Tunneling between excited states and energy splitting of parabolic DQWs

The frequency corresponding to excited state energy splitting is $\omega'' = \frac{8V_0}{\hbar}\sqrt{\frac{2V_0}{\hbar\omega\pi}}e^{\frac{-2V_0}{\hbar\omega}}$. For the system to change from its initial excited state to final state; it takes a time $T' \approx \frac{\pi\hbar}{8V_0}\sqrt{\frac{\hbar\omega\pi}{2V_0}}e^{\frac{2V_0}{\hbar\omega}}$. Moreover the ratio of the time T' during which the exchange takes place to the period of harmonic oscillator is given by $\frac{\omega}{2\pi}T' \approx \frac{\hbar\omega}{16V_0}\sqrt{\frac{\hbar\omega\pi}{2V_0}}e^{\frac{2V_0}{\hbar\omega}}$. The ratio of the frequency corresponding to excited state energy splitting to the ground state energy splitting is, $\frac{\omega''}{\omega'} = \frac{4V_0}{\hbar\omega} \Rightarrow \omega'' = \frac{4V_0}{\hbar\omega}\omega'$. This clearly shows the frequency corresponding to the excited state energy splitting is slightly greater than the frequency of ground state energy splitting. For the parameters adopted above the tunneling time and the ratio of tunneling time to the period of harmonic oscillator

of the excited state energy splitting are ($T^{'} = 9.194 \times 10^{-11}s$) and $T^{'}\frac{\omega}{2\pi} = 14.64$ respectively. The calculation reveals that the tunneling time for ground state energy splitting is larger than the excited state energy splitting as it is expected. Fig.1.3 describes the time taken for a particle to change a state from its initial state to a final state and the ratio of the time $T^{'}$ during which the exchange takes place to the period of harmonic oscillator for excited state energy splitting.

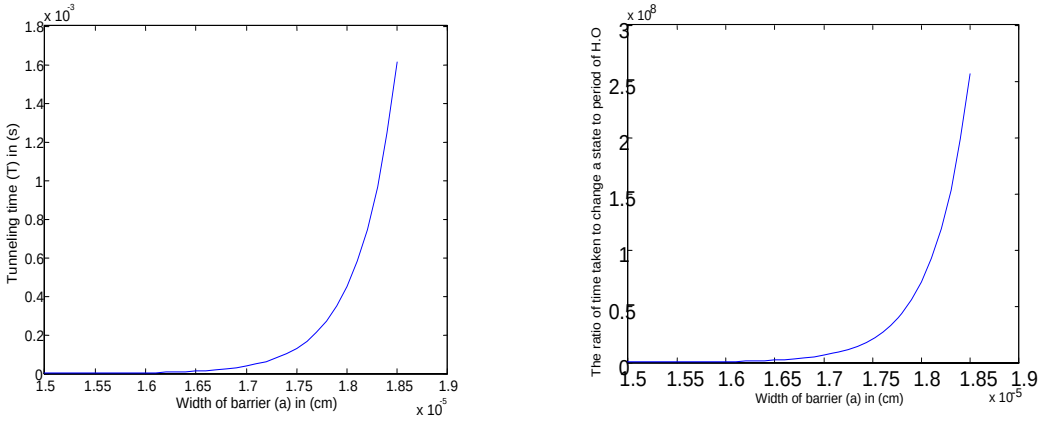

Figure 1.3: *The time taken for the system to change from its initial state to a final state and the ratio of the time during which the exchange takes place to the period of harmonic oscillator.*

1.7 Conclusion

Calculation of the frequency corresponding to the ground state energy splitting reveals that tunneling takes place in the duration of short time when the frequency is in the THz regime. Moreover the tunneling time for the excited state energy splitting is too short to that of ground state energy splitting at THz regime. As a result the

frequency corresponding to the excited state energy splitting is slightly larger than the frequency of the ground state energy splitting. This is understandable because for parabolic quantum double wells the barrier width becomes narrower for the excited state energy levels.

Chapter 2

The energy doublets in asymmetric parabolic double quantum wells

In an asymmetric double well, the low lying energy levels related to the separate wells usually do not coincide and there is no tunneling. By changing the parameters of the double well, it is possible to organize a resonant levels with equal energies. In this case, the tunneling considerably differs comparing to the tunneling between ground states of the symmetric double well. This section is devoted to an analysis of tunneling and radiation of a charged particle in a symmetric parabolic quantum double well with a constant tuned electric field that makes it asymmetrical and arranges equal energy levels in individual wells. Particularly, it is considered the case when the ground state energy in one well coincides with the first excited state energy in another well. If the typical life time of the excited state is much smaller than the tunneling time between wells, the charged particle can radiate as a result of the quantum transition from the excited state to the ground state. In the opposite case, the asymmetric DQWs can be treated as a metastable excited nanosystem regardless of that the dipole transition from the excited state to ground state is permitted. The lifetime of this metastable state can be considerably reduced by putting the double well into a

resonant cavity. The possibility of coherent radiation of an ensemble of asymmetric DQWS is discussed.

2.1 Introduction

In this chapter, we consider the tunneling of a charged particle in an asymmetric double well. Such a well can be formed by applying the gate voltage to the symmetrical double well. For the sake of simplicity, we chose a parabolic double well. By tuning the electric field it is possible to obtain coincidence of the ground state energy in one well and the first excited state energy in other well and organize quantum tunneling between these states. This tunneling differs from the tunneling between ground state levels in a symmetric double well. In the asymmetric double well under consideration the tunneling particle may execute a quantum transition from the excited state to the ground one radiating the quanta of the electromagnetic energy with the frequency much larger than the frequency of transitions between the doublet levels. Recently, an efficient THz generation within multiple quantum wells has been reported in [57]. The quantum mechanical tunneling in symmetric double quantum wells is accompanied by quantum transitions between the split levels, which is used in masers [58, 59]. The solution of the Schrödinger equation for the asymmetric double quantum wells and finding the energy level splitting to such systems are more complex than the symmetric ones.

Spontaneous emission from a two level atom tunneling in double well potential is studied recently [60]. Below we analyze the peculiarities of the tunneling.

2.2 Statement of the problem

Here, we consider a model problem. Let a particle possessing a charge e and an effective mass m^* be in the symmetric parabolic double well with an applied external constant electric field F. The Schrödinger equation for this problem is

$$-\frac{\hbar^2}{2m}\psi'' + [\frac{m^*\omega^2}{2}(|x| - a)^2 - eFx]\psi = E\psi. \tag{2.2.1}$$

Using dimensionless variable $\xi = \sqrt{\frac{m^*\omega}{\hbar}}x$, we can rewrite (2.2.1) as follows

$$\begin{cases} \psi'' + [\epsilon - 2V_L(\xi)]\psi = 0, & -\infty < \xi \leq 0, \\ \psi'' + [\epsilon - 2V_R(\xi)]\psi = 0, & 0 \leq \xi < \infty. \end{cases} \tag{2.2.2}$$

Here we introduced the potential energies of the left and right wells (see Fig 2.1)

$$\begin{cases} V_L(\xi) = \frac{1}{2}[(\xi + \xi_0 - b)^2 + b(2\xi_0 - b)], \\ V_R(\xi) = \frac{1}{2}[(\xi - \xi_0 - b)^2 - b(2\xi_0 + b)]. \end{cases} \tag{2.2.3}$$

and the denotations $\epsilon = \frac{2E}{\hbar\omega}$, $b = \frac{eF}{\hbar\omega}\sqrt{\frac{\hbar}{m^*\omega}}$, $\xi_0 = \sqrt{\frac{m^*\omega}{\hbar}}a$.

2.3 The splitting of resonant levels of parabolic DQWs with external electric field

From (2.2.3) one can see that electric field does not change the frequency of the harmonic oscillators. It changes the positions of minima of the potential wells. New positions of minima are $-\xi_L = \xi_0 - b$ and $\xi_R = \xi_0 + b$, but the distance between minima remains the same $2\xi_0$. At $\xi = 0$, the potential energy of the wells coincides $V_L(0) = V_R(0) \equiv V_0 = \frac{\xi_0^2}{2}$ as for the symmetric parabolic double well. Moreover, the

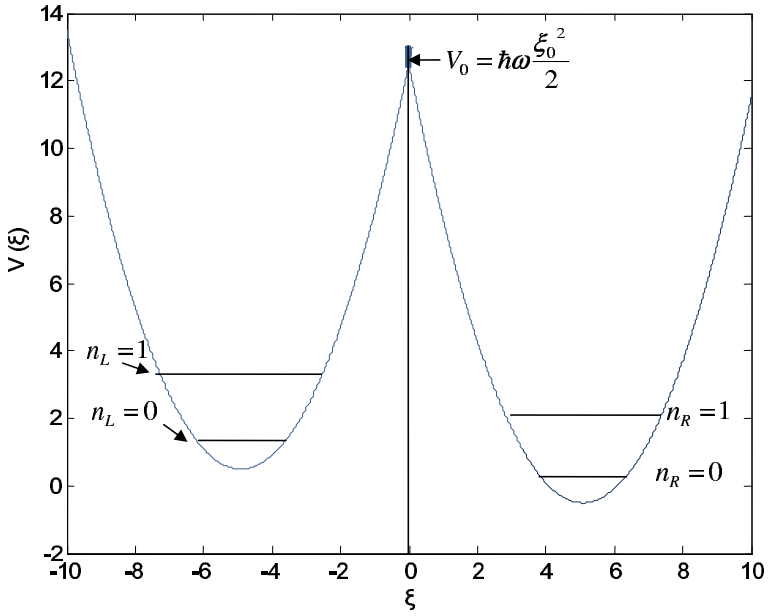

Figure 2.1: *Asymmetric double well (equation (3)). The low lying energy levels in the left and right wells (equation (4)) do not coincide at arbitrary electric field. There is no tunneling in this case.*

right well, as a whole, goes down by $\frac{b}{2}(2\xi_0 + b)$ and the left well is lifted by $\frac{b}{2}(2\xi_0 - b)$. This means that energy levels (which are equally spaced) of the left well are shifted by $2b\xi_0$ and do not coincide at arbitrary electric field as in the symmetric double well. For the far separated left and right wells $\xi_0 >> 1$, neglecting the tunneling between the wells, we obtain the following system of the low lying energy levels with wave functions localized in left and right wells:

$$\begin{cases} E_L = (n_L + \frac{1}{2}) + \frac{b}{2}(2\xi_0 - b), \\ E_R = (n_R + \frac{1}{2}) - \frac{b}{2}(2\xi_0 + b). \end{cases} \tag{2.3.1}$$

Here integers $n_L, n_R = 0, 1, ...$ cannot be large and are restricted by the inequality

$$n_L, n_R << \frac{V(0)}{\hbar\omega}. \tag{2.3.2}$$

Energy levels (2.3.1) relate to the separate left and right wells and does not coincide even at very small electric fields. Therefore, the applied electric field violates the tunneling condition. However, the tunneling between these new wells can be restored by tuning the electric field in such a way that some energy levels coincide $E_L = E_R$ (see Fig. 2.2). This resonance condition specifies the electric field, which provides the tunneling between two particular levels. For example, the tunneling between the ground state energy level of the left well and the first excited energy level of the right well is possible at $b = \frac{1}{2\xi_0}$. The necessary electric field is given by the formula

$$F = \frac{\hbar\omega}{2ea}. \tag{2.3.3}$$

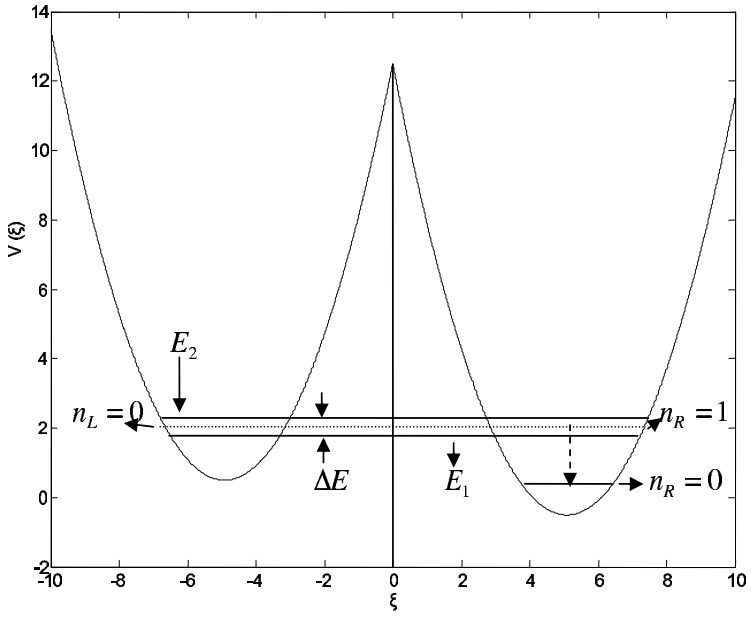

Figure 2.2: *The asymmetric double well with resonant levels: the ground state energy of the left well coincides with the first excited state of the right well. The electron captured by the left well tunneling in the right well.*

Now we calculate splitting of these coinciding levels. The normalized wave functions related to them are given by the following expressions.

$$\begin{cases} \psi_L = (\frac{1}{\pi})^{\frac{1}{4}} exp\{-\frac{1}{2}(\xi+\xi_L)^2\}, & \xi_L = -\xi_0 + \frac{1}{2\xi_0}, \\ \psi_R = (\frac{2}{\sqrt{\pi}})^{\frac{1}{2}}(\xi-\xi_R) exp\{-\frac{1}{2}(\xi-\xi_R)^2\}, & \xi_R = \xi_0 + \frac{1}{2\xi_0}. \end{cases} \tag{2.3.4}$$

The functions (2.3.4) describe levels with the same energy ground state $n_L = 0$ in the left well and the first excited state $n_R = 1$ in the right well provided that the electric field is given by (2.3.3).

The wave functions of the Schrödinger equation (2.2.1), we will seek as the linear combination of functions (2.3.4)

$$\psi = c_1\psi_L + c_2\psi_R. \tag{2.3.5}$$

It is convenient to write down the Hamiltonian of Schrödinger equation (2.2.2)

$$\hat{H}\psi = E\psi, \quad \hat{H} = -\frac{1}{2}\frac{d^2}{d\xi^2} + \begin{cases} V_L(\xi) & -\infty < \xi \le 0 \\ V_R(\xi) & 0 \le \xi < \infty \end{cases} \tag{2.3.6}$$

Multiplying the Schrödinger equation (2.3.6) by ψ_L and ψ_R according (2.3.4) and integrating over $d\xi$ we obtain a system of two linear algebraic equations.

$$\begin{cases} c_1(H_{LL} - E) + c_2(H_{LR} - sE) = 0, \\ c_1(H_{RL} - sE) + c_2(H_{RR} - E) = 0, \end{cases} \tag{2.3.7}$$

were the matrix elements of the Hamiltonian (2.3.7) with respect to wave functions (2.3.4) are

$$\begin{cases} H_{LL} = \int \psi_L \hat{H} \psi_L d\xi \\ H_{LR} = \int \psi_L \hat{H} \psi_R d\xi \\ H_{RL} = \int \psi_R \hat{H} \psi_L d\xi \\ H_{RR} = \int \psi_R \hat{H} \psi_R d\xi. \end{cases} \tag{2.3.8}$$

$$H_{LL} = \Big(\frac{1}{\sqrt{\pi}}\Big) \int_{-\infty}^{0} e^{-\frac{1}{2}(\xi+\xi_L)^2}\Big(-\frac{1}{2}\frac{d^2}{d\xi^2} + \frac{1}{2}(\xi+\xi_L)^2 + \frac{b}{2}(2\xi_0 - b)\Big)e^{-\frac{1}{2}(\xi+\xi_L)^2}d\xi + \Big(\frac{1}{\pi}\Big)^{\frac{1}{2}} \int_{0}^{\infty} e^{-\frac{1}{2}(\xi+\xi_L)^2}\Big(-\frac{1}{2}\frac{d^2}{d\xi^2} + \frac{1}{2}(\xi-\xi_L)^2 - \frac{b}{2}(2\xi_0 + b)\Big)e^{-\frac{1}{2}(\xi+\xi_L)^2}d\xi \tag{2.3.9}$$

The integral of the kinetic term of this Hamiltonian is

$$K_{LL} = \Big(-\frac{1}{2}\frac{1}{\sqrt{\pi}}\Big) \int_{-\infty}^{\infty} e^{-\frac{1}{2}(\xi+\xi_L)^2}\frac{d^2}{d\xi^2}e^{-\frac{1}{2}(\xi+\xi_L)^2}d\xi \tag{2.3.10}$$

Its solution is $K_{LL} = \frac{1}{4}$.

The integral of the potential term for $\xi_0^2 >> 1$ is

$$V_{LL} = \Big(\frac{1}{2}\frac{1}{\sqrt{\pi}}\Big) \int_{-\infty}^{\infty} (\xi+\xi_L)^2 e^{-(\xi+\xi_L)^2}d\xi + \frac{1}{\sqrt{\pi}}(\frac{b}{2}(2\xi_0 - b) \int_{-\infty}^{\infty} e^{-(\xi+\xi_L)^2}d\xi. \tag{2.3.11}$$

After some manipulation the solution of this integral is $V_{LL} = \frac{1}{4} + \frac{b}{2}(2\xi_0 - b)$.

Combining the solutions of the integral of the kinetic and potential energy terms, we obtain

$$H_{LL} = \frac{1}{2} + \frac{b}{2}(2\xi_0 - b) \tag{2.3.12}$$

$$H_{RR} = \Big(\frac{2}{\sqrt{\pi}}\Big) \int_{-\infty}^{0} (\xi-\xi_R)e^{-\frac{1}{2}(\xi-\xi_R)^2}\Big(-\frac{1}{2}\frac{d^2}{d\xi^2} + \frac{1}{2}(\xi+\xi_L)^2 + \frac{b}{2}(2\xi_0 - b)\Big)(\xi-\xi_R)e^{-\frac{1}{2}(\xi-\xi_R)^2}d\xi + \Big(\frac{2}{\pi}\Big)^{\frac{1}{2}} \int_{0}^{\infty} (\xi-\xi_R)e^{-\frac{1}{2}(\xi-\xi_R)^2}\Big(-\frac{1}{2}\frac{d^2}{d\xi^2} + \frac{1}{2}(\xi-\xi_R)^2 - \frac{b}{2}(2\xi_0 + b)\Big)(\xi-\xi_R)e^{-\frac{1}{2}(\xi-\xi_R)^2}d\xi \tag{2.3.13}$$

The integral of the kinetic term of this Hamiltonian is

$$K_{RR} = \Big(-\frac{1}{\sqrt{\pi}} \Big) \int_{-\infty}^{\infty} (\xi - \xi_R) e^{-\frac{1}{2}(\xi-\xi_R)^2} \frac{d^2}{d\xi^2} (\xi - \xi_R) e^{-\frac{1}{2}(\xi-\xi_R)^2} d\xi \tag{2.3.14}$$

Its solution is $K_{RR} = \frac{3}{2}$.

The integral of the potential term for $\xi_0^2 >> 1$ is

$$\begin{aligned} V_{RR} = \Big(\frac{1}{\sqrt{\pi}}\Big) & \\ & \int_{-\infty}^{\infty} (\xi - \xi_R)^3 e^{-(\xi-\xi_R)^2} d\xi + \frac{2}{\sqrt{\pi}} (-\frac{b}{2}(2\xi_0 + b) \int_{-\infty}^{\infty} \\ & (\xi - \xi_R)^2 e^{-(\xi-\xi_R)^2} d\xi. \end{aligned} \tag{2.3.15}$$

Its solution is $V_{RR} = -\frac{b}{2}(2\xi_0 + b)$.

H_{RR} is the sum of K_{RR} and V_{RR} and is given by

$$H_{LL} = \frac{3}{2} - \frac{b}{2}(2\xi_0 + b). \tag{2.3.16}$$

$$\begin{aligned} H_{LR} = \frac{-1}{2}\sqrt{\frac{2}{\pi}} \int_{-\infty}^{\infty} \psi_L \frac{d^2}{d\xi^2} \psi_R d\xi & \\ & + \frac{1}{2}\sqrt{\frac{2}{\pi}} \int_{-\infty}^{0} (\xi + \xi_L)^2 \psi_L \psi_R d\xi \\ & + \frac{1}{2}\sqrt{\frac{2}{\pi}} \int_{0}^{\infty} (\xi - \xi_R)^2 \psi_L \psi_R d\xi \\ & + \sqrt{\frac{2}{\pi}} \frac{b}{2} (2\xi_0 - b) \int_{-\infty}^{0} \psi_L \psi_R d\xi \\ & - \sqrt{\frac{2}{\pi}} \frac{b}{2} (2\xi_0 + b) \int_{0}^{\infty} \psi_L \psi_R d\xi, \end{aligned} \tag{2.3.17}$$

where $\psi_L \psi_R = e^{-\xi_0^2} (\xi - \xi_R) e^{-(\xi-b)^2}$.

$$K_{LR} = -\frac{1}{2}\sqrt{\frac{2}{\pi}} \int_{-\infty}^{\infty} \psi_L \frac{d^2}{d\xi^2} \psi_R d\xi. \tag{2.3.18}$$

Using integration by parts,

$$K_{LR} = \frac{1}{\sqrt{2\pi}} \int_{-\infty}^{\infty} \frac{d\psi_R}{d\xi} \frac{d\psi_L}{d\xi} d\xi = \frac{1}{\sqrt{2\pi}} e^{-\xi_0^2} \int_{-\infty}^{\infty} (\xi + \xi_L)(\xi - \xi_R)^2 e^{-(\xi-b)^2} d\xi \quad (2.3.19)$$

, and solving this integral we obtain

$$K_{LR} = \frac{1}{\sqrt{2}} e^{-\xi_0^2} \Big(\frac{3b}{2} + b^2 - \frac{\xi_0}{2} - \xi_0 b^2 - b\xi_0^2 + \xi_0^3 \Big) \quad (2.3.20)$$

For $\xi_0^2 >> 1$, taking only the leading terms

$$K_{LR} = K_{RL} = \frac{1}{\sqrt{2}} e^{-\xi_0^2} \Big(\xi_0^3 - \frac{\xi_0}{2} \Big) \quad (2.3.21)$$

The potential part of the Hamiltonian is

$$\begin{aligned} V_{LR} = \frac{1}{\sqrt{2\pi}} \int_{-\infty}^{0} (\xi + \xi_L)^2 \psi_L \psi_R d\xi & \\ + \frac{1}{\sqrt{2\pi}} \int_{0}^{\infty} (\xi - \xi_R)^2 \psi_L \psi_R d\xi & \\ + \frac{b}{2}(2\xi_0 - b) \sqrt{\frac{2}{\pi}} \int_{-\infty}^{0} \psi_L \psi_R d\xi & \\ - \frac{b}{2}(2\xi_0 + b) \sqrt{\frac{2}{\pi}} \int_{0}^{\infty} \psi_L \psi_R d\xi & \quad (2.3.22) \end{aligned}$$

Solving the integral and only taking the leading terms,

$$V_{LR} = V_{RL} = \frac{1}{\sqrt{2}} e^{-\xi_0^2} \Big(- \frac{\xi_0}{2} - \xi_0^3 \Big) \quad (2.3.23)$$

The Hamiltonian (H_{LR}) is both the sum of potential and kinetic energy terms and given by

$$H_{LR} = H_{RL} = -\frac{\xi_0}{\sqrt{2}} e^{-\xi_0^2}. \quad (2.3.24)$$

Finally, the matrix elements of the Hamiltonian (2.2.2) and the overlapping integral

are given by

$$\begin{cases} H_{LL} = \frac{1}{2} + \frac{b}{2}(2\xi_0 - b) = 1 - \frac{1}{8\xi_0^2}, \\ H_{RR} == \frac{3}{2} - \frac{b}{2}(2\xi_0 + b) = 1 - \frac{1}{8\xi_0^2}, \\ H_{LR} = H_{RL} = -\frac{\xi_0}{\sqrt{2}} exp\{-\xi_0^2\}, \\ s = \int \psi_L \psi_R d\xi = -\sqrt{2}\xi_0 e^{-\xi_0^2}.. \end{cases} \tag{2.3.25}$$

In formulas (2.3.25), we used the "tuned" electric field $b = \frac{1}{2\xi_0}$. The solution of these system can be determined by equating the determinant to zero. As it was already discussed in chapter (1) the nontrivial solution of (2.3.7) is obtained from the condition of vanishing determinant of system (2.3.7). Acting similarly as it was solved for the ground and excited state of the symmetric double quantum well in the previous chapters, we obtain the energies of the doublet of the asymmetric double well with resonance condition $b = \frac{1}{2\xi_0}$

$$E_{1,2} = \hbar\omega\Big(1 - \frac{1}{8\xi_0^2} \mp \frac{\xi_0}{\sqrt{2}} exp\{-\xi_0^2\}\Big). \tag{2.3.26}$$

The energy splitting of the coinciding levels due to an appropriate applied constant electric field is

$$\Delta E = E_2 - E_1 = 2\hbar\omega\sqrt{\frac{V_0}{\hbar\omega}} exp\Big\{ - \frac{2V_0}{\hbar\omega}\Big\}. \tag{2.3.27}$$

This result shows that splitting of the resonant levels $\Delta E/\hbar\omega \sim exp(-\xi_0^2)$ is exponentially small. It is interesting to compare this result with the splitting of the ground state level of the symmetric harmonic double well obtained by the different method in [55, 56]. A comparison gives $\Delta E/\Delta E_0 = \sqrt{\pi/2} \simeq 1.25$. The splitting (1.3.17) can be obtained acting in same manner as above with the Hamiltonian of the symmetric double well (no external electric field). This can be considered as a confirmation of the result (2.3.27) obtained with the help of the known wave functions of "far" separated wells.

2.3.1 Tunneling and radiation in asymmetric DQWs with resonant levels

In this section we show an analysis of tunneling and radiation of a charged particle in a symmetric parabolic quantum double well with a constant tuned electric field that makes the potential well asymmetric and arranges resonant levels with equal energy in individual wells. The case when the ground state energy in one well coincides with the first excited state energy in another well is considered. The splitting of these resonant levels and the tunneling time are calculated. If the typical life time of the excited state is much greater than the tunneling time, the asymmetric double well can be treated as a metastable excited nanosystem regardless that the dipole transition from the excited state to ground state is permitted. The lifetime of this metastable state can be considerably reduced by putting it in to a resonant cavity. The possibility of coherent radiation of an ensemble of asymmetric quantum double well is discussed.

The time dependent wave functions, which describe the above obtained doublet (2.3.27), may be written in the form

$$\psi(\xi,t)=\frac{1}{\sqrt{2}}\Big[e^{-\frac{i}{\hbar}E_1t}\psi_1(\xi)+e^{-\frac{i}{\hbar}E_2t}\psi_2(\xi)\Big], \tag{2.3.28}$$

where E_1 and E_2 are the lower and upper energies of the doublet, ψ_1 and ψ_2 are the wave functions of these energy levels . It is known that wave function (2.3.28)can be rewritten as [55],

$$\psi(\xi,t)=e^{-\frac{i(E_1+E_2)t}{2\hbar}}\Big[\psi_L(\xi)cos\frac{\Delta E}{2\hbar}t\pm i\psi_R(\xi)sin\frac{\Delta E}{2\hbar}t\Big], \tag{2.3.29}$$

where ΔE is the splitting given by (2.3.27). This writing shows that the charged particle in the asymmetric double well oscillates back and forth between the resonant

states ψ_L and ψ_R with a frequency $\omega = \Delta E/2\hbar$ in the left and right wells, respectively. This oscillatory "motion" can also be considered as a quantum mechanical tunneling. The frequency corresponding to asymmetric energy doublet is $\omega'' = 2\omega\sqrt{\frac{V_0}{\hbar\omega}}e^{\frac{-2V_0}{\hbar\omega}}$. For the system to change from its initial state say (right well) to final state (left well); it takes a time $T'' \approx \frac{\pi}{2\omega}\sqrt{\frac{\hbar\omega}{2V_0}}e^{\frac{2V_0}{\hbar\omega}}$. Moreover, the ratio of the time T'' during which the exchange takes place to the period of harmonic oscillator is given by $\frac{\omega}{2\pi}T'' \approx \frac{1}{4}\sqrt{\frac{\hbar\omega}{V_0}}e^{\frac{2V_0}{\hbar\omega}}$. For the parameters adopted above the tunneling time and the ratio of tunneling time to the period of harmonic oscillator of an asymmetric energy doublet are ($T'' = 1.048 \times 10^{-9}s$) and $T''\frac{\omega}{2\pi} = 166.8$ respectively. This clearly shows the tunneling time for asymmetric energy doublet is approximately comparable to the ground state energy splitting.

Now it would be relevant to discuss how to realize the state of the asymmetric double well with the tunneling electron. Let us consider the symmetric double well that obtained if the electric field in (2.2.1) is set to be zero. The ground state of this problem is the energy doublet (1.3.17) with the electron tunneling between the wells. If we switch on a very weak but finite electric field, the resonance of the ground state levels will be violated. The exponentially small splitting disappears. The level in the left well will be slightly higher and the level in the right well will be slightly lower comparing with the ground state energy at $F = 0$. The electron is captured by the left or the right well with a probability 1/2. Increasing the electric field up to the value (2.3.3), we meet the resonance condition of the ground state level in the left well and the first excited state in the right well. If the electron was in the left well, it will be in the tunneling regime. If it was in the right well, it will stay on the ground state level. The probability of realization of these states is 1/2. If we have an

ensemble of $N \gg 1$, half of them will be in the tunneling regime and can be treated as excited states. Below we deal with this states.

The typical time of this motion is $\tau_t = 4\pi\hbar/(\Delta E)$. With the help of (2.3.27), we get

$$\tau_t = \frac{2^{3/2}\pi}{\omega}\sqrt{\frac{\hbar\omega}{2V_0}}exp\Big\{\frac{2V_0}{\hbar\omega}\Big\} \tag{2.3.30}$$

Relation (2.3.30) allows one to evaluate how much time the particle spends in one of the wells. The particle "sitting" in the right well may return back to the left well but it may also perform a spontaneous quantum transition to the ground state of the right quantum well with radiation of a quant $\hbar\omega$ (see Fig.2.3). Such a transition occurs if the average life time of the first state of harmonic oscillator is much less then τ_t. The average life time of the first state of a harmonic oscillator is known [61]

$$\tau = \frac{3c^3\hbar}{4\omega^3 d_{10}^2}, \tag{2.3.31}$$

where the $d_{10} = e\sqrt{\frac{\hbar}{m^*\omega}}$ is the matrix element of dipole transition of the harmonic oscillator. Keeping in mind that $1/\tau_t$ and $1/\tau$ are the probabilities per unit time of tunneling and spontaneous radiation, respectively, we introduce the probability of tunneling

$$w_t = \frac{1/\tau_t}{1/\tau_t + 1/\tau} \tag{2.3.32}$$

and the probability of spontaneous radiation

$$w_r = \frac{1/\tau}{1/\tau_t + 1/\tau}. \tag{2.3.33}$$

The spontaneous radiation of the asymmetric parabolic double well takes place if $w_r \gg w_t$ or the following inequality holds true $\tau_t \gg \tau$. It is convenient to present the last inequality in the form

$$\sqrt{\frac{\hbar\omega}{2V_0}}exp\Big\{\frac{2V_0}{\hbar\omega}\Big\} \gg \frac{3}{8\sqrt{2}\pi}\frac{c^3 m^*}{e^2\omega}. \tag{2.3.34}$$

To solve the above inequality, it would be convenient to introduce $\omega = \omega_0 \times 10^{13}$ Hz and $a = a_0 \times 10^{-6}$ cm. This means that we measure the frequency in 10 THz and the length in 10 nm. Substituting the numerical values of the physical constants and value of the typical effective mass of electron $m^* = 0.1m_e$ (m_e is the mass of a free electron) as for GaAs, we obtain the simplified inequality

$$exp[x - 16.12] \gg \sqrt{x}, \tag{2.3.35}$$

where $x = \omega_0 \times a_0^2$. It satisfies with $x \geq 20$ and allows us to find the frequency ω for a given a or vice versa. For example, exploiting the terra Hz frequency range, we obtain that for 10 THz, $a \approx 45$ nm and for 1 THz, $a \approx 140$ nm. We can see that realization of the above proposed mechanism of radiation of the resonant levels requires the nanoscale DQWs.

With the help of (2.2.1) and above obtained ω and a one can estimate the gate voltage U and corresponding strength of the electric field F required for formation of the resonant levels in the DQWs. The results read: for 10 THz, $a \approx 45$ nm, $U = 3.28 \times 10^{-3}$ V and $F = 729$ V/cm; for 1THz, $a \approx 140$ nm, $U = 3.28 \times 10^{-4}$ V and $F = 23.4$ V/cm. These fields can be easily obtained in laboratory. It is necessary to remember that formation of the resonant levels requires the fine tuning of the gate voltage.

On the basis of the above reported, we can claim that the asymmetric quantum double well with resonant levels: the ground state in one well and the excited one in other well may be a source of spontaneous radiation in a THz frequency range. After emission of the quantum $\hbar\omega$ from the right well, the electron stays in the ground state of the right well. If we change the direction of the electric field, the system will be again in the excited state during the time $\sim \tau$.

Now we consider the case when inequality (2.3.34) is reversed. In the THz frequency range for the accepted model it requires that a distance a between the wells be smaller than (45 nm for $\omega = 10^{13}$/s and 140 nm for $\omega = 10^{12}$/s). In this case, the electron "tunnels" between the wells so fast that it has no time to make a quantum transition in the right well from the first excited state to the ground state. In other words, the system will be in the excited state with the electron tunneling between the wells. We consider this state as a metastable nanosystem.

It is possible to force the system to emit the quantum $\hbar\omega$ if we put the asymmetric quantum double well into a resonator with the electromagnetic radiation. In this case the life time of the excited state radiation decreases and may be written in the form [61]

$$\tau_{st} = \tau_r \frac{\rho_0(\omega)}{\rho_0(\omega) + \rho(\omega)}, \tag{2.3.36}$$

where τ_{st} is a typical time of the stimulated emission, $\rho_0(\omega) = \hbar\omega^3/(\pi^2 c^3)$ and $\rho(\omega)$ is a density of the external radiation of a frequency $\hbar\omega$. It is seen from (2.3.36) that at $\rho(\omega) \gg \rho_0(\omega)$, the life time of the system with respect to stimulated radiation τ_{st} can be made much smaller than the tunneling time τ_t (2.3.30).

It is necessary to note that a low lying energy levels of a harmonic oscillator are equidistant with spacing $\hbar\omega$. The splitting of resonant levels, which depend on a number of a level, violets this equidistance. However, the other models of asymmetrical quantum double wells (for example, rectangular quantum double well with a gate voltage) do not poses the equidistant resonant levels and the problem of reabsorption will be removed.

The possibility of the generation of the THz radiation in resonant tunneling structures with several quantum wells was discussed in [62]. Moreover, it is claimed in [63]

that the combined effects of the static electric field and the THz coherent radiation field can be useful in designing new optoelectronic devices.

2.3.2 Conclusion

In this paper, we obtained the condition of formation of the resonant levels for a model a charged particle in a parabolic quantum double well with an applied electric field. The tuned electric field provides the coincidence of the energies of the ground state in one well with the energy of the first excited state in another well.

The account of degeneracy of the quantum states in the wells results in the splitting of the two-fold degenerate level and in the tunneling of the particle between the wells. The typical time of tunneling τ_t or the time being in one of the wells is calculated. But unlike the tunneling of the particle in the ground state of a symmetric parabolic quantum well now it may execute also a spontaneous quantum transition from the excited state of the well with radiation of a quantum $\hbar\omega$ provided that τ_t is much larger than the typical life time of the excited state τ. In the opposite case $\tau_t \ll t$, the asymmetric quantum double well under consideration may be treated as an metastable nanosystem.

The radiation time τ_{st} of the asymmetric quantum double well with parameters $\tau_t \ll \tau$ placed into a resonator of the frequency ω may be made smaller than τ. At large enough density of the stimulated radiation it is possible to get $\tau_{st} \ll \tau_t$. This means that the metastable state of the nanosystem can be transformed in the dipole radiating state.

Chapter 3

Optical absorption coefficients and refractive index in parabolic asymmetric double quantum wells

The change in optical absorption coefficients and refractive index in GaAs/AlGaAs parabolic double quantum wells (DQWs) with applied electric field are studied in detail. Analytical expressions for the linear and nonlinear intersubband absorption coefficients and refractive index changes are obtained by using compact density matrix approach. Moreover, the calculated results show the incident optical intensity, the frequencies of the confined potentials of the parabolic DQWs, the magnitude of transition dipole moment and the applied electric field greatly change the absorption coefficient and the refractive index of the system.

3.1 Introduction

In the past few years, theoretical analysis on changes in the absorption and refractive index for intersubband optical transitions in single quantum wells, and semi parabolic quantum well structures have been reported [64-66]. Linear changes in the absorption

coefficients and refractive index in parabolic quantum well was discussed by S.L. Chung and D. Ahn [67]. However according to our knowledge these optical properties in parabolic DQWs were not studied in detail.

Asymmetric DQWs are used to the design of THz devices because their energies can be tuned so that the intersubband transitions in the conduction band lie in the THz range. In addition to that, the value of these transitions can be tailored by changing the geometry of the well and also by introducing a constant electric field in the growth direction of the layers.

We discuss the intersubband nonlinear absorption and refraction of asymmetric DQWs designed for the THz range. The dependence of absorption on various parameters of the DQWs is studied. In particular different confinement frequencies and intensities are considered. The linear and third order nonlinear absorption coefficients are obtained by using perturbative calculation of the linear and third order nonlinear susceptibility within density matrix approach. The intersubband linear and nonlinear absorption coefficients and refraction index of an asymmetric DQWs can be changed by the strength of resonant electric field which controls the asymmetry in the structure and the width of the barrier between the wells that controls the coupling.

In this chapter the change in linear and nonlinear absorption coefficients and refractive index changes are being studied theoretically in parabolic DQWs in the presence of electric field. This chapter is organized as follows: in section 3.2 the analytical expressions of the three lowest transitions coming from the ground and excited state of the right well and the ground state of the left well at resonance condition are studied. Moreover the transition dipole moments for these three lowest transitions among the energy levels are described. The optical absorption coefficients and the

change in refractive index for conduction intrsubband transitions are presented in section 3.3. Numerical calculations and detailed discussions for a typical GaAs/AlGaAs DQWs are given in section 3.4. Finally a brief summary is given in section 3.5.

3.2 Statement of the problem

As it was briefly discussed in chapter 2 the energy doublets of asymmetric DQWS due to tunneling at resonant condition are given by 2.3.26. The energy splitting of the coinciding levels due to an appropriate applied constant electric field is also described in 2.3.27. At resonance condition, when the small probability of tunneling is taken into account the energy level E splits into two levels E_1 and E_2. The three lowest transitions are demonstrated in Fig 3.1 with transition energy of

$$\begin{cases} \Delta E_{01} = \hbar\omega_0\Big(1 - \sqrt{\frac{V_0}{\hbar\omega_0}}exp\{-\frac{2V_0}{\hbar\omega_0}\}\Big), \\ \Delta E_{02} = \hbar\omega_0\Big(1 + \sqrt{\frac{V_0}{\hbar\omega_0}}exp\{-\frac{2V_0}{\hbar\omega_0}\}\Big), \\ \Delta E_{21} = 2\hbar\omega_0\sqrt{\frac{V_0}{\hbar\omega_0}}exp\Big\{-\frac{2V_0}{\hbar\omega_0}\Big\}. \end{cases} \tag{3.2.1}$$

The linear and nonlinear intersubband optical properties of asymmetric DQWs depend on the transition dipole matrix element between the relevant quantized states. The dipole moment operator is $\hat{\mu} = -e\hat{x}$, and the transition dipole moment between the two different energy levels i and j with $(i = 0, 1)$ and $(j = 1, 2)$ is given by $\mu_{ij} = \langle\psi_L(E_i)| - e\hat{x}|\psi_R(E_j)\rangle$, where $(i \neq j)$. Solving for this matrix element yields the result,

$$\begin{cases} \mu_{01} = -e\sqrt{\frac{\hbar}{m^*\omega_0}}\Big(\frac{1}{2} + \frac{\xi_0}{\sqrt{2}}exp\{-b^2\}\Big), \\ \mu_{02} = -e\sqrt{\frac{\hbar}{m^*\omega_0}}\Big(-\frac{1}{2} + \frac{\xi_0}{\sqrt{2}}exp\{-b^2\}\Big), \\ \mu_{12} = eb\sqrt{\frac{\hbar}{m^*\omega_0}} = \frac{e\hbar}{2m^*\omega_0 a} = \frac{e}{2\xi_0}\sqrt{\frac{\hbar}{m^*\omega_0}}. \end{cases} \tag{3.2.2}$$

where e the charge of electron and m^* the effective mass of the particle.

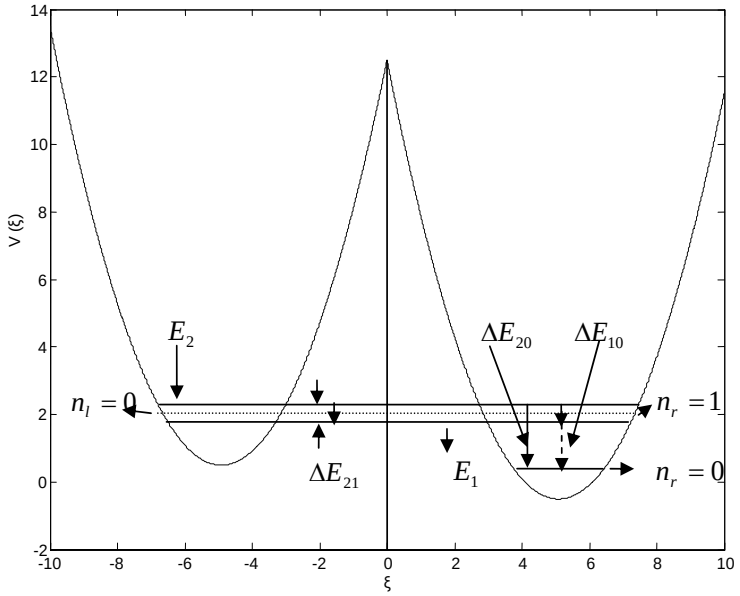

Figure 3.1: *Potential profile of parabolic DQWs with constant electric field for possible transitions at resonance condition .*

3.3 The refractive index and absorption coefficient

Employing the density matrix approach and the iterative procedure the absorption coefficients and index of refraction are calculated based on the first order $\chi^{(1)}$ and third order $\chi^{(3)}$ optical susceptibilities. The system is excited by the electric field $\tilde{\varepsilon}(t) = \varepsilon e^{i\omega t}$. The Hamiltonian $\hat{H}$ is decomposed in to two parts, the unperturbed Hamiltonian $\hat{H}_0$ for one electron in the quantum well and the time dependent interaction potential $\hat{V}(t)$ representing the perturbation.

$$\hat{H} = \hat{H}_0 + \hat{V}(t) \tag{3.3.1}$$

where $\hat{V}(t) = -\hat{\mu}.\tilde{\varepsilon}(t)$.

The density matrix is defined as

$$\hat{\rho} = |\psi\rangle\langle\psi|. \tag{3.3.2}$$

Including the phenomenological damping terms the time evolution for the density matrix is

$$\dot{\rho}_{nm} = \frac{-i}{\hbar}[\hat{H}, \hat{\rho}]_{nm} - \gamma_{nm}(\rho_{nm} - \rho_{nm}^{eq}), \tag{3.3.3}$$

where $\dot{\rho}_{nm}$ is the nm element of $\dot{\rho}$, ρ_{nm}^{eq} is the equilibrium value of ρ_{nm}, and γ_{nm} is the decay rate of ρ_{nm}. The perturbation solution of this equation is found in [68-70]. The electric polarization of the quantum system due to $\tilde{E}(t)$ can be expressed as,

$$\vec{P}(t) \approx \epsilon_0\chi^{(1)}(\omega)\varepsilon(i\omega t) + \epsilon_0\chi^{(3)}(\omega)\varepsilon(i\omega t), \tag{3.3.4}$$

where $\chi^{(1)}$ and $\chi^{(3)}$ are the linear and third-order nonlinear susceptibilities respectively. Analytical expressions of the linear and nonlinear susceptibilities for a two level quantum system are given as follows [71-73]. For the linear term,

$$\epsilon_0\chi^{(1)}(\omega) = \frac{N|\mu_{ij}|^2}{\Delta E_{ij} - \hbar\omega - i\hbar\gamma_{ij}}. \tag{3.3.5}$$

For the third-order term,

$$\epsilon_0\chi^{(3)}(\omega) = \frac{N|\mu_{ij}|^2|E|^2}{\Delta E_{ij} - \hbar\omega - i\hbar\gamma_{ij}}\Big[\frac{4|\mu_{ij}|^2}{(E_{ij} - \hbar\omega)^2 + (\hbar\omega)^2} - \frac{(\mu_{jj} - \mu_{ii})^2}{(\Delta E_{ij} - i\hbar\gamma_{ij})(\Delta E_{ij} - \hbar\omega - i\hbar\gamma_{ij})}\Big]. \tag{3.3.6}$$

where N is the number of carriers per unit surface. The change in refractive index is related to the susceptibility

$$\frac{\Delta n(\omega)}{n_r} = Re\frac{\chi(\omega)}{2n_r^2}, \tag{3.3.7}$$

where n_r is the refractive index.

By using equations (3.3.5)-(3.3.7),

$$\frac{\Delta n^{(1)}(\omega)}{n_r} = \frac{N|\mu_{ij}|^2}{2n_r^2\epsilon_0}\Big[\frac{\Delta E_{ij}-\hbar\omega}{(\Delta E_{ij}-\hbar\omega)^2+(\hbar\gamma_{ij})^2}\Big], \tag{3.3.8}$$

$$\begin{aligned}\frac{\Delta n^{(3)}(\omega)}{n_r} = \\ -\frac{\mu}{4n_r^3\epsilon_0}|\mu_{ij}|^2\frac{NI}{[(\Delta E_{ij}-\hbar\omega)^2+(\hbar\gamma_{ij})^2]^2} \\ \times\Big[4(\Delta E_{ij}-\hbar\omega)|\mu_{ij}|^2-\frac{(\mu_{jj}-\mu_{ii})^2}{(\Delta E_{ij})^2+(\hbar\gamma_{ij})^2}\{(\Delta E_{ij}-\hbar\omega) \\ \times[\Delta E_{ij}(\Delta E_{ij}-\hbar\omega)-(\hbar\gamma_{ij})^2]-(\hbar\gamma_{ij})^2(2\Delta E_{ij}-\hbar\omega)\}\Big],\end{aligned} \tag{3.3.9}$$

where $\Delta E_{ij} = E_j - E_i$ is the energy interval of two different electronic states, μ_{ij} is the dipole matrix element, μ permeability of the system and c is the speed of light in vacuum. I is the incident optical intensity and defined as,

$I = \frac{2n_r}{\mu c}|\varepsilon(\omega)|^2$.

The total refractive index change is written as,

$$\frac{\Delta n(\omega)}{n_r} = \frac{\Delta n^{(1)}(\omega)}{n_r} + \frac{\Delta n^{(3)}(\omega)}{n_r}. \tag{3.3.10}$$

Moreover, the absorption coefficient $\beta(\omega)$ is related to the susceptibility by,

$$\beta^1(\omega) = \frac{\omega}{n_r}\sqrt{\frac{\mu}{\epsilon_0}}\frac{|\mu_{ij}|^2N\hbar\gamma_{ij}}{(\Delta E_{ij}-\hbar\omega)^2+(\hbar\gamma_{ij})^2}. \tag{3.3.11}$$

$$\begin{aligned}\beta^3(\omega,I) = -\Big(\frac{I\omega}{\epsilon_0^2n_r^2c^2}\Big) \\ \times\frac{|\mu_{ij}|^2N\hbar\gamma_{ij}}{[(\Delta E_{ij}-\hbar\omega)^2+(\hbar\gamma_{ij})^2]^2} \\ \times\Big[4|\mu_{ij}|^2-\frac{|\mu_{jj}-\mu_{ii}|^2[\Delta E_{ij}^2+2\Delta E_{ij}\hbar\gamma_{ij}-\hbar\omega(\Delta E_{ij}+\hbar\gamma_{ij})-\hbar^2\gamma_{ij}^2]}{\Delta E_{ij}^2-(\hbar\gamma_{ij})^2}\Big].\end{aligned} \tag{3.3.12}$$

And the total absorption coefficient is,

$$\beta(\omega,I) = \beta^1(\omega) + \beta^3(\omega,I). \tag{3.3.13}$$

3.4 Results and discussions

In this section the change in refractive index and the absorption coefficients of three lowest transitions are calculated numerically for GaAs/AlGaAs parabolic DQWs with applied constant electric field at resonance condition. The parameters adopted in this calculation are: the phenomenological damping constant $\gamma_{ij} = 5 \times 10^{11}/s$, $N = 1.0\times10^{22}m^{-3}$, the confinement frequency of the system (ω_0=1 THz, 2 THz and 3THz), the constant electric field with respect to the above frequencies, ($\varepsilon = 2060\frac{V}{cm}$, $\varepsilon = 4121.2\frac{V}{cm}$ and $\varepsilon = 6181.9\frac{V}{cm}$), the transition energies and dipole moments for ω_0 =1 THz are ($\Delta E_{12} = 3.9052\times10^{-22}$J, $\Delta E_{01} = 4.6414\times10^{-22}$J, $\Delta E_{02} = 8.5466\times10^{-22}$J, $\mu_{12} = 2.2157\times10^{-27}$c-m, $\mu_{01} = -1.3314\times10^{-27}$c-m and $\mu_{02} = 1.3314\times10^{-27}$c-m); for ω_0 =2 THz are ($\Delta E_{12} = 7.6982\times10^{-22}$J, $\Delta E_{01} = 9.3389\times10^{-22}$J, $\Delta E_{02} = 1.7037\times10^{-21}$J), $\mu_{12} = 1.1079\times10^{-27}$c-m, $\mu_{01} = -9.4143\times10^{-28}$c-m and $\mu_{02} = 9.4143\times10^{-28}$c-m); and for ω_0 =3 THz are ($\Delta E_{12} = 9.8565\times10^{-22}$J, $\Delta E_{01} = 1.4854\times10^{-21}$J, $\Delta E_{02} = 2.471\times10^{-21}$J, $\mu_{12} = 7.3858\times10^{-28}$c-m, $\mu_{01} = -7.6868\times10^{-28}$c-m and $\mu_{02} = 7.6868\times10^{-28}$c-m), $m^* = 0.1m_0$ (m_0 is the free electron mass), the oscillation distance between the wells $a = 10nm$, the potential barrier ($V_0 = \frac{1}{2}m^*\omega_0^2a^2$) where ω_0 is the confinement frequency, the intensity ($I = 7.1893\times10^4W/cm^2$, $I = 2.8757\times10^5W/cm^2$ and $I = 6.4704\times10^5W/cm^2$) for the above frequencies respectively and the medium index of refraction $n_r = 3.2$.

In Fig. 3.2, the change in linear index of refraction $\frac{\Delta n^{(1)}(\omega)}{n_r}$, the change in third order index of refraction $\frac{\Delta n^{(3)}(\omega)}{n_r}$ and the total change in index of refraction $\frac{\Delta n(\omega)}{n_r}$ are plotted as a function of radiation energy for an incident optical intensity $I = 7.1893\times10^4W/cm^2$, confinement frequency ω_0=1 THz, change in transition energy $\Delta E_{12} = 3.9052\times10^{-22}$J and the transition dipole moment $\mu_{12} = 2.2157\times10^{-27}$c-m.

It can be observed that $n^{(1)}(\omega)$ and $n^{(3)}(\omega)$ as a function of $\hbar\omega$ are opposite in sign and this behavior dominates the magnitude of the total change in index of refraction greatly. For this transition the third order nonlinear refractive index has a very large variation and is dominant over the linear refractive index as shown in Fig 3.2. This greatly altered both the magnitude and sign of the total refractive index change.

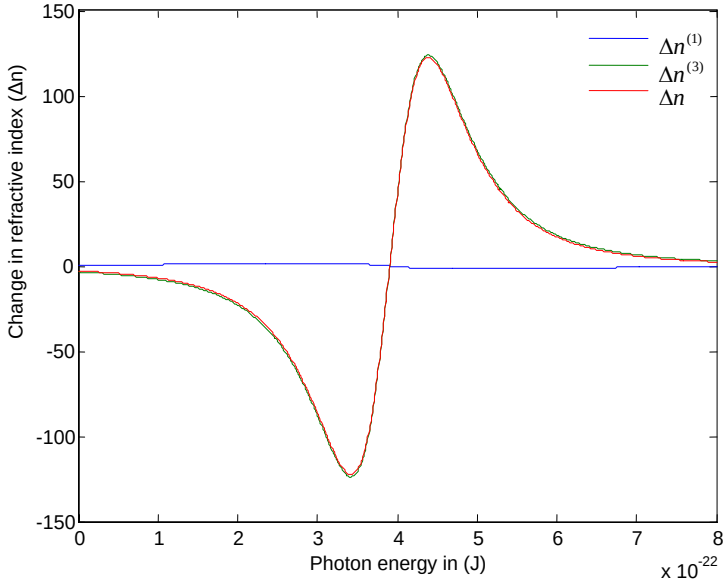

Figure 3.2: *The change in linear and third order nonlinear index of refraction versus photon energy with transition frequency*($\omega_{12} = \frac{\Delta E_{12}}{\hbar} = 9.387 \times 10^{12}/s$) .

In Fig 3.3 the change in linear index of refraction $\frac{\Delta n^{(1)}(\omega)}{n_r}$, the change in third order index of refraction $\frac{\Delta n^{(3)}(\omega)}{n_r}$ and the total change in index of refraction $\frac{\Delta n(\omega)}{n_r}$ are shown as a function of radiation energy for an incident optical intensity $I = 7.1893 \times 10^4 W/cm^2$, confinement frequency ω_0=1 THz, change in energy $\Delta E_{01} = 4.6414 \times 10^{-22}$J and the transition dipole moment $\mu_{01} = -1.3314 \times 10^{-27}$c-m. Similarly for this transition the total change in index of refraction is largely depend on large

magnitude of the change in third order index of refraction as shown in Fig 3.3. More over the total change in index of refraction for this transition is smaller than the transition explained in Fig 3.3. This is due to large magnitude of a transition dipole moment between the split states.

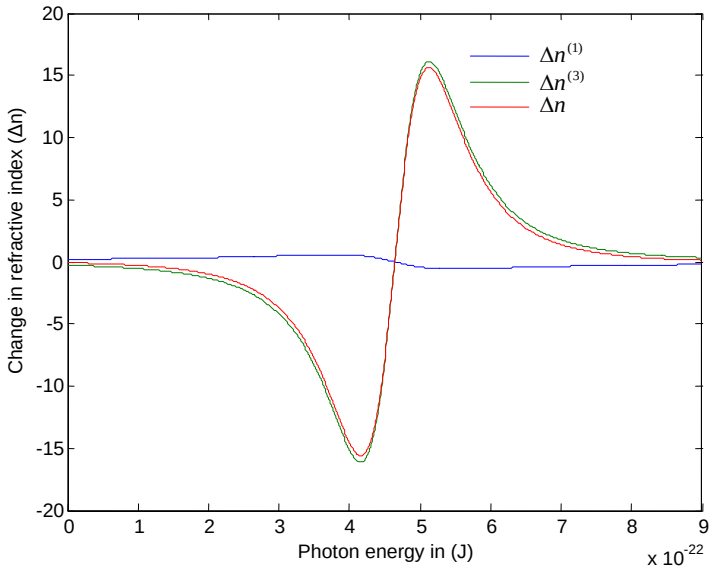

Figure 3.3: *The change in linear and third order nonlinear index of refraction versus photon energy with transition frequency*($\omega_{01} = \frac{\Delta E_{01}}{\hbar} = 1.4146 \times 10^{13}/s$)

Similarly in Fig 3.4 the change in linear index of refraction $\frac{\Delta n^{(1)}(\omega)}{n_r}$, the change in third order index of refraction $\frac{\Delta n^{(3)}(\omega)}{n_r}$ and the total change in index of refraction $\frac{\Delta n(\omega)}{n_r}$ are plotted as a function of radiation energy for an incident optical intensity $I = 7.1893 \times 10^4 W/cm^2$, confinement frequency ω_0=1 THz, change in energy $\Delta E_{02} = 8.5466 \times 10^{-22}$J and the transition dipole moment $\mu_{02} = 1.3314 \times 10^{-27}$c-m. This transition is almost the same as the transition described in Fig. 3.3 due to the same magnitude of a transition dipole moment.

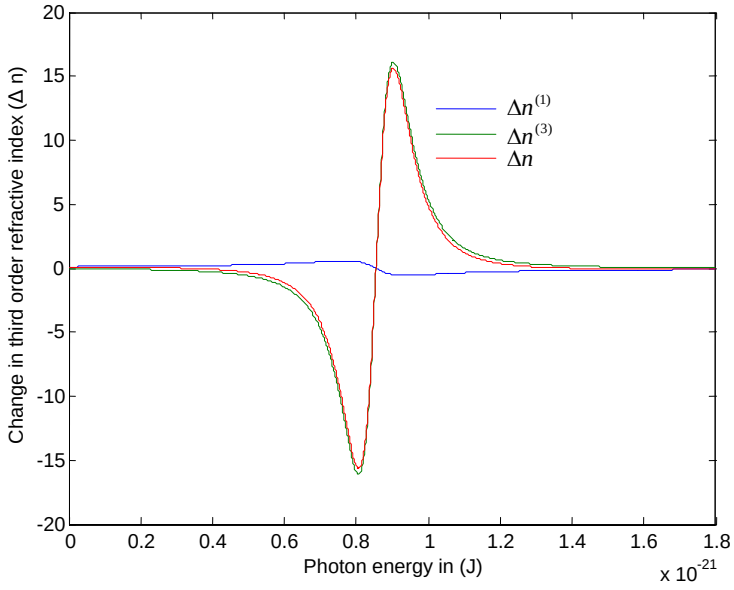

Figure 3.4: *The change in linear and third order nonlinear index of refraction versus photon energy with transition frequency*($\omega_{02} = \frac{\Delta E_{02}}{\hbar} = 2.3534 \times 10^{13}/s$)

In Fig. 3.5, the change in linear absorption coefficient $\Delta\beta^{(1)}(\omega)$, the change in third order nonlinear absorption coefficient $\Delta\beta^{(3)}(\omega)$ and the total absorption coefficient $\Delta\beta(\omega)$ are plotted as a function of photon energy for an incident optical intensity $I = 7.1893 \times 10^4 W/cm^2$, confinement frequency ω_0=1 THz, change in energy $\Delta E_{12} = 3.9052 \times 10^{-22}$J and the transition dipole moment $\mu_{12} = 2.215 \times 10^{-27}$c-m. It can be observed that $\beta^{(1)}(\omega)$ and $\beta^{(3)}(\omega)$ as a function $\hbar\omega$ have a peak at the same position due to the one photon resonance enhancement. Moreover linear change in absorption coefficient produced by the imaginary part of $\chi^{(1)}$ is opposite in sign to the nonlinear change produced by the third order nonlinear susceptibility. The third order nonlinear absorption coefficient at this frequency is three order larger than the linear absorption coefficient. The total absorption coefficient is comparable to the third order nonlinear

absorption coefficient. Aa a result the total change in absorption coefficient is large in magnitude and negative in sign.

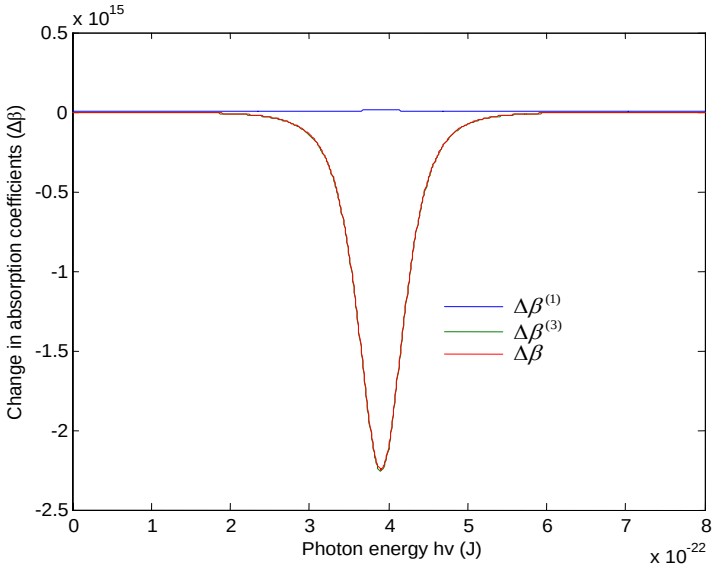

Figure 3.5: *The change in linear, third order nonlinear and total absorption coefficient versus photon energy with transition frequency*($\omega_{12} = \frac{\Delta E_{12}}{\hbar} = 9.387 \times 10^{12}/s$).

Fig. 3.6 shows the change in linear absorption coefficient $\Delta\beta^{(1)}(\omega)$, the change in third order nonlinear absorption coefficient $\Delta\beta^{(3)}(\omega)$ and the change in total absorption coefficient $\Delta\beta(\omega)$ as a function of photon energy for the same incident optical intensity $I = 7.1893 \times 10^4 W/cm^2$ and confinement frequency ω_0=1 THz with change in energy for optical transition $\Delta E_{01} = 4.6414 \times 10^{-22}$J and the transition dipole moment $\mu_{01} = -1.3314 \times 10^{-27}$c-m. For this transition the third order non linear absorption coefficient is five order greater than the linear absorption coefficient.

In Fig. 3.7 the change in linear absorption coefficient $\Delta\beta^{(1)}(\omega)$, the change in third order nonlinear absorption coefficient $\Delta\beta^{(3)}(\omega)$ and the change in total absorption

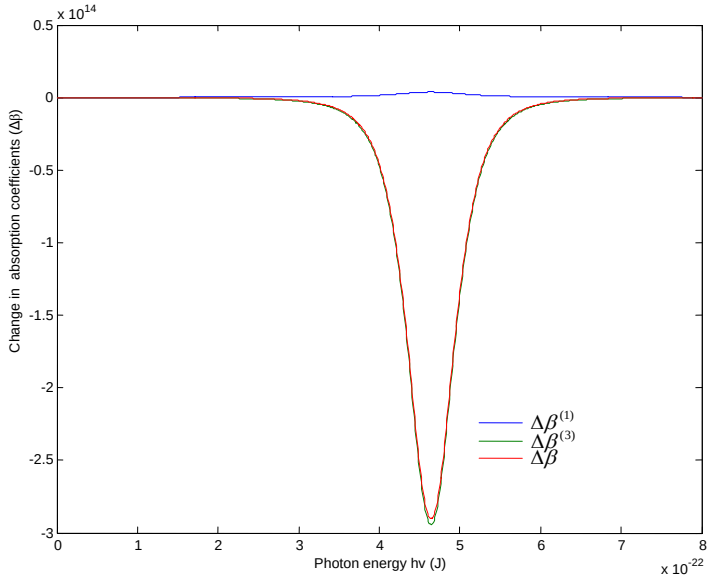

Figure 3.6: *The change in linear, third order nonlinear and total absorption coefficient versus photon energy for transition frequency*($\omega_{01} = \frac{\Delta E_{01}}{\hbar} = 1.4146 \times 10^{13}/s$).

coefficient $\Delta\beta(\omega)$ are plotted as a function of photon energy for the same incident optical intensity $I = 7.1893 \times 10^4 W/cm^2$ and confinement frequency ω_0=1 THz with change in energy for optical transition $\Delta E_{02} = 8.5466 \times 10^{-22}$J and the transition dipole moment $\mu_{02} = 1.3314 \times 10^{-27}$c-m. For this transition the third order non linear absorption coefficient is five order greater than the linear absorption coefficient. This transition has almost the same magnitude of absorption coefficients with that demonstrated in Fig. 3.4. At this frequency the third order nonlinear absorption coefficient is too large.

In Fig. 3.8 the linear and the third order nonlinear refractive index changes $n^{(1)}(\omega)$ (Fig 3.8A) and $n^{(3)}(\omega)$ (Fig 3.8B) are plotted as a function of photon energy $\hbar\omega$ for three confinement frequencies ω_0= 1 THz, 2 THz and 3 THz respectively,

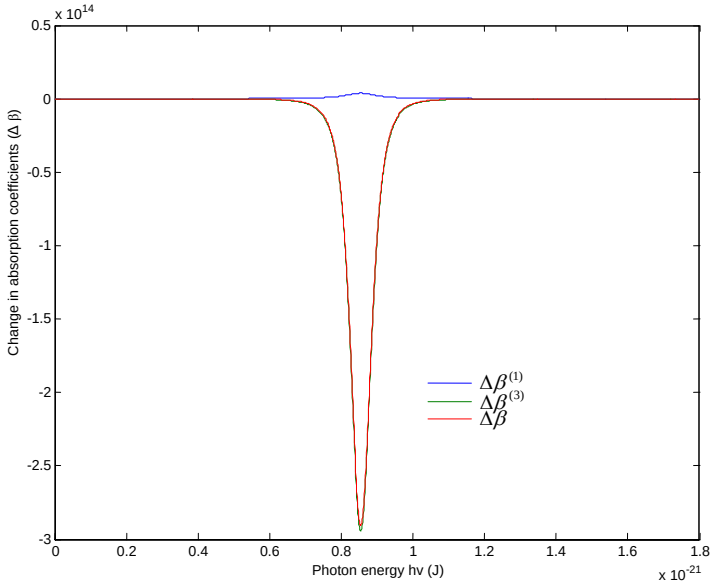

Figure 3.7: *The change in linear, third order nonlinear and total absorption coefficient versus photon energy for transition frequency*($\omega_{02} = \frac{\Delta E_{02}}{\hbar} = 2.3534 \times 10^{13}/s$).

for the transition energy of ($\Delta E_{12} = 3.9052 \times 10^{-22}$J, 7.6982×10^{-22}J, and 9.8565×10^{-22}J), the electric dipole moment $\mu_{12} = 2.2157 \times 10^{-27}$ c-m, 1.1079×10^{-27} c-m and, 7.3858×10^{-28} c-m respectively, the resonant electric field ($\varepsilon = 2060\frac{V}{cm}$, $4121.2\frac{V}{cm}$ and $6181.9\frac{V}{cm}$)and intensity ($I = 7.1893 \times 10^4 \frac{W}{cm^2}$, $2.8757 \times 10^5 \frac{W}{cm^2}$ and $6.4704 \times 10^5 \frac{W}{cm^2}$) with respect to the above given frequencies. This figure reveals that the change in linear refractive index, the change in third order nonlinear refractive index, and in turn the change in total index of refraction depend on the confinement frequency of parabolic quantum double well. As a confinement frequency ω_0 increased, the resonant peak will shift to the right of the curve and as a result a strong confinement creates a blue shift. The magnitude of linear and nonlinear refractive index in such a system decrease by increasing the confinement frequency.

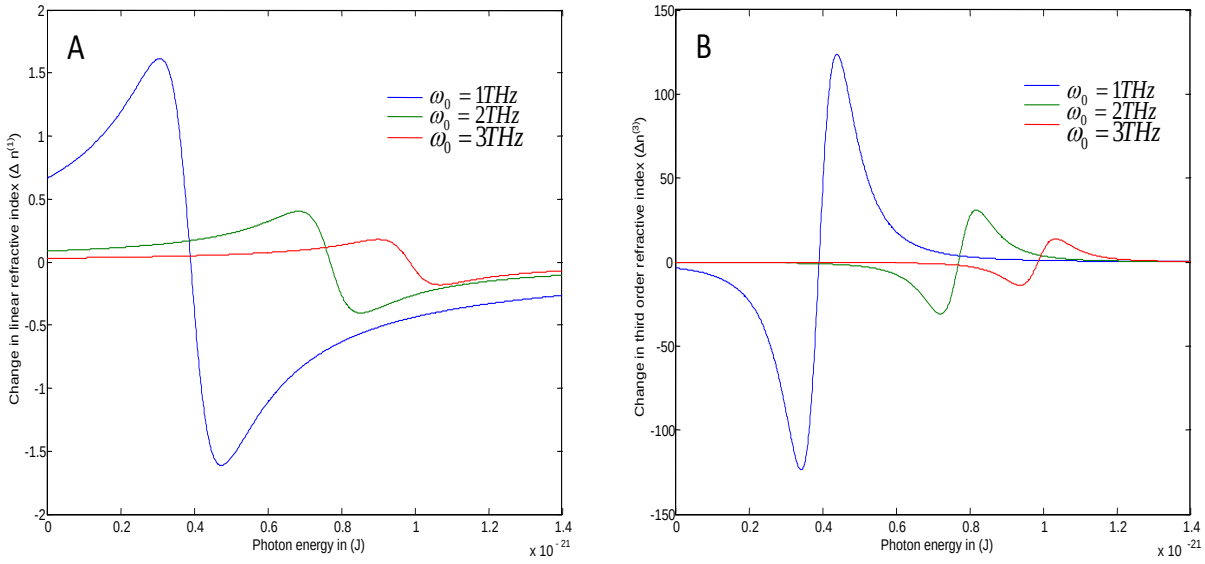

Figure 3.8: *The linear and third order refractive index versus photon energy for three different values of* ω_0 *= 1 THz, 2 THz and 3 THz.*

In Fig. 3.9 the linear and the third order nonlinear absorption coefficients $n^{(1)}(\omega)$ (Fig 3.9A) and $n^{(3)}(\omega)$ (Fig 3.9B) are plotted as a function of photon energy $\hbar\omega$ for three confinement frequencies ω_0= 1 THz, 2 THz and 3 THz respectively, for the transition energy of ($\Delta E_{12} = 3.9052 \times 10^{-22}$J, 7.6982×10^{-22}J, and 9.8565×10^{-22}J), the electric dipole moment $\mu_{12} = 2.2157 \times 10^{-27}$ c-m, 1.1079×10^{-27} c-m and, 7.3858×10^{-28} c-m respectively, the resonant electric field ($\varepsilon = 2060\frac{V}{cm}$, $4121.2\frac{V}{cm}$ and $6181.9\frac{V}{cm}$)and intensity ($I = 7.1893 \times 10^4 \frac{W}{cm^2}$, $2.8757 \times 10^5 \frac{W}{cm^2}$ and $6.4704 \times 10^5 \frac{W}{cm^2}$) with respect to the above given frequencies. This figure shows that the change in absorption coefficient, the change in third order nonlinear absorption coefficient, and in turn the change in total absorption coefficient depend on the confinement frequency of parabolic quantum double wells. Increasing a confinement frequency ω_0 creates a

blue shift. However the magnitude of linear and nonlinear absorption coefficient decrease by increasing the confinement frequency.

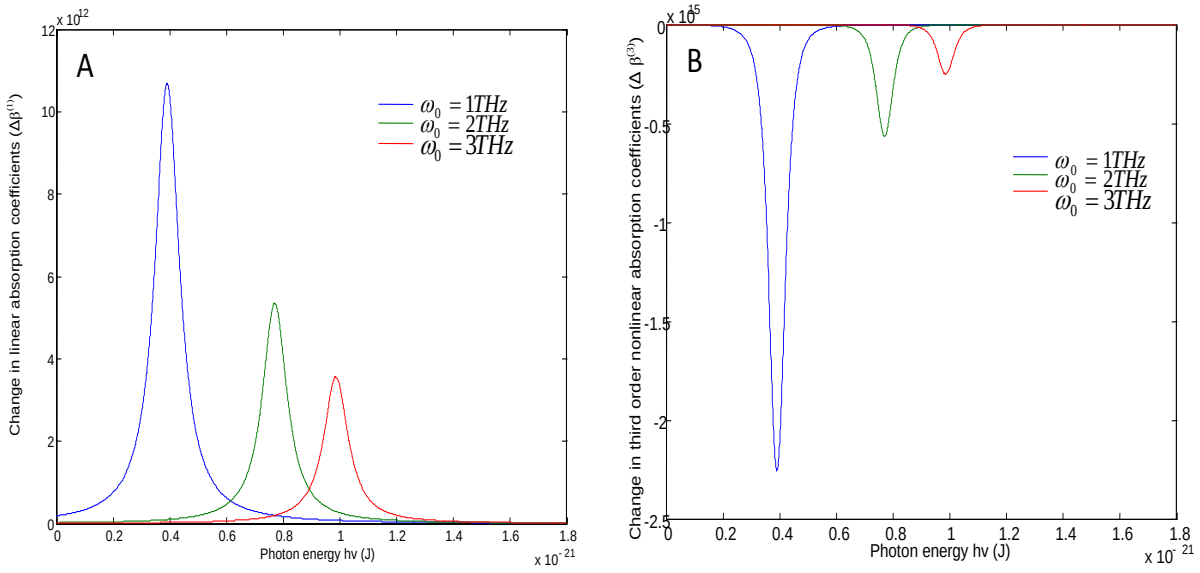

Figure 3.9: *The linear and third order nonlinear absorption coefficients versus photon energy for three different values of* ω_0 *= 1 THz, 2 THz and 3 THz.*

In Fig. 3.10 the linear and the third order nonlinear refractive index changes $n^{(1)}(\omega)$ (Fig 3.10A) and $n^{(3)}(\omega)$ (Fig 3.10B) are plotted as a function of photon energy $\hbar\omega$ for three confinement frequencies ω_0= 1 THz, 2 THz and 3 THz respectively, for the transition energy of ($\Delta E_{01} = 4.6414 \times 10^{-22}$J, 9.3389×10^{-22}J, and 1.4854×10^{-21}J), the electric dipole moment $\mu_{01} = -1.3314 \times 10^{-27}$ c-m, -9.4143×10^{-28} c-m and, -7.6868×10^{-28} c-m respectively, the resonant electric field ($\varepsilon = 2060\frac{V}{cm}$, $4121.2\frac{V}{cm}$ and $6181.9\frac{V}{cm}$)and intensity ($I = 7.1893\times10^4\frac{W}{cm^2}$, $2.8757\times10^5\frac{W}{cm^2}$ and $6.4704\times10^5\frac{W}{cm^2}$) with respect to the above given frequencies. This figure reveals that the change in linear refractive index, third order nonlinear refractive index, and in turn the total

index of refraction depend on the confinement frequency of parabolic DQWs. As a confinement frequency ω_0 increased, the resonant peak will shift to the right of the curve and as a result a strong confinement creates a blue shift. Fig. 10 reveals that magnitude of linear refractive index decreases with increment of confinement frequency. However the third order refractive index in such system remains constant with increment of the confinement frequency.

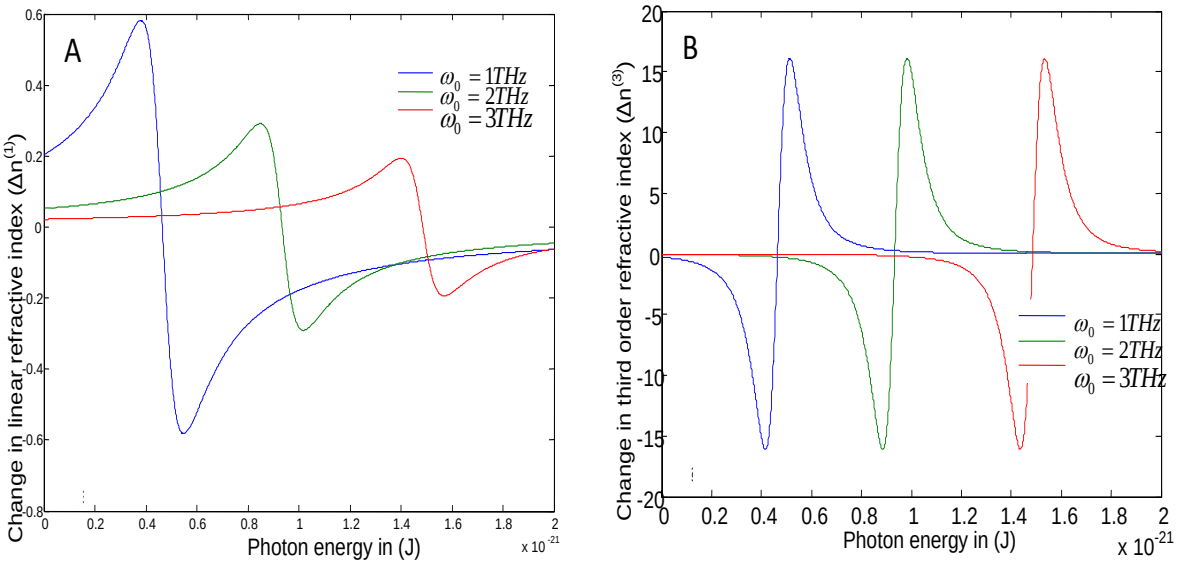

Figure 3.10: *The linear and third order refractive index versus photon energy for three different values of* ω_0 *= 1 THz, 2 THz and 3 THz.*

In Fig. 3.11 the linear and the third order nonlinear absorption coefficients $n^{(1)}(\omega)$ (Fig 3.11A) and $n^{(3)}(\omega)$ (Fig 3.11B) are plotted as a function of photon energy $\hbar\omega$ for three confinement frequencies ω_0= 1 THz, 2 THz and 3 THz respectively, for the transition energy of ($\Delta E_{01} = 4.6414 \times 10^{-22}$J, 9.3389×10^{-22}J, and 1.4854×10^{-21}J), the electric dipole moment $\mu_{01} = -1.3314 \times 10^{-27}$ c-m, -9.4143×10^{-28} c-m and,

-7.6868×10^{-28} c-m respectively,the resonant electric field ($\varepsilon = 2060\frac{V}{cm}$, $4121.2\frac{V}{cm}$ and $6181.9\frac{V}{cm}$)and intensity ($I = 7.1893 \times 10^4 \frac{W}{cm^2}$, $2.8757 \times 10^5 \frac{W}{cm^2}$ and $6.4704 \times 10^5 \frac{W}{cm^2}$) with respect to the above given frequencies. This figure shows that the change in absorption coefficient, the change in third order nonlinear absorption coefficient, and in turn the change in total absorption coefficient depend on the confinement frequency of parabolic quantum double wells. Increasing a confinement frequency ω_0 creates a blue shift. However, increasing the confinement frequency does not affect the magnitude linear and third order absorption coefficients.

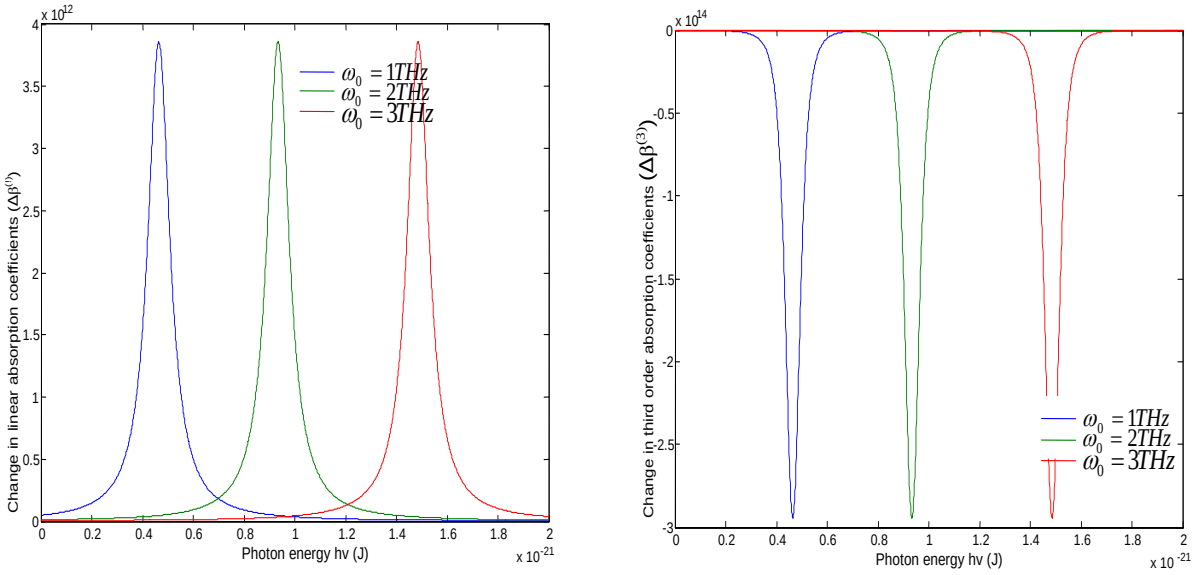

Figure 3.11: *The linear and third order nonlinear absorption coefficients versus photon energy for three different values of* ω_0 *= 1 THz, 2 THz and 3 THz.*

In Fig. 3.12 the linear and the third order nonlinear refractive index changes $n^{(1)}(\omega)$ (Fig 3.12A) and $n^{(3)}(\omega)$ (Fig 3.12B) are plotted as a function of photon energy $\hbar\omega$ for three confinement frequencies ω_0= 1 THz, 2 THz and 3 THz respectively, for the

transition energy of ($\Delta E_{02} = 8.5466\times10^{-22}$J, 1.7037×10^{-21}J, and 2.471×10^{-21}J),the electric dipole moment $\mu_{01} = 1.3314\times10^{-27}$ c-m, 9.4143×10^{-28} c-m and, 7.6868×10^{-28} c-m respectively, the resonant electric field ($\varepsilon = 2060\frac{V}{cm}$, $4121.2\frac{V}{cm}$ and $6181.9\frac{V}{cm}$)and intensity ($I = 7.1893\times10^{4}\frac{W}{cm^2}$, $2.8757\times10^{5}\frac{W}{cm^2}$ and $6.4704\times10^{5}\frac{W}{cm^2}$) with respect to the above given frequencies. This figure reveals that the change in linear refractive index, third order nonlinear refractive index, and in turn the total index of refraction depend on the confinement frequency of parabolic DQWs. As a confinement frequency ω_0 increases, the resonant peak will shift to the right of the curve and as a result a strong confinement creates a blue shift. The magnitude of linear refractive index in such a system decrease by increasing the confinement frequency. However the magnitude of third order nonlinear refractive index is not affected.

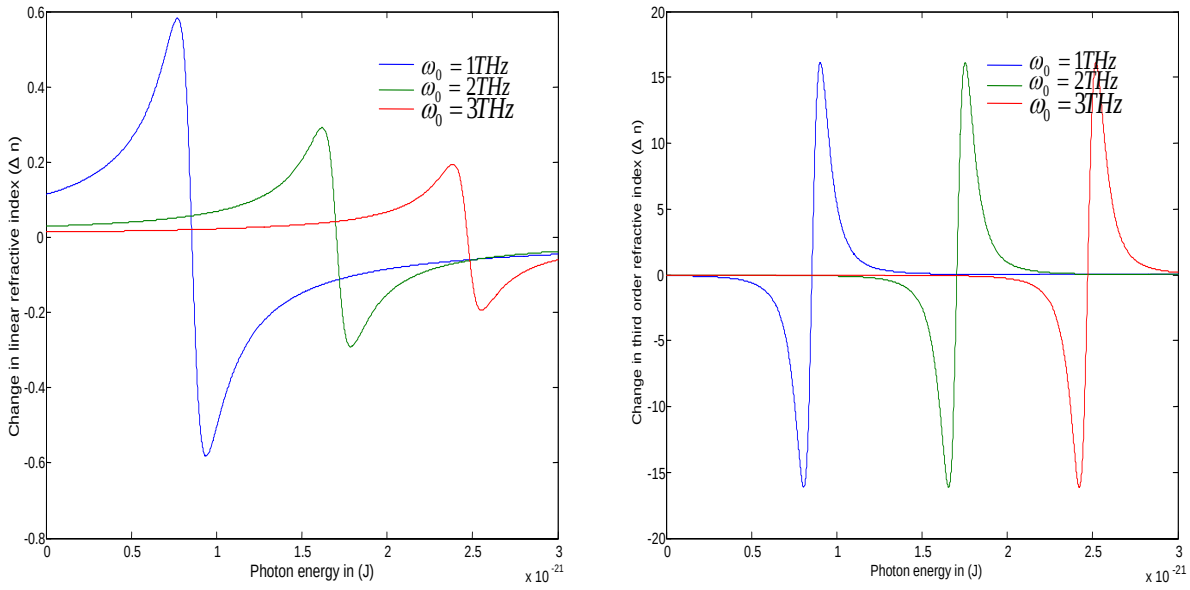

Figure 3.12: *The linear and third order refractive index versus photon energy for three different values of* ω_0 *= 1 THz, 2 THz and 3 THz.*

In Fig. 3.13 the linear and the third order nonlinear absorption coefficients $n^{(1)}(\omega)$ (Fig 3.13A) and $n^{(3)}(\omega)$ (Fig 3.13B) are plotted as a function of photon energy $\hbar\omega$ for three confinement frequencies ω_0= 1 THz, 2 THz and 3 THz respectively, for the transition energy of ($\Delta E_{02} = 8.5466\times10^{-22}$J, 1.7037×10^{-21}J, and 2.471×10^{-21}J), the electric dipole moment $\mu_{12} = 1.3314\times10^{-27}$ c-m, 9.4143×10^{-28} c-m and, 7.6868×10^{-28} c-m respectively,the resonant electric field ($\varepsilon = 2060\frac{V}{cm}$, $4121.2\frac{V}{cm}$ and $6181.9\frac{V}{cm}$)and intensity ($I = 7.1893 \times 10^4\frac{W}{cm^2}$, $2.8757 \times 10^5\frac{W}{cm^2}$ and $6.4704 \times 10^5\frac{W}{cm^2}$) with respect to the above given frequencies. This figure shows that the change in absorption coefficient, the change in third order nonlinear absorption coefficient, and in turn the change in total absorption coefficient depend on the confinement frequency of parabolic quantum double wells. Increasing a confinement frequency ω_0 creates a blue shift. However, the magnitude of linear and nonlinear absorption coefficients are not affected by increasing the confinement frequency.

3.5 Conclusion

In this chapter we have derived the energy splitting due to quantum tunneling in asymmetric parabolic DQWs as a result of constant applied electric field at resonant condition. At resonant condition the ground state energy level of the left well coincides with the excited state energy level of the right well and energy splitting takes place due to tunneling. As the result three possible transitions takes place among the ground state energy level and the two split state energy levels due to anti crossing effect. We calculated the transition dipole moments (μ_{12}, μ_{01} and μ_{02}) between the ground state in the right well and the two split states of the excited energy level in the

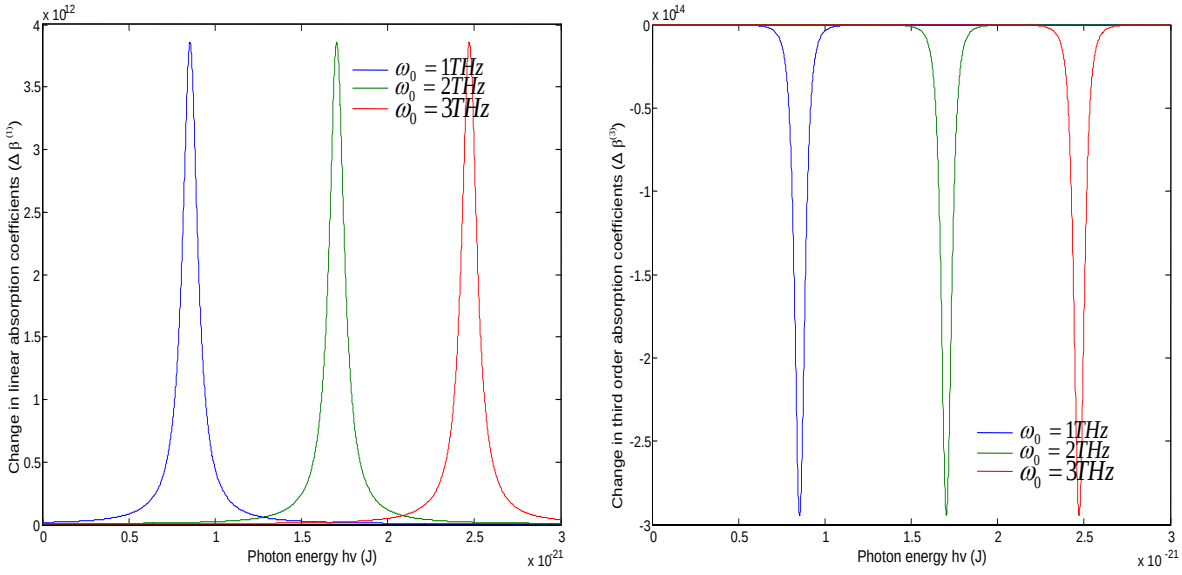

Figure 3.13: *The linear and third order nonlinear absorption coefficients versus photon energy for three different values of* ω_0 *= 1 THz, 2 THz and 3 THz.*

left and right well due to tunneling. We also calculated the change in transition energies (ΔE_{12}, ΔE_{01} and ΔE_{02}) for possible transitions. At the confinement frequency $\omega_0 = 1$ THz, the calculated transition frequencies are $\omega_{12} = 0.592$ THz, $\omega_{01} = 0.704$ THz and $\omega_{02} = 1.296$ THz. Moreover we have determined the analytical expressions of absorption coefficients and refractive index changes for parabolic DQWs using the compact density matrix approach. The calculation shows that a very large magnitude of change in third order nonlinear refraction index and absorption coefficients are produced for all possible transitions. Due to this effect the magnitude of change in total refractive index and absorption coefficients are negative in sign. As a confinement frequency increases the maximum change in the index of refraction will move to the right of the curve which predicts that a strong confinement induces blue shift

of the resonant absorption in DQWs. These features make it a very good candidate for nonlinear optical material. The total changes in absorption coefficients and index of refraction are greatly influenced by third order nonlinear terms. Moreover, it is observed that the variation of change in linear, nonlinear and total index of refraction and absorbtion coefficients extremely depend on the magnitude of the transition dipole moment and transition energy between two different states. This result may make a contribution to experimental studies and provide direction for practical applications such as tera hertz (THz) detectors, electro optical modulators and electro optical switches. After all Figs. 3.2-3.4, 3.8, 3.10 and 3.12 indicate that it is possible to achieve, with in some frequency ranges, negative values of the refractive index, that is the media with asymmetric DQWs become left handed. This result is of great importance for metamaterials science and can contribute substantially to the present search for simple and inexpensive left handed media. However, to put this result in the experimental context, further investigation of the same effects at realistic field intensities would be necessary.

Chapter 4

Two electron quantum dots with parabolic confinement (low lying para- and ortho- states)

Three low lying energy levels of 3D two-electron quantum dot (QD) with parabolic confinement are obtained by the variational method. The proposed interpolation formulas of the variation parameters allow one to recover the energy levels in the wide range of the Coulomb interaction coupling constant. The quantum states of the QD are divided into the para- and ortho- states like in the theory of helium atom. The quantum transitions from the ortho- state to the para- state are possible only with account of the spin-orbit interaction. At low temperatures an ensemble of the two-electron QDs contains dots in the ground para- state and in the first excited ortho- state, which are metastable. These QDs have the entangled spin wave functions that relate to the EPR states desirable for the quantum information protocol.

4.1 Introduction

The models of quantum wells and quantum dots (QDs) with one electron are widely used in the nano physics [74, 75]. The modern technology provides possibility to create QDs with two and more electrons where the Coulomb interaction between them must be taken in to account [76]. Due to the nano scale localization of the electrons the Coulomb interaction can exceed the average kinetic energy of electrons that considerably complicates the analytic solution of the Schrodinger equation.

In this chapter, we consider three low lying states of the two-electron spherically symmetric QDs with parabolic confinement. The Coulomb interaction in the typical 10 nm semiconductor QD cannot be treated as a small and the problem is solved with the help of the variational method. The two-electron trial functions are chosen on the bases of one-electron wave functions of the QD with parabolic confinement. We calculated the energies of the first three states and carried out the classification of the corresponding spectral terms.

At low temperatures T, (much smaller than the distance between the ground and first excited states) the ensemble of QDs consists of dots in the para- and ortho- states. The singlet spin wave functions correspond to the para- states. The triplet spin wave functions correspond to the ortho- states. The lowest ortho- state is metastable. The singlet spin wave function of the ground state and one of the triplet spin wave functions associated with the lowest ortho- state relate to Einstein-Podolskii-Rosen (EPR) states desirable for the quantum information protocols [86-89].

The Chapter is organized as follows. In Section 4.2, we introduce the variational wave functions and explain the peculiarities of calculation of the variation parameters. Sections 4.3 and 4.4 are devoted to calculation of the variation parameters and the

energy levels of the QD. Section 4.5 discusses the para- and ortho- states of the two-electron quantum dot. The Conclusion summarizes the results obtained and discusses the hypothetic many-electron quantum dots manufactured from materials with gigantic dielectric constants.

4.2 Statement of the problem

Two interacting electrons in 3D spherically symmetric quantum dot with the parabolic confinement potential are described by the following dimensionless Hamiltonian

$$\hat{H} = -\frac{1}{2}\nabla_1^2 - \frac{1}{2}\nabla_2^2 + \frac{1}{2}(r_1^2 + r_2^2) + \frac{\lambda}{|\vec{r_1} - \vec{r_2}|}. \tag{4.2.1}$$

Here the dimensionless coordinates of the first and second electrons r_1 and r_2 are measured in units $\sqrt{\hbar/(m^*\omega)}$ (m^* is the effective mass of electron and ω is a frequency of the confinement potential), $\lambda = \frac{1}{\varepsilon}\sqrt{(Ry/\hbar\omega)m^*/m}$ is the constant characterizing the Coulomb interaction between electrons, ε is the dielectric constant of the quantum dot. Keeping in mind that the Rydberg constant $Ry = me^4/\hbar^2 = 27.2$ eV and setting $\omega \approx$ 10 THz, we obtain $\lambda \simeq 20/\varepsilon$. If we assume that $\varepsilon \simeq 10$ (GaAs) then $\lambda \simeq 2$. This means that the Schrodinger equation corresponding to the Hamiltonian (4.2.1) for the semiconductor QD cannot be solved with the help of the perturbation theory. It requires variational or numerical methods. In this chapter we use the variational method, which allows us to obtain analytic formulas.

The classification of the states of the two-electron QD is convenient to perform with the help of the quantum numbers for noninteracting electrons. Due to the symmetry of the problem we use the spherical coordinate system. The one-electron wave functions are known [81]. The energy of the two-electron QD with noninteracting

electrons can be written as

$$E_{N_1N_2} = N_1 + N_2 + 3 = 2(n_1 + n_2) + l_1 + l_2 + 3, \tag{4.2.2}$$

where $N_i = 2n_i + l_i$ with $n_i = 0, 1, 2...$, are the radial quantum numbers, $l_i = 0, 1, 2...$, are the orbital quantum numbers, and $m_i = 0, \pm 1, \pm 2... \pm l_i$ are magnetic quantum numbers ($i = 1, 2$). The energy levels (4.2.2) are described by the symmetrized combinations of products of the one-electron wave functions $\psi_{n_1 l_1 m_1}(r_1, \theta_1, \phi_1)\psi_{n_2 l_2 m_2}(r_2, \theta_2, \phi_2)$. The one-electron wave functions are presented in the standard form $R_{nl}(r)Y_{lm}(\theta, \phi)$.

The ground state of the QD corresponds to a set of quantum numbers $\{n_1 = n_2 = 0,\ l_1 = l_2 = 0, m_1 = m_2 = 0\}$. We choose the normalized ground state trial wave function of the two-electron QD in the form

$$\psi_0(\vec{r_1}, \vec{r_2}) = \left(\frac{\alpha}{\pi}\right)^{\frac{3}{2}} \exp\{-\frac{\alpha}{2}(r_1^2 + r_2^2)\}, \tag{4.2.3}$$

where α is a variational parameter.

The following two sets of quantum numbers $\{n_1 = n_2 = 0, l_1 = 1, m_1 = 0, \pm 1, l_2 = 0, m_2 = 0\}$ and $\{n_1 = n_2 = 0, l_1 = 0, m_1 = 0, l_2 = 1, m_2 = 0, \pm 1\}$ correspond to the first excited state. Below for the sake of simplicity, we consider only states with $m = 0$.

The wave function of the first excited state is given by the symmetrized combination

$$\begin{cases} \psi_1^{s,a}(\vec{r_1}, \vec{r_2}) = \frac{1}{\sqrt{2}}\{\psi_{010}(\vec{r_1})\psi_{000}(\vec{r_2}) \pm \psi_{010}(\vec{r_2})\psi_{000}(\vec{r_1})\}, \\ \psi_{010}(r_1)\psi_{000}(r_2) = N_0 \exp\{-\frac{1}{2}(\beta r_1^2 + \alpha r_2^2)\} r_1 cos\theta_1. \end{cases} \tag{4.2.4}$$

Here s and a stand for the symmetric and antisymmetric combinations, respectively, $N_0 = \frac{\sqrt{2}\alpha^{3/4}\beta^{5/4}}{\pi^{3/2}}$ is the normalization constant; β is one more variational parameter. It appears because the electrons are in different states.

The following five sets of quantum numbers $\{n_1 = n_2 = 0, l_1 = l_2 = 1\}; \{n_1 = 1, n_2 = 0, l_1 = l_2 = 0\}; \{n_1 = 0, n_2 = 1, l_1 = l_2 = 0\}; \{n_1 = 0, n_2 = 0, l_1 = 2, l_2 = 0\}; \{n_1 = 0, n_2 = 0, l_1 = 0, l_2 = 2\}$ correspond to the second excited state of the QD. The trial wave function corresponding to the first set is

$$\psi_2^{(1)}(\vec{r_1}, \vec{r_2}) = \frac{2\beta^{\frac{5}{2}}}{\pi^{\frac{3}{2}}} e^{-\frac{\beta}{2}(r_1^2 + r_2^2)} r_1 cos\theta_1 r_2 cos\theta_2. \tag{4.2.5}$$

with the same variational parameter β as in (4.2.4). Four more trial wave functions corresponding to the second, third, fourth and fifth sets of the quantum numbers are

$$\begin{cases} \psi_2^{(2)s,a}(\vec{r_1}, \vec{r_2}) = \frac{1}{\sqrt{2}}\{\psi_{100}(\vec{r_1})\psi_{000}(\vec{r_2}) \pm \psi_{100}(\vec{r_2})\psi_{000}(\vec{r_1})\}, \\ \psi_{100}(\vec{r_1})\psi_{000}(\vec{r_2}) = N_1\Big(\frac{3}{\alpha+\gamma} - r_1^2\Big)e^{-\frac{1}{2}(\gamma r_1^2 + \alpha r_2^2)}, \end{cases} \tag{4.2.6}$$

and

$$\begin{cases} \psi_2^{(3)s,a}(\vec{r_1}, \vec{r_2}) = \frac{1}{\sqrt{2}}\{\psi_{020}(\vec{r_1})\psi_{000}(\vec{r_2}) \pm \psi_{020}(\vec{r_2})\psi_{000}(\vec{r_1})\}, \\ \psi_{020}(\vec{r_1})\psi_{000}(\vec{r_2}) = N_2 e^{-\frac{1}{2}(\eta r_1^2 + \alpha r_2^2)} r_1^2(3cos^2\theta_1 - 1). \end{cases} \tag{4.2.7}$$

$N_1 = \Big[\frac{4\alpha^{\frac{3}{2}}\gamma^{\frac{7}{2}}(\alpha+\gamma)^2}{3\pi^3(5\alpha^2 - 2\alpha\gamma + 5\gamma^2)}\Big]^{\frac{1}{2}}$ and $N_2 = \Big[\frac{\alpha^{\frac{3}{2}}\eta^{\frac{7}{2}}}{3\pi^3}\Big]^{\frac{1}{2}}$ are the normalization constants.

The variational parameters α and β will be obtained after calculation of the ground and second excited state energies with the help of wave functions (4.2.3) and (4.2.5), respectively. The variational parameters γ and η will be obtained after calculating the average of the Hamiltonian (4.2.1) with the help of the following wave functions

$$\psi_3^{(1)}(\vec{r_1}, \vec{r_2}) = N_3^{(1)} \prod_{i=1}^{2} \Big(\frac{3}{\alpha+\gamma} - r_i^2\Big)e^{-\frac{\gamma}{2}r_i^2}, \tag{4.2.8}$$

$$\psi_3^{(2)}(\vec{r_1}, \vec{r_2}) = N_3^{(2)} \prod_{i=1}^{2} e^{-\frac{\eta}{2}r_i^2}(3cos^2\theta_i - 1), \tag{4.2.9}$$

where $N_3^{(1)} = \frac{4\gamma^{\frac{7}{2}}(\alpha+\gamma)^2}{3\pi^{\frac{3}{2}}(5\alpha^2-2\alpha\gamma+5\gamma^2)}$ and $N_3^{(2)} = \frac{\eta^{\frac{7}{2}}}{3\pi^{\frac{3}{2}}}$ are the normalization constants.

One can easily check that all these functions are mutually orthogonal. It is necessary to note that $\psi_3^{(1)}(\vec{r_1}, \vec{r_2})$ contains two variational parameters α and γ. The average energy calculated on this function $E_3^{(1)}(\alpha, \gamma)$ depends on these parameters as well. We take α from the calculations of the ground state energy and minimize $E_3^{(1)}(\alpha, \gamma)$ only with respect to γ.

For noninteracting electrons ($\lambda = 0, \gamma = \eta = 1$) wave functions (4.2.8) and (4.2.9) relate to the fourth excited state of the QD. With account of the Coulomb interaction ($\lambda \neq 0$) they describe different energies. In this paper, we use the trial functions with one variational parameter. Such approach definitely gives good results for the ground state of the QD. For the higher states the quantitative reliability of this approach decreases. One can also argue that the style of the trial functions can change with increasing of the interaction parameter λ. The limiting λ, after which the style of the wave function changes considerably can be specified only by numeric solution of the Schrodinger equation. It would be relevant to refer paper [82], where the ground state energy of the 2D electron QD have been obtained with the help of one- two- and three parameter variation functions and compared with the exact numerical solution. It happened to be that for $\lambda < 2$ all these energies practically coincide. We use the same Gaussian type of trial wave functions that allows us to hope our results are reliable for the ground state and satisfactory for the first low lying levels for $\lambda \simeq 2$.

In the next sections we obtain the variational parameters α, β, γ, and η from the minimization of the corresponding energies.

4.3 Ground state of two-electron QD

The ground state of the two-electron QD is described by the symmetric wave function (4.2.3). Calculating the average of the Hamiltonian (4.2.1) with this wave function we obtain

$$E_0(\lambda) = \frac{3}{2}(\alpha + \frac{1}{\alpha}) + K_0. \tag{4.3.1}$$

The first term represents the kinetic and potential energy of the non interacting electrons in the parabolic potential well. The second term is the Coulomb interaction of electrons in the ground state

$$K_0 = \int \psi_0^*(\vec{r_1}, \vec{r_2}) \frac{\lambda}{r_{12}} \psi_0(\vec{r_1}, \vec{r_2}) dv_1 dv_2. \tag{4.3.2}$$

For calculation of K_0 we use the formula

$$\frac{1}{r_{12}} = \frac{1}{r_1} \sum_{l=0}^{\infty} \left(\frac{r_2}{r_1}\right)^l P_l(cos\theta), \qquad r_1 > r_2, \qquad \frac{1}{r_{12}} = \frac{1}{r_2} \sum_{l=0}^{\infty} \left(\frac{r_1}{r_2}\right)^l P_l(cos\theta), \qquad r_1 < r_2, \tag{4.3.3}$$

where $P_l(cos\theta)$ is the Legendre polynomial, θ is the angle between $\vec{r_1}$ and $\vec{r_2}$. According to the addition theorem for spherical harmonics [83, 84]

$$P_l(cos\theta) = P_l(cos\theta_1) P_l(cos\theta_2) + 2 \sum_{m=1}^{l} \frac{(l-m)!}{(l+m)!} P_l^m(cos\theta_1) P_l^m(cos\theta_2) cos\, m(\phi_1 - \phi_2), \tag{4.3.4}$$

where θ_1, ϕ_1 and θ_2, ϕ_2 are the polar angles of the vectors $\vec{r_1}$ and $\vec{r_2}$, respectively. When the above formulas are substituted into (4.3.2) and integrated with respect to ϕ_1, ϕ_2 and θ_1, θ_2, we obtain that the second term of (4.3.4) vanishes and contribution into the integral comes out of $P_0(cos\theta_1) = P_0(cos\theta_2) = 1$. With usage of the wave function (4.2.2), we obtain

$$K_0 = \lambda \Big(\frac{\alpha}{\pi}\Big)^3 (4\pi)^2 \int_0^{\infty} \Big[\int_0^{r_1} \frac{1}{r_1} e^{-\alpha(r_1^2 + r_2^2)} r_2^2 dr_2 + \int_{r_1}^{\infty} \frac{1}{r_2} e^{-\alpha(r_1^2 + r_2^2)} r_2^2 dr_2 \Big] r_1^2 dr_1. \tag{4.3.5}$$

Table 4.1: The ground state energy E_0 and variational parameter α for different λ.

λ	0.0	0.5	1.0	1.5	2.0	2.5	3.0	3.5	4.0
α	1.000	0.938	0.883	0.834	0.791	0.752	0.718	0.686	0.658
$E_0(\lambda)$	3.000	3.393	3.773	4.143	4.502	4.852	5.194	5.529	5.855

Performing integration in (4.3.5), we get

$$K_0 = \lambda\sqrt{\frac{2\alpha}{\pi}}. \tag{4.3.6}$$

The variational parameter α, which provides the minimum of energy (4.3.1), is obtained from the condition $\frac{dE_0(\alpha)}{d\alpha} = 0$. With account (4.3.5) it gives the following equation

$$\alpha^2 + \frac{\lambda}{3}\sqrt{\frac{2}{\pi}}\alpha^{\frac{3}{2}} - 1 = 0. \tag{4.3.7}$$

In the case $\lambda = 0$, the equation (4.3.7) has the solution $\alpha = 1$. For $\lambda \ll 1$, (4.3.7) can be solved with the help of expansion by small parameter ($\alpha = 1 + \lambda\alpha_1 + \lambda^2\alpha_2 + ...$). The result is

$$\alpha = 1 - \frac{\lambda}{3\sqrt{2\pi}} + \frac{\lambda^2}{18\pi}, \quad \lambda \ll 1. \tag{4.3.8}$$

Substituting (4.3.8) in (4.3.1) with account (4.3.6), we obtain the ground state energy with the same accuracy

$$E_0(\lambda) = 3 + \lambda\sqrt{\frac{2}{\pi}} - \frac{\lambda^2}{12\pi}, \quad \lambda \ll 1. \tag{4.3.9}$$

If λ, is not small the equation (4.3.7) can be solved numerically. In Table 4.1, we present the calculated ground state energy E_0 and variational parameter α for different λ.

With the help of equation (4.3.1) and numerical values α calculated for different

λ we can propose the following interpolation formulas for the variational parameter

$$\alpha(\lambda) = \frac{1}{1 + \frac{\lambda}{3\sqrt{2\pi}}}. \tag{4.3.10}$$

One can check the ground state energy $E_0(\lambda)$ (4.3.1) of the two-electron QD with α given by (4.3.10) is in excellent agreement with the data of Table 1.

4.4 First and second excited states

The first excited state wave functions (4.2.4) contain of the already calculated variational parameter α and still unknown variational parameter β. As it was mentioned before, we find it with the help of wave function (4.2.5). The calculation of the average Hamiltonian (4.2.1) with the help of the wave function (4.2.5) gives the following result

$$E_2^{(1)}(\lambda) = \frac{5}{2}(\beta + \frac{1}{\beta}) + K_2^{(1)}. \tag{4.4.1}$$

The first term in this equation is the kinetic and potential energy of two noninteracting electrons in the second excited state. The Coulomb interaction of two-electrons $K_2^{(1)}$ is given by the integral

$$K_2^{(1)} = \int \psi_2^{(1)*}(\vec{r_1}, \vec{r_2}) \frac{\lambda}{r_{12}} \psi_2^{(1)}(\vec{r_1}, \vec{r_2}) dv_1 dv_2. \tag{4.4.2}$$

To calculate this integral we use (4.2.5), (4.3.3), (4.3.4) and the relation $cos^2\theta_{1,2} = \frac{1}{3}[P_0 + 2P_2(cos\,\theta_{1,2})]$. The integration with respect to $d\phi_1 d\phi_2$ kills the sum over m in (4.3.4) and integration with respect to $d\theta_1 d\theta_2$ gives a contribution from the Legendre polynomials with $l = 0, l = 2$ only. The final result of integration in (4.4.2) is

$$K_2^{(1)} = \frac{49\lambda\sqrt{\beta}}{30\sqrt{2\pi}}. \tag{4.4.3}$$

Table 4.2: The excited state energy $E_2^{(1)}$ and variational parameter α for different λ when two electrons are in the state $n = 0, l = 1, m = 0$.

λ	0.0	0.5	1.0	1.5	2.0	2.5	3.0	3.5	4.0
β	1.000	0.968	0.939	0.911	0.885	0.860	0.837	0.815	0.794
$E_2^{(1)}(\lambda)$	5.000	5.323	5.641	5.955	6.263	6.568	6.868	7.164	7.456

The variational parameter β is found from the condition $\frac{dE_2^{(1)}(\lambda)}{d\beta} = 0$ with the help of (4.4.1) and (4.4.3). We obtain the following equation for β

$$\beta^2 + \frac{49\lambda}{150\sqrt{2\pi}}\beta^{\frac{3}{2}} - 1 = 0. \tag{4.4.4}$$

At $\lambda = 0$, the equation (4.4.4) has the solution $\beta = 1$. For $\lambda \ll 1$ it can be solved by expansion with respect to small parameter. The result is

$$\beta = 1 - \frac{49\lambda}{300\sqrt{2\pi}} + \Big(\frac{49}{300}\Big)^2 \frac{\lambda^2}{2\pi}, \quad \lambda \ll 1. \tag{4.4.5}$$

The energy of the second excited state, which corresponds to the symmetric wave function (5), with the same accuracy is

$$E_2^{(1)}(\lambda) = 5 + \frac{49\lambda}{30\sqrt{2\pi}} - \frac{(49)^2\lambda^2}{(300)^2 8\pi}, \quad \lambda \ll 1. \tag{4.4.6}$$

In Table 4.2 we present the calculated excited state energy $E_2^{(1)}$ and variational parameter β for different values of λ.

For arbitrary λ, we can propose the following interpolation formula

$$\beta(\lambda) = \frac{1}{1 + \frac{49\lambda}{300\sqrt{2\pi}}}. \tag{4.4.7}$$

One can check the second excited state energy $E_2^{(1)}(\lambda)$ (4.4.1), (4.4.3) of the two-electron QD with β given by (4.4.7) is in excellent agreement with the data of Table 2.

Now we consider the first excited state of our QD, which correspond to the state when one electron is in the ground state with $n = 0, l = 0, m = 0$ and the second one is in the first excited state with $n = 0, l = 1, m = 0$ represented by symmetrized wave function (4.2.4). The variation parameters α and β are given by the relations (4.3.10) and (4.4.7), respectively. The calculation of the average Hamiltonian (4.2.1) with the help of wave functions (4.2.4), polynomials expansions (4.3.3), and (4.3.4) gives the following result

$$E_1^{(s,a)}(\lambda) = \frac{3}{4}(\alpha + \frac{1}{\alpha}) + \frac{5}{4}(\beta + \frac{1}{\beta}) + K_1 \pm A_1. \tag{4.4.8}$$

$$K_1 = \int |\psi_{010}(\vec{r_1})|^2 \frac{\lambda}{r_{12}} |\psi_{000}(\vec{r_2})|^2 dv_1 dv_2. \tag{4.4.9}$$

$$A_1 = \int \psi_{010}(\vec{r_1})\psi_{000}(\vec{r_1}) \frac{\lambda}{r_{12}} \psi_{010}(\vec{r_2})\psi_{000}(\vec{r_2}) dv_1 dv_2. \tag{4.4.10}$$

After integration we get

$$K_1 = \frac{2\lambda}{3\sqrt{\pi}} \Big[\frac{\sqrt{\alpha\beta}(2\alpha + 3\beta)}{(\alpha + \beta)^{\frac{3}{2}}} \Big] \tag{4.4.11}$$

the energy of the Coulomb interaction between electrons and

$$A_1 = \frac{\lambda}{3\sqrt{\pi}} \Big(\frac{8\alpha^{\frac{3}{2}}\beta^{\frac{5}{2}}}{(\alpha + \beta)^{\frac{7}{2}}} \Big) \tag{4.4.12}$$

the exchange energy. In Table 4.3, we present the calculated energies $E_1^{(s)}(\lambda)$, $E_1^{(a)}(\lambda)$, the Coulomb interaction energy K_1, and the exchange energy A_1, respectively, for different λ using the calculated values of variational parameters α and β.

The second excited state of the two-electron QD can also be organized by putting either one electron in the ground state with the energy 3/2 ($n_1 = 0, l_1 = 0, m_1 = 0$)

Table 4.3: The first excited state energies $E_1^{(s)}(\lambda)$, $E_1^{(a)}(\lambda)$, the Coulomb interaction energy K_1, and the exchange energy A_1 for different λ using the values of variational parameters α and β.

λ	K_1	A_1	$E_1^{(s)}(\lambda)$	$E_1^{(a)}(\lambda)$
0.5	0.326	0.066	4.396	4.264
1.0	0.638	0.131	4.785	4.524
1.5	0.939	0.194	5.1685	4.781
2.0	1.229	0.256	5.545	5.033
2.5	1.509	0.316	5.915	5.282
3.0	1.780	0.375	6.278	5.528
3.5	2.043	0.433	6.636	5.770
4.0	2.298	0.489	6.988	6.009

and another one in the excited state with the energy 7/2 ($n_2 = 1, l_2 = 0, m_2 = 0$) represented by a wave function (4.2.6) or putting one electron in the ground state with the energy 3/2 ($n_1 = 0, l_1 = 0, m_1 = 0$) and the other in the excited state with the energy 7/2 ($n_2 = 0, l_2 = 2, m_2 = 0$) described with the wave function (4.2.7). For the noninteracting electrons its energy is 5. The variational parameters γ and η can be determined from the wave functions (4.2.8) and (4.2.9) respectively.

The unknown variational parameter γ will be used below along with the already known parameter α for constructing the second excited state variational wave function of the two-electron QD. The calculation of the average Hamiltonian (4.2.1) with the help of the wave function (4.2.8) gives the following result

$$E_3^{(1)}(\gamma) = \frac{1}{2(5\alpha^2 - 2\alpha\gamma + 5\gamma^2)}\left[\gamma\delta + \frac{\sigma}{\gamma}\right] + K_3^{(1)}, \tag{4.4.13}$$

where $\delta = 11\alpha^2 + 10\alpha\gamma + 35\gamma^2$ and $\sigma = 35\alpha^2 + 10\alpha\gamma + 11\gamma^2$. The first term in this equation is the kinetic and potential energy of two noninteracting electrons in the fourth excited state. The Coulomb interaction of two-electrons $K_3^{(1)}$ is given by the

Table 4.4: The excited state energy $E_3^{(1)}(\alpha,\gamma)$ and variational parameters α and γ for different values of λ when two-electrons are in the state $n=1$, $l=0$, and $m=0$.

λ	0.0	0.5	1.0	1.5	2.0	2.5	3.0	3.5	4.0
α	1.000	0.938	0.883	0.834	0.791	0.752	0.0.718	0.0.686	0.658
γ	1.000	0.974	0.947	0.920	0.894	0.869	0.844	0.820	0.798
$E_3^{(1)}(\lambda)$	7.000	7.270	7.539	7.807	8.074	8.340	8.606	8.872	9.137

integral

$$K_3^{(1)} = \int \psi_3^{(1)*}(\vec{r_1},\vec{r_2})\frac{\lambda}{r_{12}}\psi_3^{(1)}(\vec{r_1},\vec{r_2})dv_1dv_2, \tag{4.4.14}$$

where $\psi_3^{(1)}(\vec{r_1},\vec{r_2})$ is given by (4.2.8). To calculate this integral we use (4.3.3), (4.3.4), (4.4.14) and the final result is

$$K_3^{(1)} = \lambda\frac{\sqrt{\gamma}(755\alpha^4 - 868\alpha^3\gamma + 2178\alpha^2\gamma^2 - 1540\alpha\gamma^3 + 1571\gamma^4)}{24\sqrt{2\pi}(5\alpha^2 - 2\alpha\gamma + 5\gamma^2)^2}. \tag{4.4.15}$$

The variational parameter γ is found from the condition $\frac{dE_3^{(1)}(\alpha,\gamma)}{d\gamma} = 0$ with the help of (4.4.13) and (4.4.15). In Table 4.4, we present the calculated $E_3^{(1)}(\alpha,\gamma)$ and variational parameters α and γ for different λ.

For not very large λ ($\lambda < 10$) we can propose the following interpolation formulas for $\gamma(\lambda)$ and $E_3^{(1)}(\lambda)$

$$\gamma(\lambda) = 1 - 0.0531\lambda - 0.00053\lambda^2 + 0.0003\lambda^3, \tag{4.4.16}$$

$$E_3^{(1)}(\lambda) = 7 + 0.54183\lambda - 0.003\lambda^2 + 0.0003\lambda^3. \tag{4.4.17}$$

Similarly the variational parameter η can also be used along with the already known parameter α for constructing the second excited state variational wave function of the two-electron QD. The calculation of the average Hamiltonian (4.2.1) with the help of

Table 4.5: The excited state energy $E_3^{(2)}(\lambda)$ and variational parameter η for different λ when two-electrons are in the state $n = 0, l = 2, m = 0$.

λ	0.0	0.5	1.0	1.5	2.0	2.5	3.0	3.5	4.0
η	1.000	0.945	0.896	0.852	0.812	0.776	0.743	0.713	0.686
$E_3^{(2)}(\lambda)$	7.000	7.804	8.586	9.349	10.093	10.819	11.530	12.226	12.908

wave function (4.2.9) gives the following result.

$$E_3^{(2)}(\eta) = \frac{7}{2}(\eta + \frac{1}{\eta}) + K_3^{(2)}. \tag{4.4.18}$$

The first term in this equation is the kinetic and potential energy of two noninteracting electrons in the considered excited state. The Coulomb interaction of two-electrons $K_3^{(2)}$ is given by the integral

$$K_3^{(2)} = \int \psi_3^{(2)*}(\vec{r_1}, \vec{r_2}) \frac{\lambda}{r_{12}} \psi_3^{(2)}(\vec{r_1}, \vec{r_2}) dv_1 dv_2, \tag{4.4.19}$$

where $\psi_3^{(2)}(\vec{r_1}, \vec{r_2})$ is given by equation (4.2.9). With the help of (4.3.3), (4.3.4) and (4.4.19) we obtain

$$K_3^{(2)} = \lambda \frac{229\sqrt{\eta}}{56\sqrt{2\pi}}. \tag{4.4.20}$$

The variational parameter η is found using (4.4.18) and (4.4.20) from the condition $\frac{\partial E_3^{(2)}(\eta)}{\partial \eta} = 0$. It gives the following equation for η

$$\eta^2 + \lambda \frac{229}{392\sqrt{2\pi}} \eta^{\frac{3}{2}} - 1 = 0. \tag{4.4.21}$$

In Table 4.5 we present the calculated excited state energy $E_3^{(2)}(\lambda)$ and variational parameter η for different λ.

For arbitrary λ we can propose the following interpolation formula for the variational parameter η.

$$\eta = \frac{1}{1+\lambda\frac{229}{784\sqrt{2\pi}}}. \tag{4.4.22}$$

It is possible to check that the fourth excited state energy $E_3^{(2)}(\lambda)$ (4.4.18), (4.4.20) of the two electron QD with η given by (4.4.22) is also in excellent agreement with data of Table (4.5).

Now we consider the second excited state of our QD, which corresponds to the state when one-electron in the ground state with $n_1 = 0, l_1 = 0, m_1 = 0$ and the second one in the excited state with $n_2 = 1, l_2 = 0, m_2 = 0$ as described with symmetrized wave function (4.2.6). The calculation of the average Hamiltonian (4.2.1) with the help of wave functions (4.2.6) and Legendre polynomial expansions (4.3.3), (4.3.4) gives the following result

$$E_2^{(2)s,a}(\lambda) = \frac{1}{4}\Big\{3\alpha + \frac{3}{\alpha} + \frac{1}{5\alpha^2+2\alpha\gamma+5\gamma^2}\Big[\gamma(11\alpha^2+10\alpha\gamma+35\gamma^2) + \frac{11\gamma^2+10\alpha\gamma+35\alpha^2}{\gamma}\Big]\Big\} + K_2^2 \pm A_2^2. \tag{4.4.23}$$

$$K_2^{(2)} = \int |\psi_{100}(\vec{r_1})|^2 \frac{\lambda}{r_{12}} |\psi_{000}(\vec{r_2})|^2 dv_1 dv_2. \tag{4.4.24}$$

$$A_2^{(2)} = \int \psi_{100}(\vec{r_1})\psi_{000}(\vec{r_1}) \frac{\lambda}{r_{12}} \psi_{100}(\vec{r_2})\psi_{000}(\vec{r_2}) dv_1 dv_2. \tag{4.4.25}$$

After integration we get the energy of the Coulomb interaction between electrons

$$K_2^{(2)} = \lambda \frac{2\sqrt{\alpha\gamma}(8\alpha^2-4\alpha\gamma+15\gamma^2)}{3\sqrt{\pi}\sqrt{\alpha+\gamma}(5\alpha^2-2\alpha\gamma+5\gamma^2)}, \tag{4.4.26}$$

Table 4.6: The excited state energies $E_2^{(2)s}(\lambda)$, $E_2^{(2)a}(\lambda)$, the Coulomb interaction energy $K_2^{(2)}$, and the exchange energy $A_2^{(2)}$ for different λ using the calculated values of variational parameters α and γ.

λ	$K_2^{(2)}$	$A_2^{(2)}$	$E_2^{(2)s}(\lambda)$	$E_2^{(2)a}(\lambda)$
0.5	0.313	0.0505	5.387	5.286
1.0	0.619	0.102	5.769	5.565
1.5	0.918	0.153	6.145	5.839
2.0	1.209	0.204	6.560	6.152
2.5	1.492	0.254	6.932	6.425
3.0	1.767	0.303	7.298	6.692
3.5	2.034	0.351	7.656	6.955
4.0	2.294	0.398	8.008	7.213

and the exchange energy

$$A_2^{(2)} = \lambda \frac{8\alpha^{\frac{3}{2}}\gamma^{\frac{7}{2}}}{\sqrt{\pi}(\alpha+\gamma)^{\frac{5}{2}}(5\alpha^2 - 2\alpha\gamma + 5\gamma^2)}. \tag{4.4.27}$$

In Table 4.6, we present the calculated energies $E_2^{(2)s}(\lambda)$, $E_2^{(2)a}(\lambda)$, the Coulomb interaction energy $K_2^{(2)}$, and the exchange energy $A_2^{(2)}$, respectively, for different values of λ using the values of variational parameters α and γ.

Finally, we consider the second excited state of our QD, which correspond to the state when one electron is in the ground state with $n_1 = 0, l_1 = 0, m_1 = 0$ and the second one in the excited state with $n_2 = 0, l_2 = 2, m_2 = 0$. The wave functions of this state is given by (4.2.7). The variation parameters α and η are given by the relations (4.3.10) and (4.4.22), respectively. The calculation of the average Hamiltonian (4.2.1) with the help of wave functions (4.2.7) and expansions (4.3.3) and (4.3.4) gives the following result

$$E_2^{(3)s,a}(\lambda) = \frac{3}{4}(\alpha + \frac{1}{\alpha}) + \frac{7}{4}(\eta + \frac{1}{\eta}) + K_2^3 \pm A_2^3. \tag{4.4.28}$$

$$K_2^{(3)} = \int |\psi_{020}(\vec{r_1})|^2 \frac{\lambda}{r_{12}} |\psi_{000}(\vec{r_2})|^2 dv_1 dv_2, \tag{4.4.29}$$

$$A_2^{(3)} = \int \psi_{020}(\vec{r_1})\psi_{000}(\vec{r_1}) \frac{\lambda}{r_{12}} \psi_{020}(\vec{r_2}) \times \psi_{000}(\vec{r_2}) dv_1 dv_2. \tag{4.4.30}$$

After integration we get the energy of the Coulomb interaction between electrons

$$K_2^{(3)} = \lambda \frac{2\alpha^{\frac{3}{2}}\sqrt{\eta}(15(\alpha+\eta)^2 - 7\alpha(\alpha+\eta) - 3\alpha\eta)}{15\sqrt{\pi}\alpha(\alpha+\eta)^{\frac{5}{2}}} \tag{4.4.31}$$

and the exchange energy

$$A_2^{(3)} = \lambda \frac{2\alpha^{\frac{3}{2}}\eta^{\frac{7}{2}}}{5\sqrt{\pi}(\alpha+\eta)^{\frac{9}{2}}}. \tag{4.4.32}$$

In Table 5.7, we present the calculated energies $E_2^{(3)s}(\lambda)$ for the para-state with total spin zero and $E_2^{(3)a}(\lambda)$ for the ortho-state with the total spin unit, the Coulomb interaction energy $K_2^{(3)}$, and the exchange energy $A_2^{(3)}$, respectively, for different λ using the calculated values of variational parameters α and η.

4.5 Para- and ortho- states of two-electron QD with parabolic confinement

The total wave functions of the two-electron QD including spin variables must be antisymmetric to permutation of electrons. In Section 4.2 we introduced the variation coordinate wave functions of our QD. The ground state wave function (4.2.3) is symmetric with respect to interchange of the electron coordinates and requires the

Table 4.7: The excited state energies $E_2^{(3)s}(\lambda)$, $E_2^{(3)a}(\lambda)$, the Coulomb interaction energy $K_2^{(3)}$, and the exchange energy $A_2^{(3)}$ for different λ using the calculated values of variational parameters α and η.

λ	$K_2^{(3)}$	$A_2^{(3)}$	$E_2^{(3)s}(\lambda)$	$E_2^{(3)a}(\lambda)$
0.5	0.277	0.005	5.291	5.282
1.0	0.541	0.010	5.583	5.564
1.5	0.790	0.014	5.874	5.846
2.0	1.028	0.018	6.164	6.127
2.5	1.256	0.022	6.453	6.408
3.0	1.475	0.026	6.738	6.687
3.5	1.684	0.030	7.024	6.963
4.0	1.887	0.034	7.307	7.238

antisymmetric spin function

$$S_{ent}^{(a)} = \frac{1}{\sqrt{2}}(|\uparrow_1\downarrow_2\rangle - |\downarrow_1\uparrow_2\rangle). \tag{4.5.1}$$

It is the entangled singlet state and (a) indicates "antisymmetric". Therefore, the total ground state wave function is $\Psi_0(1,2) = \psi_0(\vec{r_1},\vec{r_2})S_{ent}^{(a)}$ (1 and 2 denote the space and spin variables of the first and second electrons, respectively). In agreement with the theory of helium atom we call it para-state of the two-electron [85] QD.

All symmetric combinations of coordinate wave functions (4.2.4), (4.2.6), (4.2.7) including function (4.2.5) require the antisymmetric spin functions (4.5.1). Those are the singlet states with spin zero relating to the para states of the QD.

The antisymmetric combinations of the coordinate wave functions (4.2.4), (4.2.6), (4.2.7) require the symmetric spin wave functions that organize the following triplet

$$S_1 = |\uparrow_1\rangle\ |\uparrow_2\rangle, S_2 = |\downarrow_1\rangle\ |\downarrow_2\rangle, \tag{4.5.2}$$

$$S_{ent}^{(s)} = \frac{1}{\sqrt{2}}(|\uparrow_1\downarrow_2\rangle + |\downarrow_1\uparrow_2\rangle). \tag{4.5.3}$$

The spin functions S_1 and S_2 corresponds to projections of spin ± 1, respectively. The spin function (4.5.3) is the symmetric entangled state corresponding to the spin projection 0. The states (4.2.4), (4.2.6), (4.2.7) relate to the ortho-states.

The system of energy levels of the two-electron QD splits into two classes - singlet (para-) and triplet (ortho-) accordingly to the symmetry of the spin functions like in a helium atom. The transitions between the para- and ortho- states are possible only with account of the spin-orbit interaction. The probability of such transitions is very small. This allows us to claim that there are two "modifications" of two-electron QDs: para- and ortho-dots. In agreement with the spectroscopic nomenclature, we can introduce the following spectral terms. Para states: ground state ${}^1S_0(\psi_0\ (3))$, first excited state ${}^1P_1(\psi_1^{(s)}(4))$, the second excited states: ${}^1D_2(\psi_2^1(5)$; ${}^1S_0(\psi_2^{(2)s}(6))$; ${}^1D_2(\psi_2^{(2)s}(7))$. Ortho- states: lowest state ${}^3P_2(\psi_1^{(a)}(4))$ (metastable), the second excited states: ${}^3S_1(\psi_2^{(2)a}(6))$; ${}^3D_3(\psi_2^{(2)a}(7))$. These spectral terms do not coincide with the ones of helium atom because in our case, the radial and orbital quantum numbers n and l are independent. The energy levels of the two-electron QD schematically depicted in Fig.4.1.

The most interesting characteristic of the energy levels of the two-electron QD is that they are very close to linear functions of the parameter λ as it can be seen from Fig.4.2. The familiar behavior was found for the ground state energy of 2D two-electron QD in [82].

The calculated energies E_0, $E_1^{(s)}$, $E_1^{(a)}$, $E_2^{(2)s}$ and $E_2^{(2)a}$) as a function of λ are shown in Figure 5.2. Let us focuss on the lowest energy levels of the QD. For $\lambda \leq 1$ the distance between the ground and first excited states $\hbar\omega$ with the typical $\omega = 10^{13}$ is order of $T = 100K$. At $T \ll \hbar\omega$, the transition from ortho- state ${}^3P_2$ to the

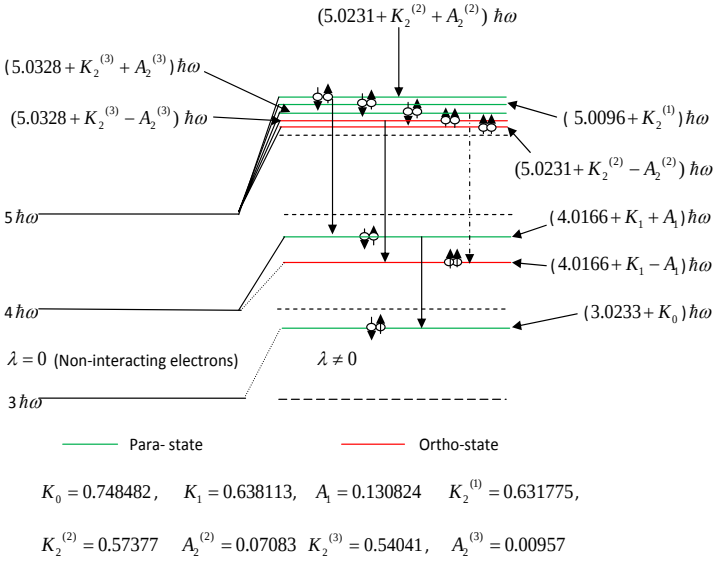

Figure 4.1: *Energy levels of para- and ortho- states of QD with* $\lambda = 1$ *(para- and ortho- states are denoted by green and red lines, respectively).*

ground para state $^1S_0$ has very small probability and the ortho state can be treated as metastable one. The ensemble of the two-electron QD at $T \ll 100K$ contains "para dots" and "ortho dots". They posses the entangled spin functions $S_{ent}^{(a,s)} = \frac{1}{\sqrt{2}}(|\uparrow_1\downarrow_2\rangle \mp |\downarrow_1\uparrow_2\rangle)$ for a long enough time.

From Fig. 4.2, one can see that the energy levels of the ground- and the lowest ortho- states getting closer with increment in λ. According to Section two for the typical QDs $\lambda < 2$ that allows us to hope that the presented variational calculations are reliable. As it was stated above the ensemble of two electron QDs according to our theory contains para- and ortho- dots. We considered the parabolic potential with the infinite confinement. The more realistic situation corresponds when the potential barrier has a finite height U_0. If $\hbar\omega \ll U_0$ then the low lying energy levels of the

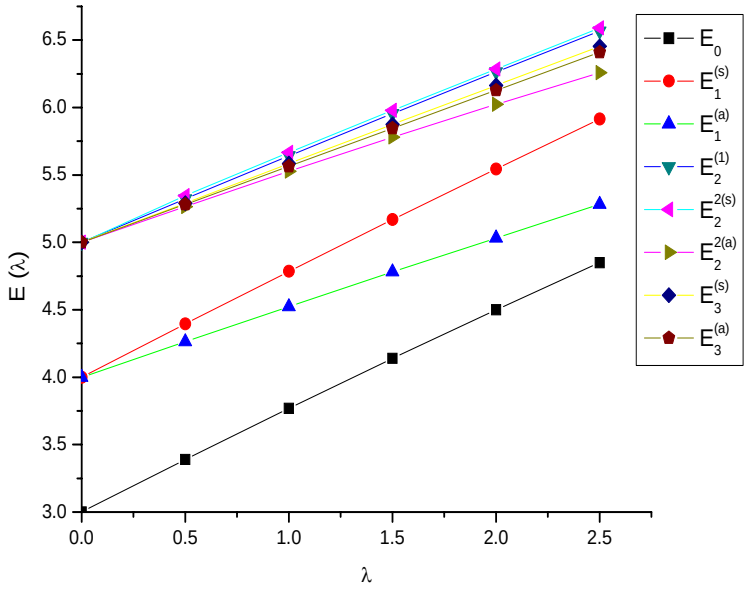

Figure 4.2: *Energy of para- and ortho- states of QD versus* λ.

two-electron QDs calculated above will be slightly affected due to the finite barrier height. It is clear that at very low temperatures the ionization potential of the para-dot is given by $I_{para} = U_0 - E_0(\lambda)$. At the same time, the ionization potential of the ortho-dot is given by $I_{ortho} = U_0 - E_1^a(\lambda)$. The values of $E_0(\lambda)$ and $E_1^a(\lambda)$ are given in Table1 and Table 3 (see also Fig. 4.2). The ionization potential of the para-dot is larger than the one of the ortho-dot. Their difference is $\Delta I = E_1^a(\lambda) - E_0(\lambda)$. For example, using a typical value of $\lambda = 2$, we get $\Delta I = 5.3$ THz.

These considerations remain true for any shape of the confining potential of QDs. The measurements of the ionization potential of the QDs can confirm existence of two-electron QDs with para- and ortho-states. As it was stated above the ensemble of two electron QDs according to our theory contains para- and ortho- dots. We considered the parabolic potential with the infinite confinement. The more realistic situation

corresponds when the potential barrier has a finite height U_0. If $\hbar\omega \ll U_0$ then the low lying energy levels of the two-electron QDs calculated above will be slightly affected due to the finite barrier height. It is clear that at very low temperatures the ionization potential of the para- dot is given by $I_{para} = U_0 - E_0(\lambda)$. At the same time, the ionization potential of the ortho-dot is given by $I_{ortho} = U_0 - E_1^a(\lambda)$. The values of $E_0(\lambda)$ and $E_1^a(\lambda)$ are given in Table1 and Table 3 (see also Fig.4.2). The ionization potential of the para-dot is larger than the one of the ortho-dot. Their difference is $\Delta I = E_1^a(\lambda) - E_0(\lambda)$. For example, using a typical value of $\lambda = 2$ we get $\Delta I = 5.3$ THz.

These considerations remain true for any shape of the confining potential of QDs. The measurements of the ionization potential of the QDs can confirm existence of two-electron QDs with para- and ortho-states.

4.6 Conclusion

We have calculated the first three energy levels of the two-electron QD with the parabolic confinement by using the variational functions. The analysis of our numeric calculations allowed us to propose the interpolation formulas for the variational parameters that recover the energy levels for the typical parameters of the QDs.

There are two classes of the electron states in the two electron QDs: para- states with total spin zero and ortho- states with total spin unit. The lowest energy level of the ortho-state is metastable. We claim that experimental realization of the quantum transition of the two-electron QDs will give para- and ortho- QDs. The lowest energy state of the QD has the symmetric coordinate wave function and antisymmetric singlet spin wave function $^1S_0$ and relates to the para state. All para- states have total spin

zero and should not manifest a multiple structure. These QDs must be related to the para- QDs. The ortho- QDs have energy levels that form close triplets with the total spin unit. The lowest energy state of the ortho-dot $^3P_2$ is metastable. The only transition from this state is $^3P_2 \longrightarrow ^1 S_0$ with change of spin direction of one electron. At low temperatures $T \ll \hbar\omega$ such a transition has low probability and we deal with two types of the entangled spin states with $S = 0$ and $S = 1$.

It would be interesting to mention about the hypothetic QDs manufactured from the materials with gigantic dielectric constant $\varepsilon \sim 10^3$ [86]. The Coulomb interaction in this case is practically negligible. The energy levels and wave functions of a such many-electron system are well known that considerably simplify description of the physical properties of such QDs.

Chapter 5

Optical properties of two - electron quantum dots with rigid confinement

Two low lying energy levels of 3D two-electron quantum dot (QD) with rigid confinement (the wave functions vanish at the surface of a QD) are obtained by the variational method. Moreover, these energy levels for rigid confinement were computed, through perturbation method. Similar to the parabolic confinement the quantum states of the QD with rigid confinement are divided into the para- and ortho- states like in the theory of helium atom. The optical properties of two electron QD are analyzed. The absolute strength of the optical constants such as the real and imaginary part of the dielectric constant, the index of refraction and the absorption coefficients for two electron QD are comparable to that of one electron QD. However, blue shift is observed in two electron QD.

5.1 Introduction

A large number of theoretical and experimental work has been devoted to the study of optical properties in low dimensional semiconductor microstructure with carrier confined in one direction (quantum wells), and two dimensions (quantum wires) [87]. The remarkable advancement in micro fabrication technology has now made it possible to realize structures particularly with quantum confinement in all three dimensions (quantum dots) [88, 89]. Some basic linear optical properties of QD's are already understood theoretically. The interband absorption spectrum should change from continuous band to a set of discrete lines, as a size of crystallite is decreased [90]. The study of optical property in such QD structures is therefore considered to be a subject of fundamental interest and significant attention has been developed to it since last decade [91, 92]. A system of electrons fully confined in all three dimensions will have discrete charge and electronic states, as do atoms and molecules [93]. As we make semiconductor crystal smaller the physical properties change in many ways. In a large crystal the overall shape and size of the crystal make little or no difference to its internal properties [94]. As a crystal becomes smaller, however, the effect of the surface becomes increasingly important. The most extreme consequence is that as a fraction of atoms at the surface becomes larger, the arrangement of the nuclei changes in order to relax the energy of the system as a whole [95]. In the case of strong confinement the image force effects are very small and can be neglected since the effects are not large enough to distort the wave functions significantly. So it is very simple to calculate the single particle energy levels of the quantum dot. The quantum confinement will split the bulk conduction and valence bands in to a series of discrete energy shells in spherical quantum dot.

QDs have been the subject of intense research studies over the last years. The interest in these structures is motivated by the physical effects and the potential device applications [101].

The two electron QD is an essential component for the preparation of entangled electronic states and this entanglement has a potential use to secure quantum communications protocol, quantum information processing and fundamental tests of quantum mechanics. These new physical properties are due to the size quantization effect of charge carriers [102, 103].

In this Chapter, we consider the low lying states of one and two-electron spherically symmetric QDs with rigid confinement where the wave function is set to be zero on the QD surface. The Coulomb interaction in the typical 10 nm semiconductor QDs cannot be treated as a small. We solved the problem with the help of the variational method and perturbation technique for hypothetic semiconductor QDs with large dielectric constant.

Under experimental realization of the two-electron quantum dots one will obtain two modifications of dots in the para and ortho states. But the strong Coulomb interaction between electrons in the typical semiconductor quantum QDs can create problems in tailoring such systems. It is worth attention to the materials with gigantic dielectric functions [104]. The electrostatic interaction of electrons in quantum dots made from this dielectrics can be very small. In this case, the two electron problem can be treated with the help of the perturbation theory and clarify the influence of the confinement on the structure of the wave functions.

This Chapter is organized as follows. In Section 5.2, we introduce the variational wave functions and the peculiarities of calculation of the variation parameters. We

also introduce the exact wave functions which, are used to determine the energies through perturbation techniques. Section 5.3 and 5.4 are devoted to calculation of the variation parameters and the energy levels of the QD. Moreover the energies calculated by perturbation technique and variational method are compared. Section 5.5 discusses the para- and ortho- states of the two-electron quantum dot. Section 5.6 is devoted to the study of optical properties of the two electron GaAs QD and comparing them with the known ones of the one electron GaAs QD.The Conclusion summarizes the results obtained and discusses the hypothetic many-electron quantum dots manufactured from materials with gigantic dielectric constants.

5.2 Statement of the problem

Two interacting electrons in 3D spherically symmetric quantum dot with the rigid confinement potential of a radius a are described by the following dimensionless Hamiltonian

$$\hat{H} = -\frac{1}{2}\nabla_1^2 - \frac{1}{2}\nabla_2^2 + \frac{\lambda}{|\vec{r_1} - \vec{r_2}|}. \tag{5.2.1}$$

The dimensionless coordinates of the first and second electrons r_1 and r_2 are measured in units of the radius of QD a, $\lambda = \frac{1}{\varepsilon}\frac{e^2 m^* a}{\hbar^2}$ is a coupling constant, and the energy is measured in $\frac{\hbar^2}{m^* a^2}$. Here m^* is an effective mass of electron, e is its charge, ε is the dielectric constant. In this model, the wave function must vanish on the surface of the shpere. This type of confinement is called a rigid confinement.

Let us evaluate λ for a typical semiconductor. Using the following parameters $m^* = 0.067m$ (m is the mass of free electron), $\varepsilon = 10$, we obtain $\lambda = 1.5438 \times 10^6 a$. For $a = 10$ nm $=10^{-6}$ cm, $\lambda = 1.5438$. This means that the perturbation theory to

the semiconductor two-dimension QD can be applied if $a \ll 10$ nm. For QD with $a \approx 10$ nm one has to use the numeric calculations or the variational method. It requires variational or numerical methods. In this chapter we use the variational method, which allows us to obtain analytic formulas.

The trial wave function when two electrons are in the ground state may be chosen as

$$\psi_0(\vec{r_1}, \vec{r_2}) = N_n(1 - r_1^\alpha)(1 - r_2^\alpha), \tag{5.2.2}$$

where $N_n = \frac{6\alpha^2+27\alpha+27}{2\alpha^2}$ is the normalization constant and α is a variational parameter. The wave function (5.2.2) vanishes on the surface of the QD when $r_1 = 1$, $r_2 = 1$. This style of the wave function is dictated by the exact ground state wave function of the one-electron QD [81]

$$\psi_0 \sim \frac{sin\pi r}{r}. \tag{5.2.3}$$

This function is nonzero at $r \to 0$ and zero on the surface of the QD at $r = 1$. The exact wave function of noninteracting electrons is

$$\psi_0(\vec{r_1}, \vec{r_2}) = \frac{1}{2\pi}\frac{sin\pi r_1}{r_1} \cdot \frac{sin\pi r_2}{r_2}. \tag{5.2.4}$$

The wave function of the first excited state is given by the symmetrized combination

$$\psi_1(\vec{r_1}, \vec{r_2})^{(s,a)} = \frac{1}{\sqrt{2}}\{\psi_0(\vec{r_1})\psi_1(\vec{r_2}) \pm \psi_0(\vec{r_2})\psi_1(\vec{r_1})\}, \tag{5.2.5}$$

where, $\psi_0(\vec{r_1})\psi_1(\vec{r_2}) = N_l(1-r_1^\alpha)r_2(1-r_2^\beta)cos\theta_2$ with $N_l = \frac{\sqrt{3}}{4\pi}\left(\frac{6\alpha^2+27\alpha+27}{2\alpha^2}\right)^{\frac{1}{2}}\left(\frac{5(5+\beta)(5+2\beta)}{2\beta^2}\right)^{\frac{1}{2}}$. Here s and a stand for the symmetric and antisymmetric combinations, respectively.

The exact function of the first excited state for rigid confinement when one electron is in the ground state and the other electron is in the excited state. The corresponding

wave function for small coupling constant λ is:

$$\psi_1(\vec{r_1},\vec{r_2}) = \frac{1}{\sqrt{2}}[\psi_0(\vec{r_1})\psi_1(\vec{r_2})) \pm \psi_0(\vec{r_2})\psi_1(\vec{r_1}))]. \tag{5.2.6}$$

Where $\psi_0(\vec{r_1}) = N_0\frac{sin\pi r_1}{r_1}$, $\psi_1(\vec{r_2}) = N_1[\frac{sinkr_2}{(kr_2)^2} - \frac{coskr_2}{kr_2}]cos\theta_2$ are the ground and first excited states wave functions, respectively, $N_0 = \frac{1}{\sqrt{2\pi}}$, $N_1 = 6.51011\sqrt{\frac{3}{4\pi}}$ are the normalization constants and $k = 4.49341$ is the second root of the spherical Bessel function. These wave functions vanish at the surface of the quantum dot ($\psi_0(1) = \psi_1(1) = 0$).

The trial wave function for the second excited state is chosen as

$$\psi(\vec{r_1},\vec{r_2}) = N_m r_1(1-r_1^\beta)r_2(1-r_2^\beta)cos\theta_1 cos\theta_2, \tag{5.2.7}$$

where $N_m = \frac{3}{4\pi}\frac{5(5+\beta)(5+2\beta)}{2\beta^2}$ and β is the variational parameter.

5.3 Ground state of two-electron QD

Calculating the average of the Hamiltonian (5.2.1) with wave function (5.2.2), we obtain the variation energy of the ground state E_0^v

$$E_0^v = T + K_0, \tag{5.3.1}$$

where the first term is the average kinetic energy of electrons

$$T = \frac{N_n\alpha^2}{2\alpha+1}, \tag{5.3.2}$$

the second term is the average energy of the Coulomb interaction

$$K_0 = \lambda\frac{8}{3}\frac{\alpha^4 N_n^2(12\alpha^2+89\alpha+124)}{(3+\alpha)(3+2\alpha)\prod_{j=0}^{4}(5+j\alpha)} \tag{5.3.3}$$

where $\prod_j$ stands for product with respect to j. For obtaining (5.2.6), we have to calculate the integral

$$K_0 = \int \psi_0^*(\vec{r_1}, \vec{r_2}) \frac{\lambda}{r_{12}} \psi_0(\vec{r_1}, \vec{r_2}) dv_1 dv_2, r_{12} = |\vec{r_1} - \vec{r_2}| \tag{5.3.4}$$

with the wave function (5.2.2) and usage of the known Legendre polynomial expansion

$$\frac{1}{r_{12}} = \frac{1}{r_1} \sum_{l=0}^{\infty} \left(\frac{r_2}{r_1}\right)^l P_l(cos\theta), \qquad r_1 > r_2, = \frac{1}{r_2} \sum_{l=0}^{\infty} \left(\frac{r_1}{r_2}\right)^l P_l(cos\theta), \qquad r_1 < r_2. \tag{5.3.5}$$

Here θ is the angle between $\vec{r_1}$ and $\vec{r_2}$. According to the addition theorem for spherical harmonics [83, 84] and

$$P_l(cos\theta) = P_l(cos\theta_1) P_l(cos\theta_2) + 2 \sum_{m=1}^{l} \frac{(l-m)!}{(l+m)!} \times P_l^m(cos\theta_1) P_l^m(cos\theta_2) cos\, m(\phi_1 - \phi_2), \tag{5.3.6}$$

where θ_1, ϕ_1 and θ_2, ϕ_2 are the polar angles of the vectors $\vec{r_1}$ and $\vec{r_2}$, respectively. When the above formulas are substituted into (5.3.4) and integrated with respect to ϕ_1, ϕ_2 and θ_1, θ_2, we obtain that the second term of (5.3.6) vanishes and contribution into the integral comes out of $P_0(cos\theta_1) = P_0(cos\theta_2) = 1$. With this in mind, we obtain

$$K_0 = \int_0^1 \Big[\int_0^{r_1} \frac{1}{r_1} \psi_0^2(\vec{r_1}, \vec{r_2}) r_2^2 dr_2 + \int_{r_1}^1 \psi_0^2(\vec{r_1}, \vec{r_2}) r_2 dr_2 \Big] r_1^2 dr_1. \tag{5.3.7}$$

Performing the integration, we get (5.3.3).

The minimum of energy (5.3.1) is obtained from the condition $\frac{dE_0^v(\alpha)}{d\alpha} = 0$. In Table 6.1 we present the calculated values of the variational parameter α and the variational ground state energy E_0^v for different values of λ. It is interesting to note that the trial function (5.2.2) gives ground state energy of two non interacting electrons $E_0^v =$

Table 5.1: The ground state energy E_0^v and variational parameter α for different λ

λ	0	0.5	1	1.5	2	2.5	3	3.5	4
α	1.081	1.135	1.189	1.244	1.299	1.356	1.413	1.471	1.529
$E_0^v(\lambda)$	9.993	10.875	11.752	12.623	13.490	14.352	15.209	16.062	16.910

9.99342. The exact wave function (5.2.4) of noninteracting electrons gives the ground state energy $E_0 = \pi^2$. For interacting electrons it gives

$$E_0(\lambda) = \pi^2 \frac{\hbar^2}{m^* a^2} + 1.78607 \frac{e^2}{\varepsilon a}. \tag{5.3.8}$$

This yields the ground state energy which is below the energy calculated employing the variational method below. The accuracy of the variational calculations with the trial function (5.2.2) gives only 1.3% deviation from the exact value.

The analysis of the numerical data from Table 5.1 allows one to propose the interpolation formula for calculation of the ground state energy of the two electron QD with rigid confinement for $0 \leq \lambda \leq 4$

$$E_0^v = 9.9944 \frac{\hbar^2}{m^* a^2} + 1.76049 \frac{e^2}{\varepsilon a}. \tag{5.3.9}$$

5.4 First excited state

The trial wave function for the state when both non interacting electrons are in the first excited state may be chosen as

$$\psi(\vec{r_1}, \vec{r_2}) = N_m r_1 (1 - r_1^\beta) r_2 (1 - r_2^\beta) cos\theta_1 cos\theta_2, \tag{5.4.1}$$

Table 5.2: The excited state energy E_2^v and variational parameter β for different λ

λ	0	0.5	1	1.5	2	2.5	3	3.5	4
β	0.371	0.392	0.413	0.434	0.456	0.477	0.499	0.521	0.543
$E_2^v(\lambda)$	20.604	21.424	22.243	23.061	23.880	24.694	25.510	26.321	27.134

where $N_m = \frac{3}{4\pi}\frac{5(5+\beta)(5+2\beta)}{2\beta^2}$ and β is the variational parameter. Calculating the average of the Hamiltonian (5.2.1) with wave function (5.4.1) we obtain

$$E_2^v = (5+\beta)(5+2\beta)\Big[\frac{5}{2(3+2\beta)} + \frac{\lambda\sum_{n=0}^{4} a_n\beta^n}{\prod_{i=0}^{2}(7+i\beta)\prod_{j=1}^{4}(9+j\beta)}\Big], \tag{5.4.2}$$

where $a_0 = 152020, a_1 = 129810, a_2 = 39046, a_3 = 4836$ and $a_4 = 208$. The minimum of energy (5.4.2) is obtained from the condition $\frac{dE_2^v(\beta)}{d\beta} = 0$. In table 6.2 we present the variational parameter β and the calculated excited state energy E_2^v for different values of λ. It is interesting to note that the trial function (5.4.1) gives excited state energy of two non interacting electrons $E_2^v = 20.604$. The exact wave function for non interacting electrons gives the energy $E_2^p = 20.25$. The accuracy of the variational calculations with the trial function (5.4.1) gives only 1.72% deviation from the exact value.

Keeping in mind the above obtained variational parameters α and β (tables 3 and 4) the symmetrized first excited state wave function of the two electron quantum dot can be written as

$$\psi(\vec{r_1},\vec{r_2})^{(s,a)} = \frac{1}{\sqrt{2}}\{\psi_0(\vec{r_1})\psi_1(\vec{r_2}) \pm \psi_0(\vec{r_2})\psi_1(\vec{r_1})\}, \tag{5.4.3}$$

where, $\psi_0(\vec{r_1})\psi_1(\vec{r_2}) = N_l(1-r_1^{\alpha})r_2(1-r_2^{\beta})cos\theta_2$ with $N_l = \frac{\sqrt{3}}{4\pi}\left(\frac{6\alpha^2+27\alpha+27}{2\alpha^2}\right)^{\frac{1}{2}}\left(\frac{5(5+\beta)(5+2\beta)}{2\beta^2}\right)^{\frac{1}{2}}$. The variation parameters α and β relates to the ground and excited state wave functions and are the roots of equations $\frac{dE_0^v(\lambda)}{d\alpha} = 0$ (with E_0^v given by (5.3.1) and $\frac{dE_2^v(\lambda)}{d\beta} = 0$

(with E_2^v given by (5.4.2).

Calculating the average of the Hamiltonian (5.2.1) with the help of trial wave function (5.4.3) and expanding $1/r_{12}$ in spherical harmonics as (5.3.5) we obtain the energy of the first excited state of the two electron quantum dot.

The calculation of the average Hamiltonian (5.2.1) with the help of the symmetrized wave function (5.2.2) gives the following result

$$E_1^v(\alpha,\beta) = \frac{(\alpha+1)(6\alpha^2+27\alpha+27)}{4(2\alpha^2+3\alpha+1)} + \frac{5(5+\beta)(5+2\beta)}{4(3+2\beta)} + K_1 \pm A_1, \tag{5.4.4}$$

$$K_1 = \int |\psi_1(\vec{r_1})|^2 \frac{\lambda}{r_{12}} |\psi_0(\vec{r_2})|^2 dv_1 dv_2, \tag{5.4.5}$$

$$A_1 = \int \psi_1(\vec{r_1})\psi_0(\vec{r_1})\frac{\lambda}{r_{12}}\psi_1(\vec{r_2}) \times \psi_0(\vec{r_2}) dv_1 dv_2. \tag{5.4.6}$$

After integration we get

$$K_1 = \frac{3\lambda}{16\alpha^2\beta^2} N_k (C+D+E), \tag{5.4.7}$$

with

$$C = \frac{32}{21} + \frac{7+3\alpha}{\prod_{i=1}^{2}(7+i\alpha)} - \frac{15(1+\alpha)}{\prod_{i=1}^{2}(3+i\alpha)}, \tag{5.4.8}$$

$$D = \frac{10(7+3\beta)}{3\prod_{i=1}^{2}(7+i\beta)} - \frac{40}{6+5\alpha+\alpha^2}\Big(\frac{7+\alpha+3\beta}{\prod_{i=1}^{2}(7+\alpha+i\beta)}\Big), \tag{5.4.9}$$

$$E = \frac{10}{3+5\alpha+2\alpha^2}\Big(\frac{7+2\alpha+3\beta}{\prod_{i=1}^{2}(7+2\alpha+i\beta)}\Big) - \frac{10\alpha^2(5+3\beta)}{(2+3\alpha+\alpha^2)\prod_{i=1}^{2}(5+i\beta)}. \tag{5.4.10}$$

The energy of exchange interaction A is given by

$$A = \frac{5\lambda}{4\alpha^2\beta^2} N_k (F+G+H), \tag{5.4.11}$$

Table 5.3: The excited state energy $E_1^{(s)}$, and $E_1^{(a)}$ variational parameters α and β, the normal Coulomb interaction energy K_1, and the exchange energy A_1 for different λ

λ	K_1	A_1	$E_1^{(s)v}(\lambda)$	$E_1^{(a)v}(\lambda)$
0	0	0	15.299	15.299
0.5	0.798	0.176	16.275	15.922
1	1.591	0.353	17.249	16.543
1.5	2.380	0.530	18.223	17.163
2	3.164	0.707	19.195	17.780
2.5	3.944	0.885	20.165	18.396
3	4.719	1.062	21.134	19.009
3.5	5.491	1.240	22.101	19.621
4	6.258	1.418	23.067	20.230

with

$$F = \frac{2\alpha^2(17+2\alpha)}{35(5+\alpha)\prod_{i=1}^{2}(7+i\alpha)} - \frac{5\alpha(\alpha-1)}{3(\alpha-3)(2+\alpha)(5+\beta)}, \tag{5.4.12}$$

$$G = \frac{203+38\beta}{15\prod_{i=1}^{2}(7+i\beta)} + \frac{4}{21+6\alpha+6\beta} + \frac{\alpha(5+\alpha)}{3(6+5\alpha+\alpha^2)(5+\alpha+\beta)}, \tag{5.4.13}$$

$$H = \frac{6(7+\alpha+\beta) - 3(20+\alpha(7+\alpha)(7+2\alpha+\beta))}{(2+\alpha)(5+\alpha)\prod_{i=1}^{2}(7+\beta+i\alpha)} + \frac{24}{(-9+\alpha^2)(7+\alpha+2\beta)}, \tag{5.4.14}$$

$$N_k = \prod_{i=1}^{2}(3+i\alpha)\prod_{j=1}^{2}(5+j\beta). \tag{5.4.15}$$

Now we consider the energy of the exact first excited state (5.2.6) for rigid confinement when one electron is in the ground state and the other electron is in the excited state. For solving the problem we have to use the general formula (5.3.5) to expand $1/r_{12}$ in spherical harmonics. The expectation value of the normal interaction energy between electrons (5.4.5) and expanding $1/r_{12}$ in spherical harmonics (5.3.5)

becomes

$$K = 84.76\lambda \int_0^1 \Big\{ \frac{sin^2\pi r_1}{r_1^3} \int_0^{r_1} \Big(\frac{sinkr_2}{(kr_2)^2} - \frac{coskr_2}{kr_2} \Big)^2 r_2^2 dr_2 + \frac{sin^2\pi r_1}{r_1^2} \int_{r_1}^1 \Big(\frac{sinkr_2}{(kr_2)^2} - \frac{coskr_2}{kr_2} \Big)^2 r_2 dr_2 \Big\} r_1^2 dr_1 \quad (5.4.16)$$

Integration in (5.4.16)is performed with the help of *Mathematica* and yields

$$K = 1.62159 \frac{e^2}{\varepsilon a}. \tag{5.4.17}$$

Similarly when the two states $\psi_0(\vec{r_1})$ and $\psi_1(\vec{r_2})$ relate to electrons in the ground and first excited state, the exchange energy can also be found by employing equations (5.4.11) and (5.2.5) and (5.4.16). The result is

$$A = 0.359655 \frac{e^2}{\varepsilon a}. \tag{5.4.18}$$

The calculation of the Hamiltonian (5.2.1) with the help of symmetrized wave function (5.2.6) yields

$$E_1 = \Big(\frac{\pi^2}{2} + \frac{4.5^2}{2} \Big) \frac{\hbar^2}{m^* a^2} + 1.62159 \frac{e^2}{\varepsilon a} \pm 0.359655 \frac{e^2}{\varepsilon a}. \tag{5.4.19}$$

In table 6.4. the ground state energies (5.3.9) and (5.4.1) and excited state energies (5.4.5) and (5.4.19), which are obtained by employing the variational method with trial wave functions (5.2.2) and (5.2.5) and perturbation technique with exact wave functions (5.2.4) and (5.2.6) are compared, respectively.

5.5 Para- and ortho- states of two-electron QD

The total wave functions of the two-electron QD including spin variables must be antisymmetric to permutation of electrons. In Section 2 we introduced the variation coordinate wave functions of our QD. The ground state wave function (5.2.2) or (5.2.3)

Table 5.4: Comparison of the ground state energies (5.3.9), (5.4.1) and excited state energies (5.4.5) and (5.4.19) obtained by variational method and perturbation technique.

λ	E_0^p	E_0^V	$E_1^{(s)p}$	$E_1^{(a)p}$	$E_1^{(s)v}(\lambda)$	$E_1^{(a)v}(\lambda)$
0	9.899	9.993	15.059	15.059	15.298	15.298
0.5	10.763	10.875	16.054	15.691	16.275	15.922
1	11.656	11.752	17.041	16.322	17.249	16.543
1.5	12.549	12.623	18.032	16.953	18.223	17.163
2	13.442	13.490	19.022	17.584	19.195	17.780
2.5	14.335	14.352	20.013	18.215	20.165	18.396
3	15.228	15.209	21.004	18.846	21.134	19.009
3.5	16.121	16.061	21.994	19.477	22.101	19.621
4	17.014	16.910	22.985	20.108	23.067	20.230

is symmetric with respect to interchange of the electron coordinates and requires the antisymmetric spin function 4.5.1. Therefore, the total ground state wave function is $\Psi_0(1,2) = \psi_0(\vec{r_1}, \vec{r_2})S_{ent}^{(a)}$ (1 and 2 denote the space and spin variables of the first and second electrons, respectively). It belongs to para-state of the two-electron QD.

All symmetric combinations of coordinate wave functions; (5.2.5) and (5.2.6) require the antisymmetric spin functions (4.5.1). Those are the singlet states with spin zero relating to the para states of the QD.

The antisymmetric combinations of the coordinate wave functions variational wave functions (5.2.5) and exact wave functions (5.2.6) require the symmetric spin wave functions that organize the triplet described in (4.5.2) and (4.5.3).

The spin function (4.5.3) is the symmetric entangled state corresponding to the spin projection 0. The states (5.2.5)and (5.2.6) relate to the ortho-states.

Similar to the parabolic confinement the system of energy levels of the two-electron QD in rigid confinement splits into two classes - singlet (para-) and triplet (ortho-)

accordingly to the symmetry of the spin functions like in a helium atom. Only under the condition of the spin-orbit interaction the transition between these two different states is possible. The probability of such transition is very small. This confirms that there are two "modifications" of two-electron QDs: para- and ortho-dots.

The most interesting characteristic of the energy levels of the two-electron QD is that they are very close to linear functions of the parameter λ as it is seen from Fig.5.1. The familiar behavior was found for the ground state energy of 2D two-electron QD in [82]. Moreover, for large dielectric constant ($\varepsilon \geq 10^2$) the perturbation technique gives a good result as compared to the variational method. This is understandable since the perturbation technique is more applicable when the coupling constant is very small ($\lambda \ll 1$) and the variation function does not coincides with the exact one at $\lambda \to 0$.

The calculated energies E_0, $E_1^{(s)}$, and $E_1^{(a)}$ as a function of λ are shown in Figure 5.1. Let us focuss on the lowest energy levels of the QD. For $\lambda \leq 1$ the distance between the ground and first excited states $\hbar\omega$ with the typical $\omega = 10^{13}$ is order of $T = 100K$. At $T \ll \hbar\omega$, the transition from ortho- state to the ground para state has very small probability and the ortho state can be treated as metastable one. The ensemble of the two-electron QD at $T \ll 100K$ contains "para dots" and "ortho dots". They posses the entangled spin functions $S_{ent}^{(a,s)} = \frac{1}{\sqrt{2}}(|\uparrow_1\downarrow_2\rangle \mp |\downarrow_1\uparrow_2\rangle)$ for a long enough time.

From Fig. 5.1 one can see that the energy levels of the ground- and the lowest ortho- states getting closer with increment in λ. According to Section two for the typical QDs $\lambda < 2$ that allows us to hope that the presented variational calculations are reliable.

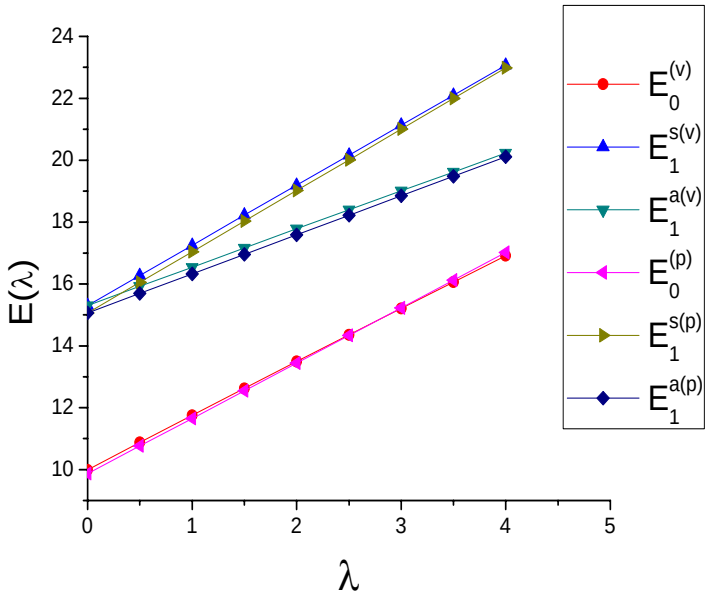

Figure 5.1: *Energy of para- and ortho- states of QD versus* λ.

5.6 Linear optical properties of GaAs QD with two electrons

If the QD with energy levels is subjected to an oscillating electric field, the perturbing Hamiltonian $\hat{H}(t) = H_p e^{i\omega_p t}$, induces a transition from the initial state i of energy E_i to the final state f of energy E_f. Using Fermi's golden rule, the transition probability for the QD [100] is

$$W(\omega) = \frac{2\pi}{\hbar}\frac{e^2 A_0^2}{m^{*2}c^2}|P_{cv}|^2\frac{1}{V}\rho^{0D}, \tag{5.6.1}$$

where, A_0 is the amplitude of the vector potential, P_{cv} is the moment matrix element between the valence and conduction band, V is the volume of the QD and ρ^{0D} is the joint density of states for a spherical quantum dot. The moment matrix element is

described as [88]

$$|P_{cv}|^2 = \frac{3m_e^2 E_x(E_x + \Delta x_0)}{2(3E_x + 2\Delta x_0)}\Big(\frac{1}{m_e^*} - \frac{1}{m_e}\Big), \tag{5.6.2}$$

where, E_x is the band gap of the QD, Δx_0 the spin- orbit splitting of valence bands, m_e^* is the electron effective mass, and m_e is the electron mass. For 2.8 nm radius of spherical GaAs quantum dot with one electron $E_x = 2.16$ eV. For a QD with two electrons the energy difference between the ground and the first excited para-state is $E_x = 2.1962$ eV including the Coulomb interaction and the exchange energy. We assume that $\Delta x_0 = 0.34$ eV is the same for one and two electron QDs and $m_e^* = 0.067 m_e$.

The optical absorption coefficient $\alpha(\omega)$ is proportional to a number of optical transitions per unit volume and time. It is given by the absorbed energy per unit time $\hbar\omega W(\omega)$ divided by the energy flux $\frac{A_0^2\omega}{\lambda} = \frac{A_0^2\omega^2 n(\omega)}{2\pi c}$, $\alpha(\omega) = \frac{\hbar\omega W(\omega)}{A_0^2\omega^2 n(\omega)} 2\pi c$ or

$$\alpha(\omega) = \frac{1}{V}\frac{4\pi^2 e^2}{m^{*2}\omega n(\omega) c}|P_{cv}|^2 \rho^{0D}, \tag{5.6.3}$$

where $n(\omega)$ is the real part of refractive index, which depends on frequency. The optical absorption coefficient relates to the imaginary part of the susceptibility $\chi(\omega)$ can also be written as

$$\alpha(\omega) = \frac{4\pi\omega}{cn(\omega)} Im\chi. \tag{5.6.4}$$

Relating equation (5.6.3) and (5.6.4) we obtain,

$$Im\chi = \frac{f}{V}\sum_{n,l}(2l+1)\delta(E - E_{nl}^e - E_{nl}^h), \tag{5.6.5}$$

where E_{nl}^e and E_{nl}^h are energy levels of electrons and holes, $f = \frac{2\pi e^2\hbar^2}{m^{*2}E^2}|P_{cv}|^2$.

In the vicinity of the resonance the dielectric constant ($\varepsilon = \varepsilon_1 + i\varepsilon_2$) for the quantum dot is [88],

$$\varepsilon = \varepsilon_\infty + \frac{\beta(\delta + i)}{1 + \delta^2}, \tag{5.6.6}$$

where $\beta = \frac{4\pi f}{\hbar\Gamma_x V}$ and $\delta = \frac{\hbar\Omega - \hbar\omega}{\hbar\Gamma_x}$ with $\hbar\omega$ being the photon energy, $\hbar\Omega = E_x$ being the lowest transition energy, $\hbar\Gamma_x = E_b$ being the broadening, and ε_∞ the back ground dielectric constant. The real and imaginary parts of the dielectric constant for a quantum dot are given by

$$\varepsilon_1 - \varepsilon_\infty = \Big(\frac{9\pi e^2\hbar^2 E_x(E_x + \Delta x_0)}{E_b R^3 E^2(3E_x + \Delta x_0)}\Big)\Big(\frac{m_e - m_e^*}{m_e m_e^*}\Big)\Big(\frac{(E_x - E)/E_b}{1 + ((E_x - E)/E_b)^2}\Big), \tag{5.6.7}$$

$$\varepsilon_2 = \Big(\frac{9\pi e^2\hbar^2 E_x(E_x + \Delta x_0)}{E_b R^3 E^2(3E_x + \Delta x_0)}\Big)\Big(\frac{m_e - m_e^*}{m_e m_e^*}\Big)\Big(\frac{1}{1 + ((E_x - E)/E_b)^2}\Big). \tag{5.6.8}$$

The refractive index and the absorption coefficient can be written as

$$n_r(\omega) = \Big(\frac{1}{2}\varepsilon_1(\omega) + \frac{1}{2}\Big\{[\varepsilon_1(\omega)]^2 + [\varepsilon_2(\omega)]^2\Big\}^{\frac{1}{2}}\Big)^{\frac{1}{2}}, \tag{5.6.9}$$

$$\alpha(\omega) = \frac{\omega\varepsilon_2(\omega)}{c\Big(\frac{1}{2}\varepsilon_1(\omega) + \frac{1}{2}\Big\{[\varepsilon_1(\omega)]^2 + [\varepsilon_2(\omega)]^2\Big\}^{\frac{1}{2}}\Big)^{\frac{1}{2}}}. \tag{5.6.10}$$

The graphs in Fig. 5.2 are drawn according to (5.6.7) and (5.6.8) for two electron QDs, with $E_x = 2.1962$ eV, $E_b = 0.5$ meV, $\varepsilon_\infty = 10$, $\Delta x_0 = 0.34$ eV and the radius of QD $R = 2.8$ nm. They show the real and imaginary part of the dielectric constant. There is a blue shift in energy by $\Delta E = 0.0362$ eV as compared to the energy of one electron QD due to the Coulomb interaction and exchange energy of two electrons.

The absolute values of the refractive index and the absorption coefficient for two electron QD are practically the same as for one electron QD. Figures 3A and 3B demonstrate the refractive index and absorption coefficient respectively. These graphs are drawn according to (5.6.9) and (5.6.10).

One can see from Fig. 5.3 that both $n_r(\omega)$ and $\alpha(\omega)$ are considerably large at the resonant frequency and may be utilized for intensive application in designing of

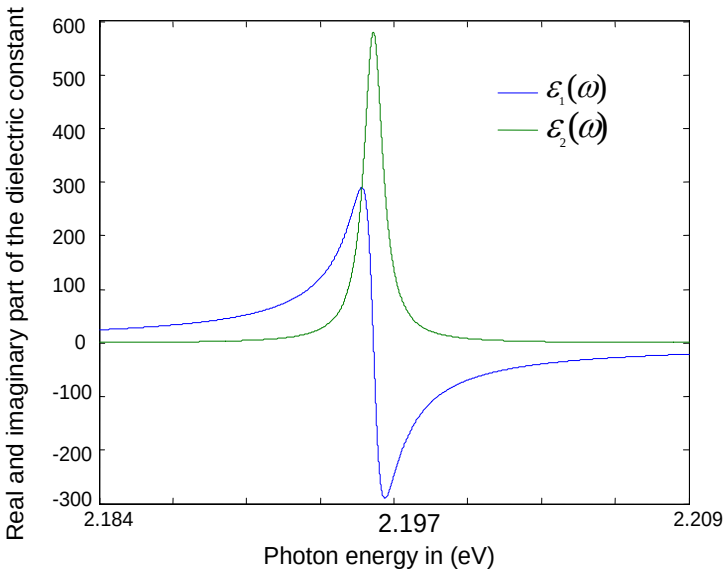

Figure 5.2: *Real and imaginary part of dielectric constant for GaAs QD with two electrons versus to photon energy*

optoelectronic devices. There are practically no difference between these quantities for one and two electron QDs. From Fig. 5.4 follows that reducing the size of the dot increases the energy gap and results in blue shift for both one and two electron QDs. Energy difference between the ground and excited states show that a blue shift in the case of two electron QD is larger than that of one electron QD. This is due to the increment of the coupling constant λ with radius of the QD. This behavior is illustrated in Fig. 5.4A and Fig. 5.4B

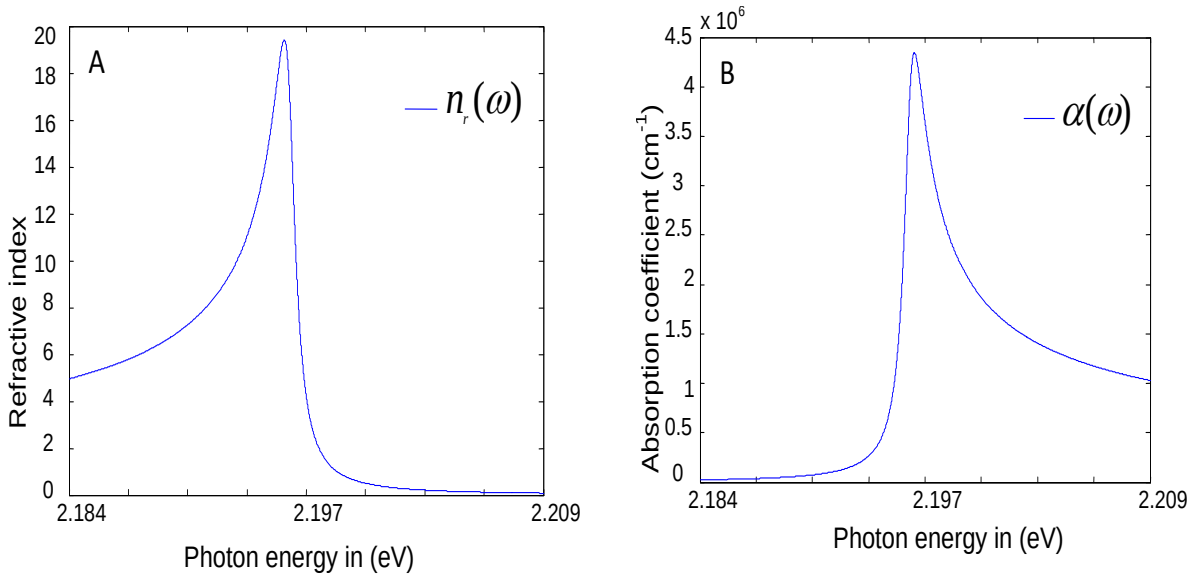

Figure 5.3: *Refractive index (A) and absorption coefficient (B) versus photon energy for GaAs quantum dot with two electrons*

5.7 Conclusion

We have calculated the first two energy levels of the two-electron QD with the rigid confinement by using the variational method (λ is not small) and perturbation technique ($\lambda \ll 1$).

There are two classes of the electron states in the two electron QDs: para- states with total spin zero and ortho- states with total spin unit. The lowest energy level of the ortho-state is metastable. We claim that experimental realization of the quantum transition of the two-electron QDs will give para- and ortho- QDs. The lowest energy state of the QD has the symmetric coordinate wave function and antisymmetric singlet spin wave function $^1S_0$ and relates to the para state. All para- states have total spin zero and should not manifest a multiple structure. These QDs must be related to

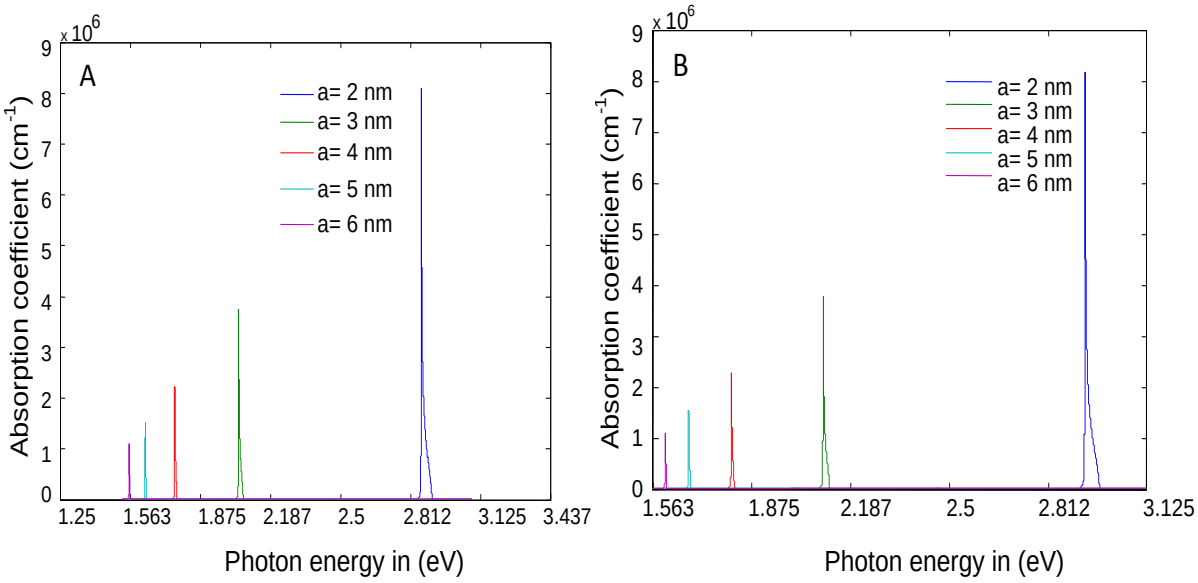

Figure 5.4: *Optical absorption spectra for one electron (4A) and two electron (4B) GaAs QDs of different radii versus photon energy*

the para- QDs. The ortho- QDs have energy levels that form close triplets with the total spin unit. The lowest energy state of the ortho-dot $^3P_2$ is metastable. The only transition from this state is $^3P_2 \longrightarrow ^1 S_0$ with change of spin direction of one electron. At low temperatures $T \ll \hbar\omega$ such a transition has low probability and we deal with two types of the entangled spin states with $S = 0$ and $S = 1$.

The linear absorption spectrum will be rigorously a series of lines. The change in absorption coefficient and index of refraction could be very large. Blue shift exhibited in the case of two electron QD is larger than that of one electron QD. This enhancement comes from the Coulomb interaction energy. Reducing the size of a QD induces a blue shift for both one and two electron QDs. But the blue shift in the case of two electron QD is larger than that one electron QD due to the interaction between electrons.

Chapter 6

Summary and Outlook

In this dissertation we have described the asymmetric DQWs with resonant levels. The splitting of these levels and tunneling times were calculated. When the tunneling time is much smaller than the average life time of the excited state, a charged particle makes a quantum transition from the excited state to the ground state by emitting a photon energy $\hbar\omega$. However for the reverse process the particle tunnels between the wells so fast that it has no time to make a quantum transition from the excited state to the ground state. In such a case we consider the system as a metastable nanosystem. The stimulated radiation time τ_{st} of asymmetric DQWs with parameters $\tau_t \ll \tau$ placed into resonator of the frequency ω may be made considerably smaller than the tunneling time τ_t. In such a case the metastable state of the nanosystem can be transformed into the dipole radiating state.

We have also determined the change in linear and third order refractive index and absorption coefficients using density matrix approach. In the given THz frequency range the total change in refractive index and absorption coefficients has a negative value. This indicate that it is possible to achieve, within some frequency range,

negative values of refractive index. As a result the media with asymmetric DQWs become left handed. This finding is of great importance for metamaterials science and can contribute substantially to the present search for simple and inexpensive left handed media.

Moreover we considered three and two low lying energy levels of 3D 2EQD with parabolic confinement and rigid confinement respectively using variational method and perturbation technique. The analysis of our numerical calculation allowed us propose interpolation formulas for the variational parameters that recover the energy levels for the typical parameters of the QDs. The calculation shows that there are two classes of electron states in the 2eQDs: para-states with the total spin equal to zero and ortho-states with the total spin equal to unit. The lowest energy level of the ortho-state is metastable. All para-states have the total spin equal to zero and should not manifest multiplet structure. The experimental realization of an ensemble of 2eQDs gives the para- and ortho QDs. The quantum transition from the ortho-state to para-state requires change of the spin direction of one electron. At low temperature the transition between these states are possible only with account of the spin-orbit interaction and have very small probability. This allows us to claim that there are two "modifications" of 2eQDs: para- and ortho-dots. The para- and ortho- QDs have different ionization potentials. The measurement of these potentials can also confirm the existence of 2eQDs.

With the help of the obtained energy levels of 2eQD for the case of rigid confinement, we calculated the real and imaginary part of the dielectric constant, the refractive index and absorption coefficient as a function of the incident photon energy. The maxima of these quantities show the blue shift comparing with the 1eQD due to

the Coulomb and exchange interaction between electrons. Reducing the size of the QDs results in the blue shift of the maxima of the above quantities for both 1- and 2eQD due to the Coulomb interaction.

For the future further work is required to study the nonlinear optical properties of two electron QDs using the calculated para- and ortho- state energies in this thesis. Moreover we are very interested to study the quantum mechanical and optical (linear and nonlinear) properties of three, four, five, six and many controllable number of electron QDs with the help of different numerical approaches.

Bibliography

[1] R.P. Feyman, Caltech Engineering and Science, 23:5, 22 (1960).

[2] A.Y. Cho and J.R. Arthur Prog., Solidstate Chem. 10, 157 (1974).

[3] R.dingle, Wiegmann, and C.H. Henry, Phys. Rev. Letters, 33, 827 (1975).

[4] J.R. Arthur, J. appl. Phys., 39, 4032 (1968).

[5] L. Esaki, and R. Tsu, IBM, J. Res. Dev 14, 61 (1970).

[6] G. Döhler, Phys. Stat. Sol. (b)52, 79 and 533 (1972).

[7] E. Kasper, H.J. Herzog, and H. Kibbel, Appl. Phys, 8, 199 (1975).

[8] D.C. Tsui, H.L. Störmer, and A.C. Gossard, Phys. Rev. Lett., 48, 1599 (1982).

[9] Goldstein, et al., Appl. Phys. Lett., 47, 1099 (1985).

[10] Fulton and Dalton, Phys. Rev. Lett., 59, 109 (1987).

[11] L.P. Kouwenhoven, et al., Z. Phys., B-Condenced matter, 85, 367 (1991).

[12] Xiang-Hong Qi, Xiao-Jun Kong, Jian-Jun Liu Phys. Rev. B 58, 10578 (1998)

[13] Tomoaki Kaneko, Mikito Koshino, Tsuneya Ando, Phys. Rev. B 78, 245303 (2008)

[14] T.Puangmali, M. Califano, Paul Harrison, Phys. Rev. B 78, 245104 (2008)

[15] L. Pavesi and R. Guardini, Brazilian J. Phys. 26, 151 (1996).

[16] ZXCao, R. Song, LBMa, YDu, ALJi and YQ Wang J. Nano Tech.,17, 2073 (2006).

[17] H.S. Mavi, A.K. Shukla, B.S. Chauhan and S.S. Islam, J.Matter. Sc. and Engineering 107, 148 (2004).

[18] S.Vijayalakshmi, A. Lan, Z. Iqbal, H. Grebel, J. Appl. Phys., 5, 2490 (2002) .

[19] P. Mishra and K.P. Jain, J. Mater. Sc. and Engineering, 95, 202 (2002).

[20] S. Schmitt-Rink, D.A.B. Miller and D.S. Chemla, J. Phys. Rev. 15, 8113 (1987).

[21] O. Ciftja and A.A. Kumar, Phys. Rev. B 70, 205326 (2004)

[22] E.Ozturk, I. Sokmen, J. superlattice and microstructure, 47, 36 (2007).

[23] I. Karabulut, U. Atav, H. Safak, M. Tomak, Eur. Phys. J. B 55, 283 (2007) .

[24] E.Ozturk, I. Sokmen, J. superlattice and microstructure, 48, 312 (2010).

[25] D.M.T. Kuo, Y.C. Chang, Chinese J. Phys. 39 (2001).

[26] S. Panda, B.K.Panda, S.Fung, and C.D.Beling, J. Appl. Phys. 80 (1996).

[27] S. Panda, and B.K. Panda, Paramana J. Phys., 56 (2001)

[28] R. Koc, and D.Haydargil, Turk J. Phys. 28 (2004)

[29] J.P. Eienstein, L.N Pfeiffer, and K.W. West, J. Appl. Phys. 58 (1991).

[30] A. G. Davies, E.H. Linfield, and M.B. Jhonston, Phys.Med. Biol. 47, 3679 (2002).

[31] S. Ten, M.F. Krol, P.T. Guerreiro, and N. Peyghambarian, Appl. Phys. Lett. 69, 22 (1996).

[32] M. Bedoya, and A.S. Camacho, Phys. Rev. B 72 (2005).

[33] A.G. Davies, E.H. Linfield and M.B. Jonson, J. Phys. Med. Biol. 47 (2002).

[34] M. Razavy, *Quantum theory of tunelling*, 1st edn. Chapter 7 (World Scientific press, New Jersy, 2003).

[35] S.S. Rink, D.S. Chemla, and D.A.B. Miller, J. APPS, 32 (1985).

[36] J.D. Cox. Mahi and R. Singh, Nanoscale Res Lett. 484 (2010).

[37] J.J Sakurai,*Modern Quantum Mechanics*, 3rd edn. (Addison-Wesley, 1994).

[38] Y. Masumoto, T. Takagahara, "Semiconductor Quantum Dots" Springer, Berlin (2002)

[39] D. Heiss, M. Kroutvar, J.J. Finley, G. Abstreiter, Solid state commun. 135, 591 (2005) .

[40] M. Troeecoli, A. Belyanin, F. Capasso, E. Kubukcu, D.L. Sinco, A.Y. Cho, Nature 433, 845 (2005).

[41] G.H. Zaki, A.H. Phillips, and A.S. Atallah, EJTP 5, 19, 33 (2008)

[42] S. Neeleshwar, C.L. Chen, C.B. Tsai, and Y.Y. Chen, Phys. Rev. B 71, 201307 (R) (2005).

[43] Y. Masumoto and K. Sonobe, Phys. Rev. B 56, 15 (1997).

[44] N.A. Bruce, and P.A. Maksym, Phys. Rev. B 614718 (2000).

[45] D. Pfannkuche, V. Gudmundsson, and P.A. Maksym, Phys. Rev. B 472244 (1993).

[46] J-L. Zhu, Z. Zhu, Y. Kawazoe, and T. Yao, Phys. Rev. B 581375 (1998).

[47] R. Pino, and V.M. Villalba, J. Phys. Condens. matter 13, 11651 (2001).

[48] A. Harju, S. Siljamaki,and R.M. Nieminen, Phys. Rev. B 65 075309 (2002).

[49] J. Harting, O. Mulken, and P. Borrmann, Phys. Rev. B 62 10207 (2000).

[50] C.S. Park, M.G. Jeong, C.S. Park, and S.K. Yoo, Phys. Rev. A 58, 3443 (1998).

[51] K. Banergee and S.P. Bhatnager, phys. Rev. D 18, 4768 (1978).

[52] A. Patrasciou and E. Gildener, Phys. Rev. D 16, 423. (1977).

[53] F. Zhou, Z. Cao and Q. Shen, Phys. Rev. A 67, 062112 (2003).

[54] P. Pedram, M. Mirzaei, and S.S. Gousheh, J. Phys. 1 (2006)

[55] E. Merzbacher, *Quantum Mechanics*, 3rd edn., Chapter 2 (John Wiley and Sons press, New York, 1970).

[56] L.D. Landau and E.M. Liftshitz, *Quantum Mechanics*, 3rd edn., Chapter 7, (Pergamon press, London, 1977).

[57] Guan Sun, Guibao Xu, Yujie J. Ding, Hongping Zhao, Guangyu Liu, Jing Zhang,V, IEEE Journal of Selected Topics in Quantum Electronics, 17,1, (2011).

[58] J.R. Singer, *Masers* (John, Whiley, and Sons Inc, 1959).

[59] J. Vanier, C. Audoin, *The Quantum Physics of Atomic Frequency Standards*, (Adam Hilger, Bristol, 1989).

[60] D.Braun, J. Martin, Phys. Rev. A 77, 032102 (2008).

[61] D. Blokhintsev, *Quantum Mechanics*, 1st edn., (Springer press, New York 1964).

[62] S.A. Savinov and V.N. Mursin, JEEP letters, 93, 1, 155 (2011).

[63] E.C. Niculescu and A. Radu, Eur. Phys. J. B, 80, 1, 73 (2011).

[64] Z. Li, and X.H. Jing, J. Commun. Theor. Phys.,41 (2004).

[65] G.H. Wang, Q. Guo, K.X. Guo, Chinese J. phys, 41 1 (2003).

[66] Lizhang and Hong-Jing Xie, Modern Physics Letters B, 17 1 (2005).

[67] S.L. Chuang and D. Ahn, J.appl.Phys. 65, 2822 (1989).

[68] R. W. Boyd, Nonlinear optics (Academic press, New York 1992).

[69] J. Radovanvoic, V. Milanovic, Z. Ikonic, D. Indin, J. facta uneversitatis, 2, 1263 (2000).

[70] M.A.Reed, J.N.Randell, R.J.Aggarwal, R.J.Matyi, T.M.Moor, Phys. Rev. Lett., 60, 1 (1988.

[71] G. Rezaei, B. Vaseghi, F. Taghizadeh, M.R.K. Vahdani, M.J. Karimi, Superlattice and Microstructure 48, 450 (2010).

[72] M.R.K. Vahdani, G. Rezaei, Phys. Lett. A 374, 477 (2010).

[73] M.R.K. Vahdani, G. Rezaei, Phys. Lett. 373, 3079 (2009).

[74] S.S. Rink D.A.B. Miller, D.S.Chemla, Phys. Rev. B 35, 8114 (1986).

[75] Garnett W. Bryant, Phys. Rev. B 52 (1995).

[76] Li, W.Ping, Xiao, Jing-lin, Y.J. Wen, Yu Yi-Fu and Wang-Zi-Wu, Chin. Phys. Rev. B 19, 047102 (2010).

[77] A. Einstein, B. Podolsky, and N. Rosen Phys. Rev. 47, 536 (1935).

[78] W.D. Oliver, F. Yamaguchi, and Y. Yanmoto, Phys. Rev. Lett. 88, 037901, 1 (2002).

[79] L. He, G. Bester, and A. Zunger, Phys. Rev. B 72, 195307 1(2005).

[80] A. Ferron, O. Osenda, and P. Serra, Phys. Rev. A 79, 032509 (2009).

[81] P.Gombas and D. Kisdi,*Wave Mechanics*, 1st edn., (Akademiai Kiado, Budapest, 1973).

[82] O. Ciftja, and A.A. Kumar, Phys. Rev. B 70, 205326 (2004).

[83] G. Arfken, *Mathematical Methods for Physicists*, 3rd edn., (Academic Press, San Diiaego, California, 1985)

[84] L. I. Schiff, *Quantum Mechanics*, 1st edn., (Springer Press, New York 1964).

[85] I.O. Vakarchuk, *Quantum Mechanics*, 2nd edn., (Ivan Franko L'viv University, L'viv 2004 (in Ukrainian)).

[86] J.Liu, G.G. Duan, W.G. Yin, W.N. Mei, R. W. Smith, J.R. Hardy, Phys. Rev. B 70 144106 (2004).

[87] D.A.B.Miller, and S.D. Smith, Advances in Phys., 30, 697 (1981)

[88] D.A.B. Miller, D.S.Chemla, S.schmitt-Rink, Phys. Rev. B 35 1 (1986).

[89] D.A.B. Miller, D.S. Chemla, T.C.Dammen, A.C.Gossard, and W.T. Tsang, Appl. Phys. Lett. 41 1 (1982).

[90] D.A.B. Miller, D.S. Chemla, T.C.Dammen, A.C.Gossard, and W. Wiegmann, Phys. Rev. Lett. 53 1 (1984).

[91] Y.Ding and Z.L.Wang, J.Phys. Chem.B, 108, 12280 (2004).

[92] D.U.Saengr, Phys. Rev. Lett., 54 1 (1996).

[93] A.Nakamura, H.Yamada, and T.Tokizaki, Phys. Rev. Lett. 40 1 (1989).

[94] F.E.Prins, S.Y. Nikitin, G.Lehr, and H.schweizer, Phys. Rev. Lett. 49 1 (1994).

[95] S.M. Reimann, M. Manninen, Rev. Mod. Phys., 74 1 (2002).

[96] Y. Peleg, R. Pnini, and E. Zaarur, *Theory and Problems of Quantum Mechanics*, 1st edn. (McGraw-Hill, NewYork, 1998).

[97] C. Kittel, P.McEuen, *Introduction to Solid State Physics*, 8th edn. (John Wiley and Sons, USA, 2005).

[98] S.S. Rink, D.A.B. Miller, D.S. Chemla, J.Phys. Rev.B, 35 1 (1987).

[99] J.H. Davies, the Physics of Low Dimensional Semiconductors, 6th ed (Cambridge, USA, 1998).

[100] S. S. Rink, D.S. Chemla, D.A.B. Miller, J. Advances in Physics, 38, 89 (1989).

[101] Burlad G., Loss D. and Di Vincenzo, D.P., Phys. Rev., B 59: 2070 (1999).

[102] M Bayer, O. Stern, P. Hawrylk, S. Fafard, A. Forchel, Nature, 405, 923 (2000).

[103] K.G. Dvoyan, D.B. Hayrapetyan, E.M. Kazaryan, and A.A. Tshantshapanyan, Nanoscale Research Letters, Vol.4, N2, 130 (2009).

[104] Wen Xiang Yuan, Suikong Hark, and Wai Ning Mei, J. Ceramic Processing Research, 10 696 (2009).

PUBLICATIONS

1. Menberu Mengesha, V.N. Mal'nev, "Linear Optical Properties of GaAs Quantum Dot", Asian Journal of Spectroscopy-Special Issue, ISSN No. 0971-9237 (2010) 179-185

2. Menberu Mengesha, V.N. Mal'nev, and S.V. Koshvaya,"THz Radiation under Tunneling in asymmetric double quantum wells", Journal of electromagnetic analysis and application, 3 2011 (271-276).

3. Menberu Mengesha, V.N. Mal'nev, "Two electron Quantum dots with parabolic confinement (Low lying para- and ortho- states)", Ukrainian Journal of Physics, ISSN 0372-400X 2011 V56 No 11.

4. Menberu Mengesha, V. Mal'nev, "Optical properties of two electron quantum dots in low lying para- and ortho- states" J. Superlattices and microstruct, Elsevier (2012), http://dx.doi.org/10.1016/j.spmi.2012.04.008.

POSTER PRESENTATION IN INTERNATIONAL CONFERENCE

1. Menberu Mengesha, V. Mal'nev, "Low lying states of two electron quantum dots, Poster presentation [P1-8]", 2nd Nanotoday Conference, Marriott, Waikoloa beach, Hawaii, USA, December 11-15, 2011.

DECLARATION

I hereby declare that this PhD dissertation is my original work and has not been presented for a degree in any other University and that all source of materials used for the dissertation have been duly acknowledged.

Name: Menberu Mengesha

Signature: _____

email: menberuwldmrm@gmail.com

This PhD dissertation has been submitted for examination with my approval as University advisor.

Name: Prof. V. Mal'nev

Signature: _____

Place and date of submission:

Department of Physics

Addis Ababa University

February, 2012